An ultrasonic study of vibrational anharmonicity in indium between room temperature and the melting point

Flower, Stephen Clive

Award date:
1987

Awarding institution:
University of Bath

AN ULTRASONIC STUDY OF VIBRATIONAL ANHARMONICITY IN INDIUM BETWEEN ROOM TEMPERATURE AND THE MELTING POINT

submitted by Stephen Clive Flower

for the degree of Doctor of Philosophy

of the University of Bath

1987

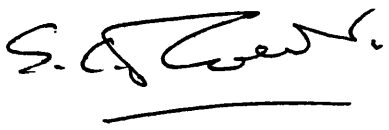

ProQuest LLC
789 East Eisenhower Parkway
P.O. Box 1346
Ann Arbor, MI 48106-1346

CONTENTS

	Page
Abstract	1
Acknowledgements	3
1.INTRODUCTION	4
1.1 Instability based theories of melting	11
2. SOUND WAVES THROUGH SOLIDS	17
2.1 Introduction	18
2.2 Elastic stiffness constants	18
2.3 Elastic wave propagation	21
2.4 Pressure derivatives of elastic constants	25
2.5 Grüneisen parameter	27
3. EXPERIMENTAL TECHNIQUES	33
3.1 Crystal growth	34
3.1.1 Introduction	34
3.1.2 Zone melting	34
3.1.3 Zone refining	35
3.1.4 Horizontal zone leveller	38
3.1.5 Crystal growth boats	38
3.1.6 Crystal growth procedure	41
3.1.7 Sample preparation	41
3.2 Ultrasonic wave velocity measurement	44
3.2.1 Introduction	44
3.2.2 Transducers	44
3.2.3 Pulse-echo overlap	45

3.3 Application of pressure 48

3.3.1 Pressure cell 48

3.3.2 Manganin resistance coil 50

3.4 Temperature control 51

3.5 Data collection and analysis 53

3.6 Experimental errors and corrections 56

4. EXPERIMENTAL RESULTS 59

4.1 Introduction 60

4.2 Ultrasonic propagation velocities 60

4.3 Second order elastic constants 74

4.4 Pressure derivatives of SOECs 88

4.5 Grüneisen parameters 101

5. DISCUSSION 111

5.1 Introduction 112

5.2 Propagation velocities 113

5.3 Elastic constants 116

5.4 Pressure derivatives of elastic constants 119

5.5 Grüneisen parameters 123

5.6 Melting curve for indium 129

6. CONCLUSIONS 144

APPENDIX A Printout of data analysis program 146

APPENDIX B Worked example of conversion between adiabatic and isothermal pressure derivatives 156

References 163

ABSTRACT

Ultrasonic techniques have been used to measure pressure and temperature dependences of elastic wave propagation velocities along various crystallographic directions in single crystal indium . The results have allowed , for the first time , a complete set of the pressure derivatives of the elastic constants of indium to be obtained for temperatures between room temperature and the melting point (429.7 deg.K). This in turn has allowed the temperature dependence of long wavelength acoustic mode Grüneisen parameters to be found over the same temperature range .The values obtained for acoustic mode Grüneisen parameters show that there is a significant increase in vibrational anharmonicity as the melting transition is approached . The mean acoustic mode Grüneisen parameter γ^{el} , for modes near the Brillouin zone centre , is seen to be larger in value than the thermal Grüneisen parameter γ^{th} (also calculated here) due mainly to the contributions from the more anharmonic slow shear modes ($\underline{k}[110],\underline{e}[1\bar{1}0]$, and $\underline{k}[101],\underline{e}[\emptyset]$). It is therefore concluded that the mean acoustic mode Grüneisen parameter for shorter wavelength modes , further out in the Brillouin zone , will be rather lower in value than the mean for modes near the zone centre . .

The data obtained here for indium close to its melting point has provided a means of properly testing a melting

curve equation based on the Lindemann melting law (Kraut and Kennedy [1966], Gilvarry [1966], Vaidya and Raja Gopal [1966]). By using high temperature data and correcting the value of the thermal Grüneisen parameter for compression, (Ramakrishnan [1978]) the equation is shown to give a much more accurate description of the pressure dependence of the melting temperature of indium , at high pressures , than could be shown previously .

ACKNOWLEDGEMENTS

My thanks go to my supervisor, George Saunders, for his enthusiasm, guidance and support, without which it would not have been possible to pursue this research.

Special thanks must go to my wife, Helen, who has had to put up with "the thesis" rather longer than originally anticipated.

I am grateful to all the research group staff, Wendy, Eddie, Bob and Barry, for their help and advice during this work.

Thanks also to Debs, Nigel, Nick and all the staff in the School of Physics for making it such a friendly and entertaining place to work.

This thesis has taken considerably longer to complete than I had originally thought it would. The fact that it got finished at all is due in no small part to the support (and nagging) of Rosemary Ford, Peter Stewart (thanks for the use of the PC and the xerox), and my parents.

I am also grateful to the S.E.R.C. for funding this work, and to my Dad for the use of his word-processor.

CHAPTER 1

INTRODUCTION

1.0 INTRODUCTION

The purpose of this work has been to investigate the vibrational anharmonicity of the long wavelength acoustic phonon modes in indium within the temperature range between room temperature and the melting point (156.7 deg.C) . This has been done by measuring hydrostatic pressure dependences of the velocities of ultrasonic waves propagating through single crystal indium .

This introduction sets out to explain what vibrational anharmonicity actually is , and to outline how ultrasound velocities relate to elastic properties of materials . It then goes on to give the reasons for carrying out such a study and for indium being chosen as the subject .

An external stress applied to a solid produces a resultant deformation , or strain . The relationship between stress and strain may be considered linear for many purposes (Hookes law) , and is described by parameters called elastic constants . This linearity only holds for infinitesimal strains .

For real solids a full description of the stress-strain relationship may only be obtained by considering stress and strain as second rank tensors , related by elastic constants that are components of a fourth rank tensor (eg. Nye 1957) .

A more general definition of elastic constants is obtained using a thermodynamic approach (Brugger 1964) . The conventional elastic constants are then defined as the second derivatives of a thermodynamic potential , such as internal energy , with respect to finite strain . These are then termed second order elastic constants (SOECs) . Elastic constants of third and higher orders may then be introduced which relate to departures from the linear Hookes law as strains become finite and the SOECs become strain dependent .

If strain energy density is expanded in a Taylor series, about the position of zero strain , one can start to form a representation of how the energy of the solid varies with deformation . The coefficients of this series are the various orders of elastic constants . An analogous expansion is that of the interatomic potential in terms of the displacement of atoms from their equilibrium lattice positions . If the forces binding atoms were purely harmonic in nature , ie. if the atom were vibrating in a perfectly parabolic potential well , only terms up to second order in the expansion would need to be considered. If this were so, solids would not show the anharmonic effects so characteristic of real materials .

For example if the temperature were raised for a system of atoms vibrating in parabolic potential wells , the atoms would have more energy and so would move higher up

the well and display a larger amplitude of vibration . However , they would still be moving about the same position in space , and therefore would still have the same mean atomic displacement . If this were the case for real materials, there would be no thermal expansion.

Real solids have various anharmonic properties associated with the higher order terms in the Taylor expansion . Third order elastic constants (TOECs) relate to the dependence of SOECs upon interatomic distances , and so are useful when investigating phenomena such as thermal expansion , phonon-phonon interactions and vibrational instabilities leading to structural phase transitions .

Elastic constants govern many of the physical properties of a material . For instance , the speed at which a pressure wave may propagate through a body will depend upon how the applied stress is converted to a resultant movement (strain) which transmits the wave . This leads us to suppose that measurement of the speed of propagation of a pressure wave through a sample might yield information enabling values of SOECs to be calculated . Thurston [1965] describes the relations between SOECs and the propagation velocities of small amplitude ultrasonic waves along different crystallographic directions for various crystal structures . Ultrasonic methods can also be used to determine TOECs . This is done by observing how the measured SOECs vary with interatomic distance (ie

by measuring how the ultrasonic velocities depend upon applied pressure) . Ultimately ultrasonic data combined with calorimetric and thermal expansion data can be used to determine the equilibrium equation of state and various thermodynamic functions for a material .

For this study the velocities , and the hydrostatic pressure dependences of the velocities , of ultrasonic waves propagating along various crystallographic directions in single crystal samples of indium were measured in the temperature range 283K to 429K (melting point for indium , T = 429.7K) . The aim of the work was to try and quantify anharmonic effects in a crystal structure right up to temperatures near the melting point and perhaps throw more light on a possible mechanism for the melting process .

Indium was chosen for this work because it is a safe material of which single crystals can readily be grown and it has a fairly easily accessible melting temperature (429.7K) . It also possesses a very simple structure containing just one atom per unit cell . This means that the only vibrational modes present are acoustic phonon modes , and optic phonon modes do not need to be considered .

Indium is a member of the group IIIB metals and crystallises with a tetragonal symmetry . It has a body-centred tetragonal (bct) structure (although it can

be represented as a face-centred tetragonal (fct)) and belongs to the 4/mmm point group . The atomic arrangement differs only slightly from cubic close packed : at room temperature the c/a ratio is only 1.08 . Although this value decreases as the temperature rises, it remains greater than unity right up to the melting point .

Indium undergoes no transformations right down to 4.2K (Swensen [1955]) , and up to 300Kbar (Vereshchagin , Kabalkina and Troitskaya [1964] , Vaygham and Drickamer [1965]) . This makes indium the most stable of the group IIIB metals in spite of the softening of the shear vibrational mode , propagating ($\underline{k}$) along the [110] direction and polarised ($\underline{e}$) along [1$\bar{1}$0] , near the Brillouin zone centre (Gunton and Saunders [1973]) . The elastic constant $(C_{11} - C_{12})/2$ associated with this mode is a measure of resistance to deformation when a shear stress is applied across a [110] plane in a [1$\bar{1}$0] direction , and its small value and rapid decrease with rise in temperature strongly suggests a shear assisted displacive transformation to face-centred cubic (fcc , point group m3m) structure at high temperature . It is thought that the only reason that this transformation does not take place is that indium melts before getting to the required temperature (Chung , Gunton and Saunders [1976]).

Alloying of indium with thallium further reduces its shear stability . Indium rich In-Tl alloys exhibit soft mode transformations , the shear modulus $(C_{11} - C_{12})/2$

tending to zero (within experimental error) as the fct/fcc transformation is approached from either the tetragonal or cubic phase (Pace and Saunders [1974]) . It is possible that such anharmonic behaviour may be responsible in part for other sorts of transitions such as the solid-liquid phase transition . This study sets out to try and quantify the temperature dependence of the vibrational anharmonicity of long wavelength acoustic phonon modes in indium as it approaches its melting point .

1.1 INSTABILITY-BASED THEORIES OF MELTING

The solid to liquid transition is one of the most common phenomena known to man , and yet, despite the large number and wide range of ideas that have been put forward, there is still no general understanding of the melting process .

Historically there have been two basic approaches to melting . The 'puritan' line emphasises the first order character of the transition and the fact that the free energies of both phases must be equal as melting occurs (see fig i) . Great importance is put upon gaining knowledge of the structure of solid and liquid either side of the transition , and , since structures of solids are relatively well known , this sort of approach generally relies on improved understanding of the structure of liquids .

The other approach is to consider that the nature of melting may be better examined by carefully studying the properties of solids as they near the transition . Part of the evidence used to support this type of theory is that , although you can get supercooled liquids , superheating of solids is very rare , suggesting perhaps that melting occurs at , or very near , an intrinsic stability limit of the solid . It is however recognised that to form any complete theory solid and liquid phases must be treated on an equal basis .

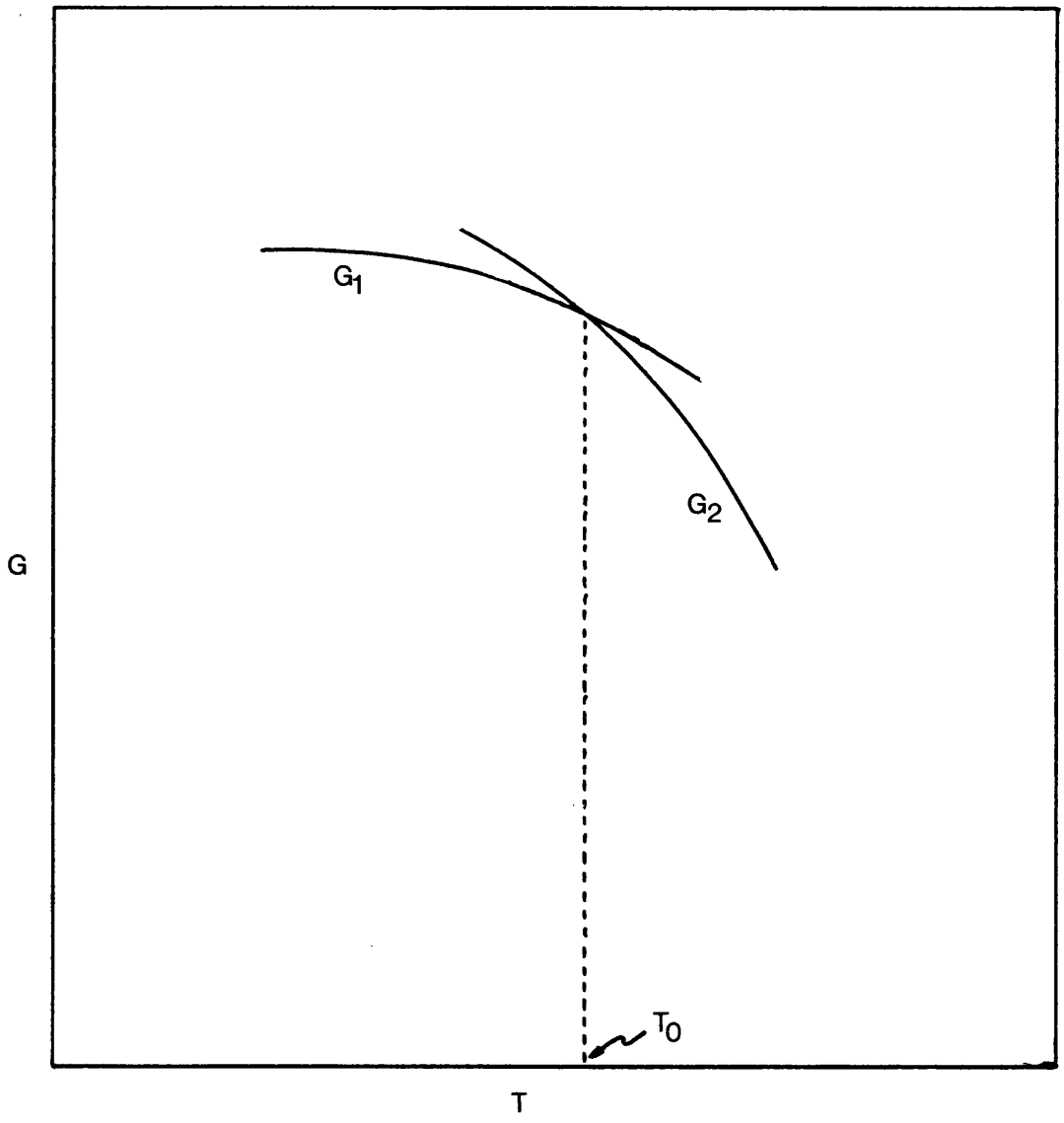

Figure i. Illustration of purely first order transition: sketch of the Gibbs free energies of phases G_1 and G_2 as a function of temperature.

This general sort of introduction may be found at the beginning of a number of papers on melting (e.g. Coterill and Madsen [1982] , Tallon [1982] , Boyer [1985]) . Here we shall go on to consider some of the instability-based theories that have been proposed in the past .

One of the simplest approaches to the problem was put forward as a theory by Lindemann [1910] . He considered a crystal as a group of independent oscillators and proposed that melting occured when the amplitude of oscillation became comparable with interatomic nearest neighbour distances . The theory has been relatively successful in that it is easy to apply and the Lindemann constant that it generates does show some agreement between crystals of similar materials . The Lindemann constant also provides a characteristic parameter that is useful when comparing the behaviour of different materials . Even now the Lindemann melting criterion still forms the basis for a number of theories of melting (Ruffa [1981], Moleko and Glyde [1982], Vaidya [1985]) .

About twenty five years after Lindemann's work Herzfeld and Goeppert Mayer [1934] did a theoretical study of the equation of state for solids which suggested that melting could be caused by a thermodynamic instability of the solid in which the isothermal compressibilty diverges at the melting point . Further work along these lines was done by Kane [1939] , but around this time Born [1939] put forward an attractive theory suggesting that melting

could be caused by the vanishing of one of the shear elastic moduli . This neatly fitted in with the fact that a solid has elastic resistance to shearing stress while a liquid does not , and the theory gained wide acceptance . The theory was only rejected by most workers when experimental results failed to find any vanishing shear mode constant at melting (Hunter and Siegel [1942] , Enck [1960]) .

More recently , however , there has been increased interest in Born's melting criterion . Jackson and Leiberman [1974] find a clear correlation between the Born instability temperature and the melting temperatures of alkali halides . Tallon , Robinson and Smedley [1977] and Tallon [1979] show that , as a function of volume , the shear modulus extrapolates approximately to zero at the volume of the liquid . Tallon [1980a , 1980b and 1982] and Tallon and Robinson [1982] go on to explain that the communal entropy of the liquid lowers the free energy from what it would be in the solid , and that it is this that causes melting to occur before the shear modulus vanishes .

Boyer [1985] has recently done some work to try and show that Born's idea and the Herzfeld and Goeppert Mayer theory are quite closely connected and that the linking of these ideas leads on to a more comprehensive explanation of the melting process . Another approach (Ruffa [1982]) emphasized the approximate validity of the Born criterion

when elastic constants are extrapolated to the liquid volume . Ruffa developed the concept of 'thermal potential' based on a representation of the of the solid in terms of Morse potentials , the parameters of which are chosen to characterize both thermal expansion and elastic properties . He was then able to relate the 'heat content' of the system , including the volume- and communal-entropy contributions to the latent heat , to the dissociation energy of the Morse potential .

There have been many other studies of intrinsic instability limits of the solid and their possible relation to melting : there has even been an attempt to relate fusion to an instability of the liquid (Newman [1980]) . Nardi and Percus [1967] proposed an instability involving 'pair exchange' energy in relation to melting in rare gas solids . They found a large ratio of pair exchange energy to kinetic energy and suggest that order-disorder considerations are more important in the melting process than energetics . Ida developed a melting theory based on the critical behaviour of 'vibrational elongation' (Ida [1969] and [1970]) .

A number of authors (Choquard [1967], Plakida and Siklos [1978], Moleko and Glyde [1983], Pershin and Pershin [1982]) have investigated the limits of stability of solids as a part of the general problem of treating anharmonicity in crystals , and all of them employ some form of selfconsistent phonon theory . One thing revealed

by these studies is that the maximum temperature for crystal stability can vary enormously depending on the level of sophistication of the theory (Moleko and Glyde [1983], Zubov [1978]) .

In recent years many researchers have turned their attention to the roles that defects and surfaces play in melting . This sort of approach can be thought of as a kind of instability theory where the instability is presumed to be directly related to the production of intrinsic defects in the crystal structure . There is a large amount of literature covering this sort of work and many of the proposed theories have been reviewed by Cotterill [1980] and Ubbelohde [1978] .

In the present study we investigate a melting curve equation based on a relation proposed by Kraut and Kennedy [1966] and modified using a reformulation of the Lindemann melting law (Gilvarry [1966], Vaidya and Raja Gopal [1966], see section 5.6). The linear relation has been shown to provide a good description of the pressure dependence of the melting temperature of a number of metals at low pressures ($P < 5$ GPa , Vaidya and Raja Gopal [1966]) , but fails to provide a good basis for extrapolation to higher pressures . The data measured here , for the pressure derivatives of SOECs and Grüneisen parameters for indium at temperatures near the melting point , will be used to test the equation to high pressure.

SOUND WAVES THROUGH SOLIDS

SOUND WAVES THROUGH SOLIDS

2.1 INTRODUCTION

Briefly described in this section are some of the relationships between a material's elastic properties, and it's ultrasonic wave propagation velocities. Included here are all the equations needed to calculate second order elastic constants, pressure derivatives, and Gruneisen parameters, from measured ultrasonic data for FCT indium. For further information look at Nye [1960], Pollard [1977], Dieulesaint and Royer [1980], Beyer and Letcher [1969].

The elastic waves propagated through samples for this study were of low amplitude and had wavelengths of a few hundred μm. The strains encountered in propagating media under these conditions are small, and classical linear elasticity theory may be applied.

2.2 ELASTIC STIFFNESS CONSTANTS

When an ultrasonic wave propagates in a crystal it disturbs the particles of the medium from their equilibrium positions. Internal restoring forces and particle inertia cause vibrations of the medium which lead to elastic wave propagation. This excitation of elastic waves has the same effect as if the crystal were being acted upon by external forces, with each part of the crystal exerting a force on its neighbouring parts. Effectively the crystal is in a state of stress.

Using a generalised Hooke's law for a perfectly elastic body, each component of stress applied is

linearly related to each component of the resultant strain. As stress and strain both have six independent components there will be, for the most anisotropic body with no symmetry elements, a set of six equations each with six terms (ie. a total of 36 coefficients). These equations may be written concisely using tensor notation (repeated suffices denoting summation):

$$T_{ij} = C_{ijkl} S_{kl}$$

where T_{ij} and S_{kl} represent second rank stress and strain tensors respectively, and C_{ijkl} is a fourth rank elastic stiffness tensor. In the most general case C_{ijkl} has 81 components, but T_{ij} and S_{kl} are both symmetric tensors, so;

$$C_{ijkl} = C_{jikl}$$

and $$C_{ijkl} = C_{ijlk}$$

This reduces the number of independent constants to 36 (as mentioned above). This number is reduced still further by taking into account thermodynamic considerations which show that the elastic constant tensor is also symmetric. This leaves 21 independent constants for the most general anisotropic body. Further simplification is only possible by considering the symmetry of the material under study. Voigt's principle states that for a crystal the symmetry of the physical process is superimposed on the symmetry of the crystal.

Indium itself has a face centred tetragonal (FCT)

structure (TI, 4/mmm). The symmetry elements of this structure further reduce the number of independent constants down to just 6. These are (in matrix notation);

$$C_{11} = C_{22} \; ; \; C_{12} \; ; \; C_{13} = C_{23} \; ;$$
$$C_{33} \; ; \; C_{44} = C_{55} \; ; \; C_{66}$$

all other constants are zero.

where C_{11} etc. are components in a second order elastic constant matrix: each of the two numbers in the suffix representing a pair of numbers according to the following rules:

$$1 - 11 \; ; \; 2 - 22 \; ; \; 3 - 33 \; ;$$
$$4 - 23=32 \; ; \; 5 - 31=13 \; ; \; 6 - 21=12$$

The second order elastic constant matrix for indium is then written;

$$\begin{pmatrix} C_{11} & C_{12} & C_{13} & 0 & 0 & 0 \\ C_{12} & C_{11} & C_{13} & 0 & 0 & 0 \\ C_{13} & C_{13} & C_{33} & 0 & 0 & 0 \\ 0 & 0 & 0 & C_{44} & 0 & 0 \\ 0 & 0 & 0 & 0 & C_{44} & 0 \\ 0 & 0 & 0 & 0 & 0 & C_{66} \end{pmatrix}$$

2.3 ELASTIC WAVE PROPAGATION IN A CRYSTALLINE SOLID

The force exerted on any element of a solid is the gradient of the stress acting on that element. This leads to a form of Newton's law for an anisotropic body which is written (reverting to expanded suffix notation),

$$\frac{\delta T_{ij}}{\delta x_i} = \rho \ddot{u}_i \qquad (2.2)$$

where ρ = volume density and u_i = displacement vector

The equation of wave motion for an anisotropic elastic body can now be found by combining Newton's law (2.2) with Hooke's law (2.1) giving;

$$\rho \ddot{u}_i = C_{ijkl} \delta_j S_{kl} \qquad (2.3)$$

where $\delta_j = \delta / \delta x_j$

Now strain may be defined by the equation ;

$$S_{kl} = 0.5(\delta_l u_k + \delta_k u_l) \qquad (2.4)$$

which when sustituted into equation (2.3) gives;

$$\rho \ddot{u}_i = C_{ijkl} (\delta_j \delta_l u_k + \delta_j \delta_k u_l)/2 \qquad (2.5)$$

But the elastic stiffness tensor is symmetric so we may interchange l and k allowing us to rewrite equation (2.5) as;

$$\rho \ddot{u}_i = C_{ijkl} \delta_i \delta_k u_l \qquad (2.6)$$

Now if we assume plane harmonic travelling waves of the form;

$$u_i = A_i \exp[i(n_j x_j - \omega t)] \qquad (2.7)$$

where A_i are displacement component amplitudes, and n_j are wave vector components, then by substituting (2.7) into (2.6) we get;

$$\rho\omega^2 u_i = C_{ijkl} n_j n_k u_l \qquad (2.8)$$

This can be put in a more homogeneous form by putting $u_i = u_l\delta_{il}$, where δ_{il} is the unit tensor, ie;

$$(\rho\omega^2 \delta_{il} - C_{ijkl} n_j n_k) u_l = 0 \qquad (2.9)$$

This equation was developed by Christoffel (1877). It represents a set of three homogeneous equations of the first degree with u_1, u_2, and u_3 as unknowns. They have non-zero solutions only if the determinant of the coefficients is zero, ie;

$$\left| C_{ijkl} n_j n_k - \rho\omega^2 \delta_{il} \right| = 0 \qquad (2.10)$$

Evaluation of (2.10) leads to a cubic equation in w, leading to three different velocities of propagation. So it is possible to calculate elastic constants knowing the various mode wave velocities. In general these modes will not be pure longitudinal or pure transverse, but

will be of some mixed type. However in certain crystallographic directions (called pure mode directions) it is possible to propagate one pure longitudinal, and two pure shear waves. For a cubic crystal these directions are [100], [110], and [111], but in crystals of lower symmetry it is necessary to propagate quasi-pure modes to obtain all the elastic constants. These are modes where the energy flux vector of the waves is not perpendicular to the plane wave fronts. Brugger (1965) evaluated the determinant (2.10) to give the expressions linking wave velocities with C_{ijkl}'s for various propagation directions in different crystal classes. The expressions for FCT indium are given in table 2.1.

TABLE 2.1 Relationships between propagation velocities and SOECs for various modes in indium.

Propagation direction	Polarisation direction	ρV^2
[100]	[100]	C_{11}
[100]	[010]	C_{66}
[100]	[001]	C_{44}
[001]	[001]	C_{33}
[001]	x-y plane	C_{44}
[110]	[110]	$C_{66} + (C_{11} - C_{12})/2$
[110]	$[1\bar{1}0]$	$(C_{11} - C_{12})/2$
[110]	[001]	C_{44}
[011]	[100]	$(C_{44} + C_{66})/2$
[011]	φ	$[A + (A^2 - B + C^2)^{0.5}]/2$
[011]	$\varphi+\pi/2$	$[A - (A^2 - B + C^2)^{0.5}]/2$

where; $A = C_{44} + (C_{11} + C_{33})/2$; $B = (C_{11} + C_{44})(C_{33} + C_{44})$; $C = C_{13} + C_{44}$; φ is measured from [001] in the (100) plane and depends on elastic constant values.

2.4 PRESSURE DERIVATIVES OF ELASTIC CONSTANTS

When evaluating the stress derivatives of the second order elastic constants, it must be remembered that the density and thickness of the sample are dependent upon the state of strain of the material. Therefore, for accurate results, the changes in the physical dimensions of the sample with stress must be taken into account.

Thurston [1965] gives an equation for the initial pressure derivative of the mode elastic constant, $(\rho V^2)'$;

$$(\rho V^2)'_{P=0} = (\rho W^2)'_{P=0} + \rho_0 V_0^2 (\chi^T - 2N_k N_m S^T_{kmii})_{P=0} \qquad (2.12)$$

where W, called the "natural" velocity, is defined as the path length at zero pressure divided by the transit time at pressure P. The quantity in final parentheses on the right hand side of the equation is the volume compressibility minus twice the linear compressibility in the direction $\underline{N}$. These terms are effectively corrections for the changes in density and path length due to pressure. The first term on the right hand side may be evaluated from measured data using the relation;

$$(\rho_0 W^2)'_{P=0} = 2\rho_0 V_0^2 f'/f_0 \qquad (2.13)$$

where V_0 and f_0 are the wave velocity and pulse-echo frequency at atmospheric pressure, and f' is the

gradient of the frequency-pressure response.

For a tetragonal crystal structure the volume compressibility is given by;

$$\chi^{T} = 2S_{11} + S_{33} + 2(S_{12} + 2S_{13}) \qquad (2.14)$$

and linear compressibility is given by;

$$S_{km_{ij}} l_i l_j = (S_{11} + S_{12} + S_{13}) - (S_{11} + S_{12} - S_{13} - S_{33}) l_3^2 \qquad (2.15)$$

where S_{11} etc. are the components of the second order compliance matrix, ie the inverse of the SOEC matrix.

2.5 Gruneisen Parameter

It was Gruneisen [1908] who discovered that a material's thermal expansion coefficient, α, could be related to it's specific heat, Cv, by the empirical relation;

$$\alpha/Cv = \text{constant} \qquad (2.16)$$

Later this was developed into the Gruneisen relation;

$$\gamma^{th} = \beta V_0 K^T / Cv \qquad (2.17)$$

where β is the volume coefficient of thermal expansion; V_0 is the molar volume, K^T is the isothermal bulk modulus, and γ^{th} is a dimensionless number called the Gruneisen constant, or thermal Gruneisen parameter.

Gruneisen also calculated γ^{th} for a range of materials from known thermal expansion data, and found that γ^{th} was usually of the order of 2 and virtually independent of temperature. Since then, evaluation of γ^{th} has provided a useful tool for the investigation of anharmonic effects such as thermal expansion, phonon-phonon interactions, thermal conductivity, and non-linear phenomenon.

On a microscopic scale γ^{th} is a measure of the fractional change of a vibrational frequency of a lattice with a fractional change in volume:

$$\gamma^{th} = -V\Delta\nu/\nu\Delta V \qquad (2.18)$$

This may be written as a weighted average of individual mode Gruneisen parameters, γ_i, where γ_i represents the

fractional change in frequency with volume for the i'th vibrational mode.

Hence;

$$\gamma^{th} = \sum_i \gamma_i C_i / C_v \qquad (2.19)$$

where C_i is the Einstein specific heat of the i'th vibrational mode, and

$$\gamma_i = -d\ln\nu_i / d\ln V \qquad (2.20)$$

The weighting factor in the above equation is essentially a measure of the degree of excitation of each vibrational mode.

At high temperatures, ie $T>>\Theta_D$ (the Debye temperature), all the normal modes will contribute equally to the specific heat and so γ^{th} is given by a summation over all the phonon modes. For elastic waves the wavelength is so long that the elastic continuum model can be used to obtain the acoustic mode Gruneisen parameters γ^{el}. In the long wavelength limit (at the centre of the Brillouin zone) the frequency, ν_i, is given by;

$$\nu_i = v_i \underline{q} \qquad (2.21)$$

where v_i is the velocity of the elastic wave propagating with wavevector $\underline{q}$. Hence the acoustic mode Gruneisen parameters may be calculated from the volume dependence of the acoustic wave velocities, which are in turn obtained from the pressure derivatives of the second order elastic constants.

Brugger [1965] gives the general relationship

expressing the isothermal acoustic mode Gruneisen parameter, $\gamma_p^T(\underline{N})$ (with unit vector in propagation direction $\underline{N}$, and polarisation index p (=1,2,3)), in terms of the second and third order elastic constants:

$$\gamma_p^T(\underline{N}) = -(2\chi^T\omega_p(\underline{N}))^{-1}[1 + S^T_{aajk}(2\omega_p'(\underline{N})U_jU_k + C_{jkmunv}N_mN_nU_uU_v)] \quad (2.22)$$

where $\underline{U}$ is a unit vector along the polarisation direction, S_{aajk} are second order compliances (obtained from inverse of second order elastic constant matrix), and C_{jlmunv} are third order elastic constants.

From this general expression Tu Hailing et al [1982] developed the form specialised to tetragonal crystals belonging to the 4/mmm (TI) Laue group:

$$\begin{aligned}\gamma_p^T(N) =& -(2\omega\chi^T)^{-1}\{1 + 2\omega[(S_{11}^T + S_{12}^T + S_{13}^T)(U_1^2 \\ &+ U_2^2) + (2S_{13}^T + S_{33}^T)U_3^2] + [(C_{111} + C_{112})(S_{11}^T \\ &+ S_{12}^T + S_{13}^T) + C_{113}(2S_{13}^T + S_{33}^T)](N_1^2U_1^2 \\ &+ N_2^2U_2^2) + 2[2C_{112}(S_{11}^T + S_{12}^T + S_{13}^T) \\ &+ C_{123}(2S_{13}^T + S_{33}^T)](N_1N_2U_1U_2) + 2[(C_{113} \\ &+ C_{123})(S_{11}^T + S_{12}^T + S_{13}^T) + C_{133}(2S_{12}^T \\ &+ S_{33}^T)](N_1N_3U_1U_3 + N_2N_3U_2U_3) \\ &+ [2C_{133}(S_{11}^T + S_{12}^T + S_{13}^T) + C_{333}(2S_{13}^T \\ &+ S_{13}^T)]N_3^2U_3^2 + [(C_{144} + C_{155})(S_{11}^T + S_{12}^T \\ &+ S_{13}^T) + C_{344}(2S_{13}^T + S_{33}^T)][N_1U_3 + N_3U_1)^2 \\ &+ (N_2U_3 + N_3U_2)^2] + [2C_{166}(S_{11}^T + S_{12}^T + S_{13}^T) \\ &+ C_{366}(2S_{13}^T + S_{33}^T)](N_1U_2 + N_2U_1)^2\} \quad (2.23)\end{aligned}$$

where C_{ijk} are third order elastic constants, S_{ij} are elastic compliances, $\underline{N}$ and $\underline{U}$ are propagation and polarisation vectors, χ^T is the isothermal compressibility ($= 2(S_{11}^T + S_{12}^T + S_{13}^T) + (2S_{13}^T + S_{33}^T)$), and

$$\omega = C_{11}(N_1^2U_1^2 + N_2^2U_2^2) + 2C_{12}N_1N_2U_1U_2 + 2C_{13}(N_1N_3U_1U_3 + N_2N_3U_2U_3) + C_{33}N_3^2U_3^2 + C_{44}((N_1U_3 + N_3U_1)^2 + (N_2U_3 + N_3U_2)^2) + C_{66}(N_1U_2 + N_2U_1)^2$$

This expression shows that to calculate the Gruneisen parameter values of second and third order elastic constants must be available. This normally requires that measurements of the change in ultrasonic mode velocities with both hydrostatic and uniaxial pressure must be made. Fortunately however, under hydrostatic pressure each vibrational mode is affected by a certain set of combined third order constants which can be related to the pressure derivatives of the thermodynamic elastic constants (Thurston et al [1966]). The relations between the pressure derivatives of the SOEC's and those of the thermodynamic elastic constants are listed for most crystal symmetries by Tu Hailing [1983] and are shown for indium in table 2.2. So by substituting thermodynamic pressure derivatives for products of compliances and combinations of third order elastic constants, the mode Gruneisen parameter may be calculated using the equation (Tu Hailing et al [1982])

Table 2.2

Relationships between pressure derivatives of thermodynamic elastic constants and the pressure derivatives of SOEC.

$$B_{11} = \delta C_{11}/\delta P + 1 - (S_2 + S_3 - 3S_1)C_{11}$$

$$B_{12} = \delta C_{12}/\delta P - 1 - (S_3 - S_1 - S_2)C_{12}$$

$$B_{13} = \delta C_{13}/\delta P - 1 - (S_2 - S_1 - S_3)C_{13}$$

$$B_{33} = \delta C_{33}/\delta P + 1 - (S_1 + S_2 - 3S_3)C_{33}$$

$$B_{44} = \delta C_{44}/\delta P + 1 - (S_1 - S_2 - S_3)C_{44}$$

$$B_{66} = \delta C_{66}/\delta P + 1 - (S_3 - S_1 - S_2)C_{66}$$

$$S_1 = S_2 = S_{11} + S_{12} + S_{13}$$

$$S_3 = 2S_{13} + S_{33}$$

where B_{ij} are the pressure derivatives of the thermodynamic second order elastic constants.

$$\gamma_p^{\tau}(\underline{N}) = -(2\omega\chi^{\tau})^{-1}\{1 + 2\omega(S_{11}^{\tau} + S_{12}^{\tau} + S_{13}^{\tau})(U_1^2 + U_2^2) + (2S_{13}^{\tau} + S_{33}^{\tau})U_3^2$$

$$- B_{11}(N_1^2U_1^2 + N_2^2U_2^2) - 2B_{12}N_1N_2U_1U_2 - 2B_{13}(N_1N_3U_1U_3 + N_2N_3U_2U_3)$$

$$- B_{33}N_3^2U_3^2 - B_{44}(N_1U_3 + N_3U_1)^2 + (N_2U_3 + N_3U_2)^2$$

$$- B_{66}(N_1U_2 + N_2U_1)^2\} \qquad (2.24)$$

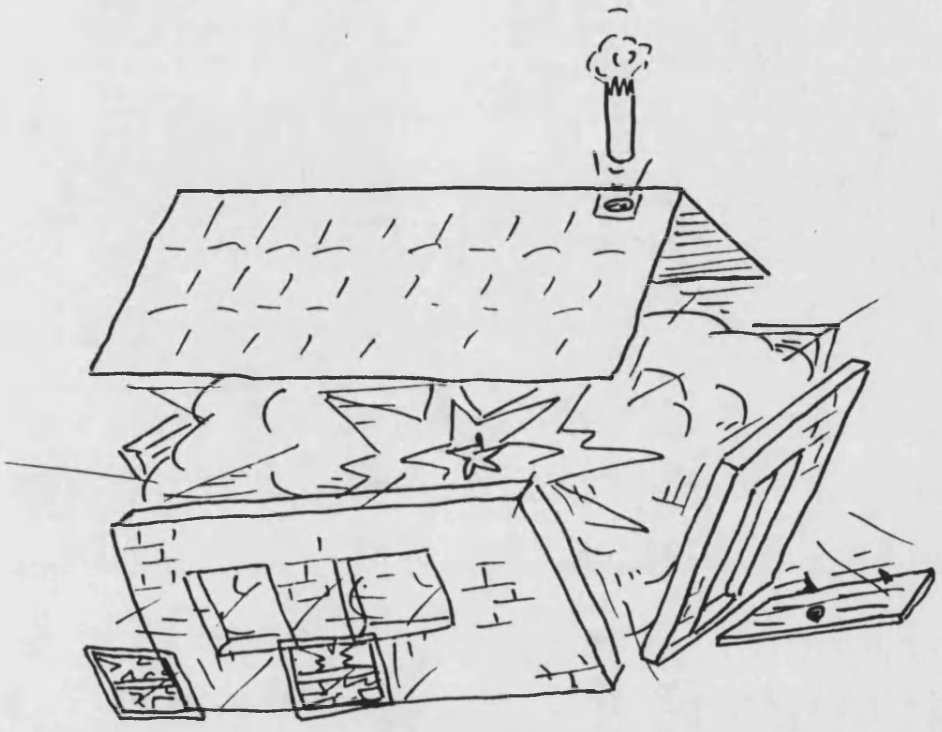

EXPERIMENTAL TECHNIQUES

EXPERIMENTAL TECHNIQUES.

3.1 CRYSTAL GROWTH.

3.1.1 INTRODUCTION

The study of anisotropic elastic properties of solids, by ultrasonic methods, requires large homogeneous single crystal samples. The specimens must be prepared correctly with flat parallel sides, cut perpendicularly to a desired crystallographic axis.

The crystals used for this study were grown by a horizontal zone melting method, then orientated using X-ray photography, and cut and polished by spark erosion.

3.1.2 ZONE MELTING

Zone melting is the term given to a family of techniques, that have in common the passage of a narrow molten zone through a long solid rod. Zone refining is used for the purification of elements or compounds, and other zone melting methods may be used to concentrate impurities, study phase diagrams, or produce crystals with a uniform distribution of impurity (zone levelling).

Previous studies on indium alloyed with cadmium, and thallium (Gunton [1973], Madhava [1977], Brassington [1982]) were made with samples prepared using a horizontal zone levelling technique. Similar methods, and much of the same equipment, have been used to prepare indium samples for the present study.

3.1.3 ZONE REFINING

The theory of zone refining is now well known (Pfann [1958]), so only a brief qualitative description need be given here.

To zone refine a specimen a molten zone must be repeatedly passed through the sample, always in the same direction. Impurities within the material will tend to travel with, or against, the zone depending on whether they lower, or raise, the melting point of the charge substance, respectively. Therefore the impurities will become concentrated at the ends of the sample, thus purifying the remainder.

The number of passes required to purify a sample will depend on the value of the distribution coefficient K, defined as the ratio of the concentration of solute in the solid to the concentration of solute in the liquid. If $K<1$ or $K>1$ then impurities will be carried to one end or the other. If $K=1$, no purification is possible.

If, say, $K<1$ then passing a zone through an ingot should produce a solute distribution as shown in Fig.3.1, where

C_o = mean impurity concentration in the original liquid,

L = length of zone.

This distribution curve has three distinct regions:

(i) Initial region: When the zone, at full length, is at the beginning of the charge, its concentration is

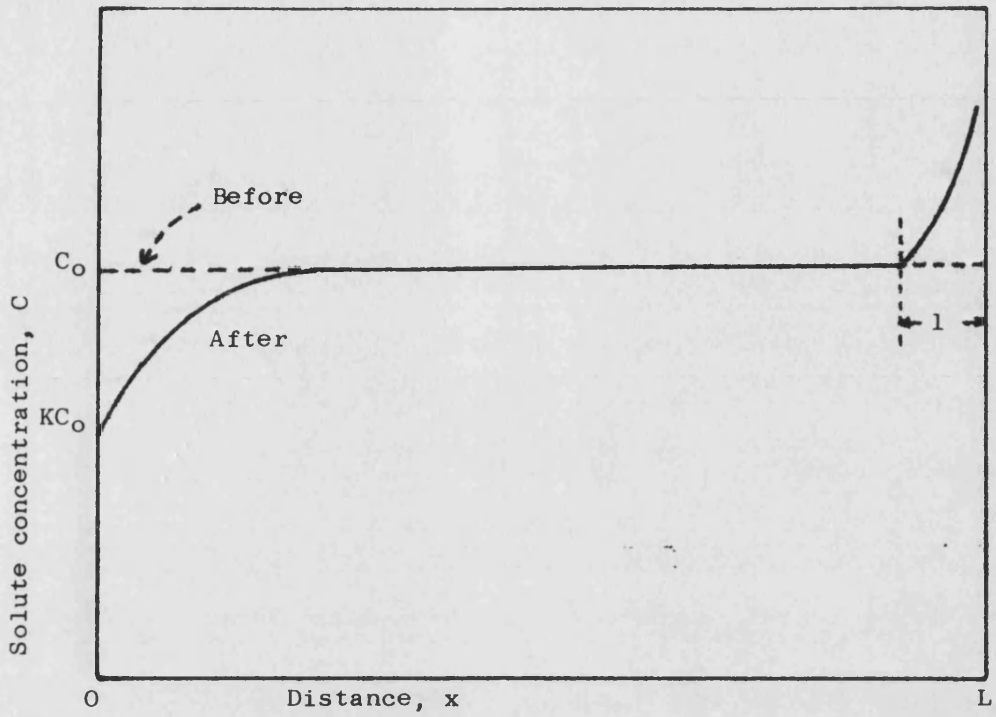

Fig 3.1 Plot of solute distribution on completion of a single pass of a molten zone.

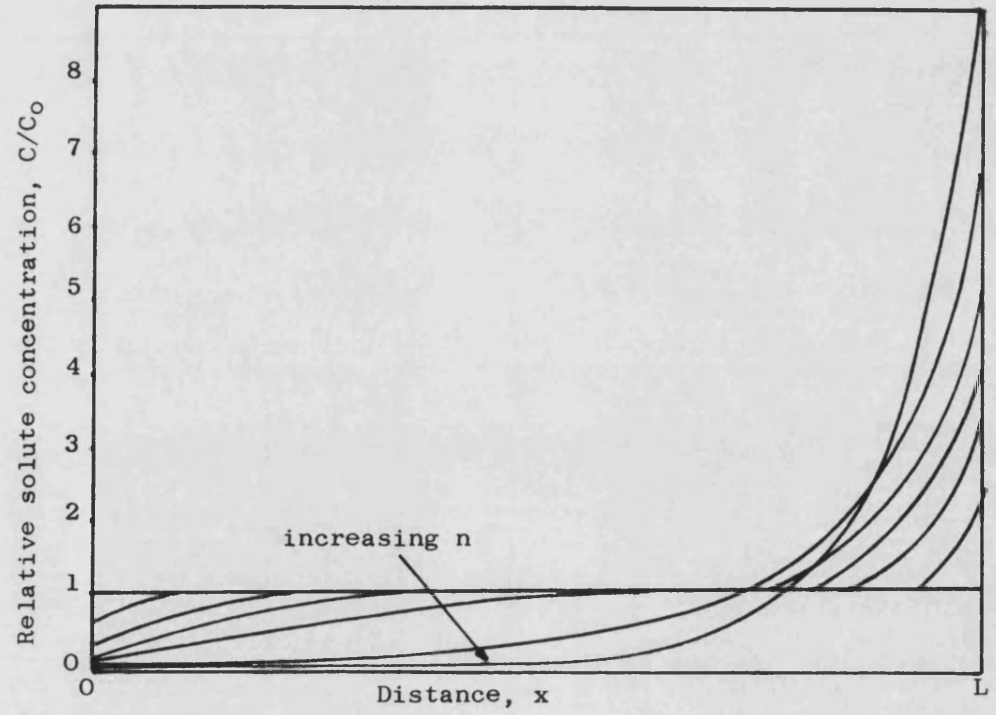

Fig 3.2 Plot of relative solute distribution against number of passes, n.

that of the melted material, C_o. As the zone advances a short distance it freezes out a layer of solid with a solute concentration of KC_o, and takes in a layer with a concentration of C_o. So the zone is enriched and subsequently freezes out material of higher solute concentration.

This is a purification region.

(ii) Level Region: As the zone progresses, enrichment will continue at a decreasing rate until the solute concentration attains the value C_o/K. From this point the concentrations in the material entering and leaving the zone are equal, and the concentration in the freezing solid remains constant (at C_o) until the zone reaches the end of the ingot.

This is a zone levelling region.

(iii) Final region: When the zone reaches the end, further movement of the heater decreases the length of the zone, causing the solute concentration to rise.

This is a normal freezing region.

Further passes of the zone will tend to leave behind a lower and somewhat longer initial region, and a higher somewhat longer, final region, decreasing the length of the intermediate level region. Ultimately the three portions blend into a smooth curve (Fig.3.2).

3.1.4 HORIZONTAL ZONE LEVELLER

The horizontal zone leveller used to grow crystals for this work is illustrated in Fig.3.3. Details of its construction are given by Gunton [1973] and Madhava [1977] and are described briefly below.

The apparatus consisted of a horizontal travelling furnace capable of uniform motion along the length of a charge, which was contained in a pyrex boat, inside an evacuated glass tube. The furnace assembly, mounted on an aluminium block, was drawn along two guide rods by a lead-screw driven by an electric motor. The traverse speed could be varied by changing the gears coupling the motor to the lead-screw. Water cooled coils either side of the furnace helped increase the temperature gradients at the zone edges (thus keeping the zone as small as possible). The whole apparatus was suspended on shock-cord to damp out mechanical vibration, and completely enclosed in a wooden box to maintain a constant (thermostatically controlled) temperature environment. Also safety cut-outs were used to ensure that the system did not overheat.

3.1.5 CRYSTAL GROWTH BOATS

The pyrex glass 'boats', used to contain the indium charges, are illustrated in Fig.3.4. They were made by melting sheet pyrex down onto a mould. The average capacity of each boat was about 13cm^3. They were

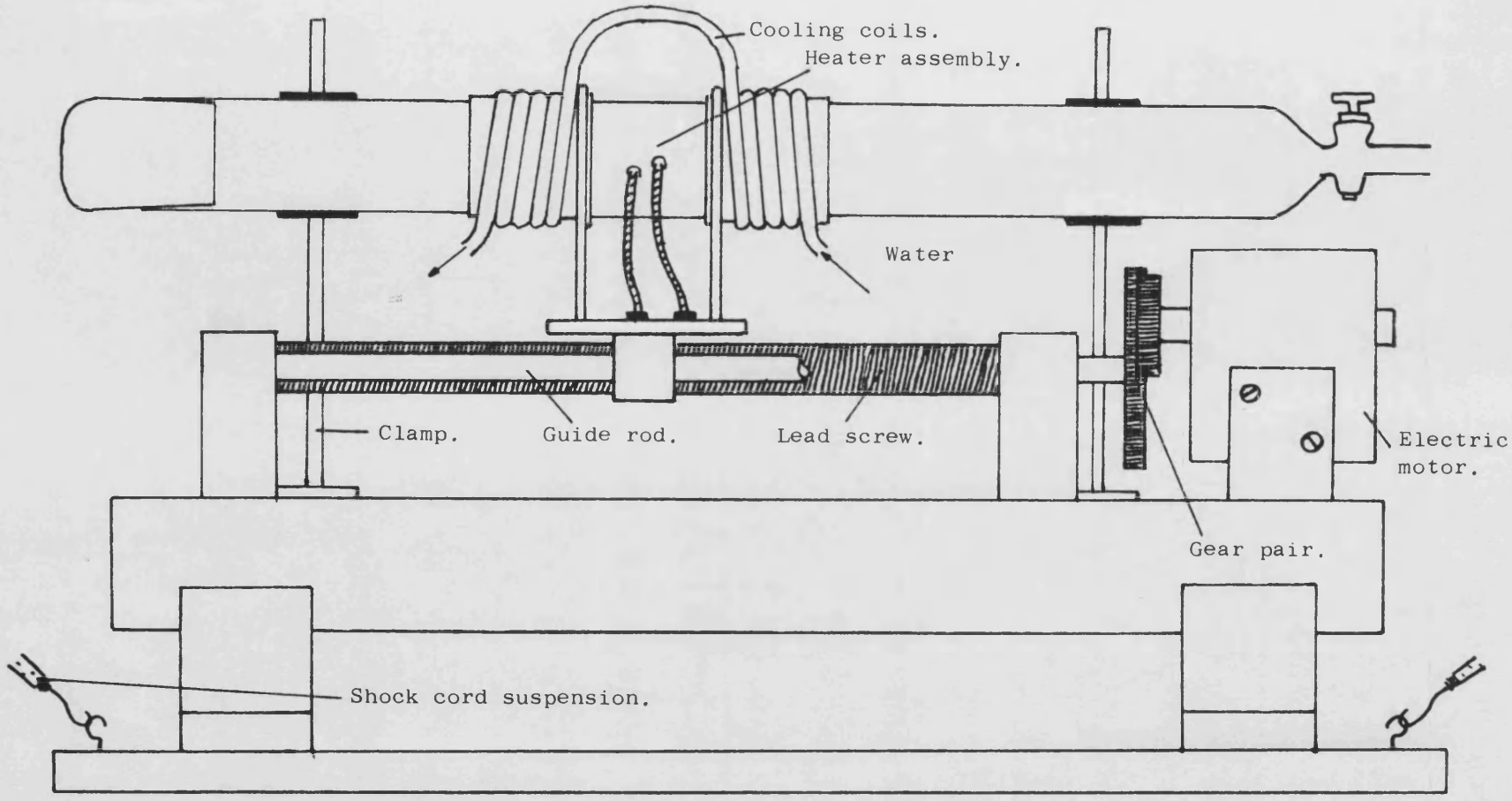

Fig 3.3 Diagram of horizontal zone leveller.

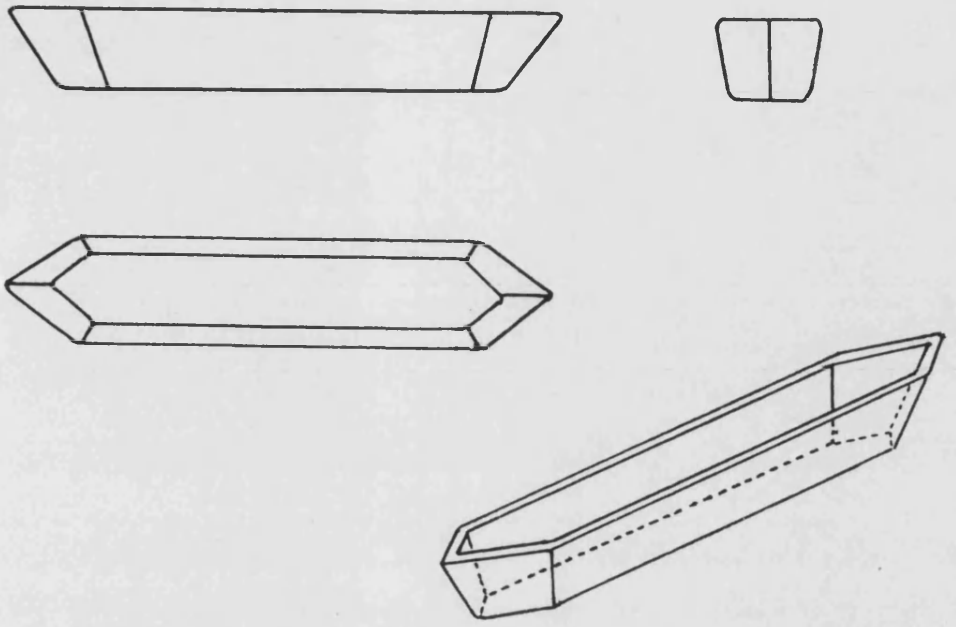

Fig 3.4 Diagram showing pyrex growth boats.
(approximately to scale)

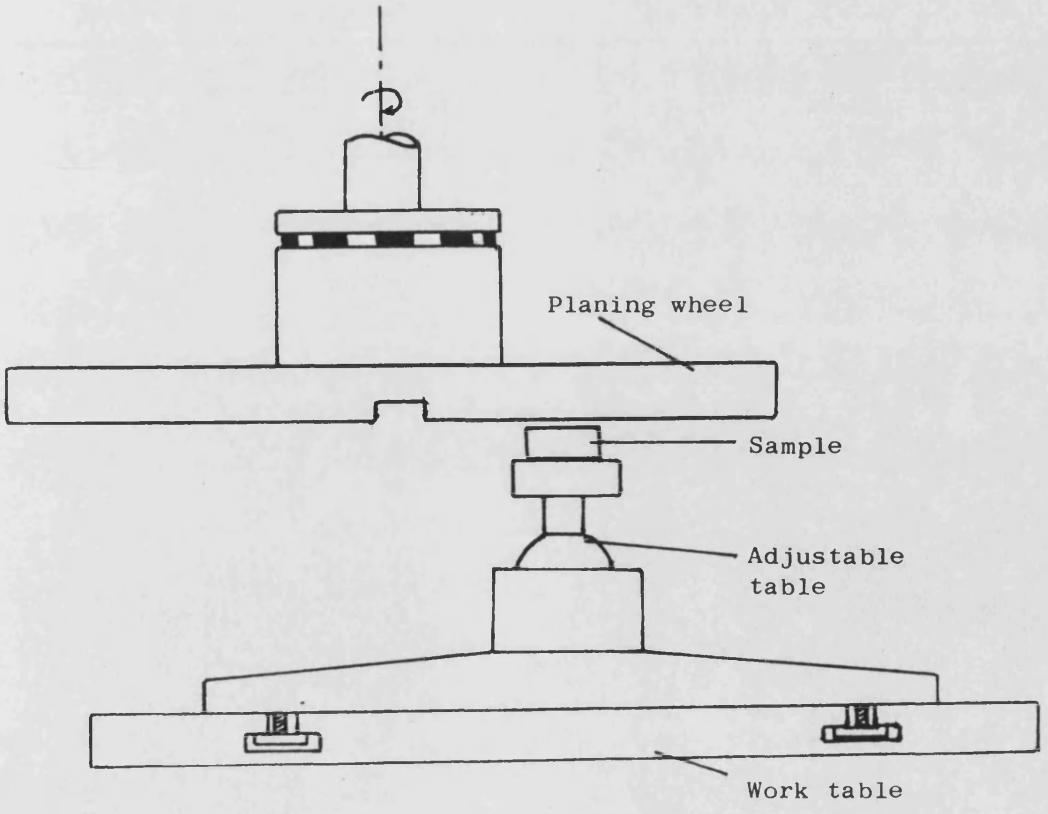

Fig 3.5 Diagram showing spark planing device.

designed with pointed ends to promote crystal growth by single grain selection, and their inner surfaces were sand-blasted to prevent the indium sticking to the glass.

3.1.6 CRYSTAL GROWTH PROCEDURE

Indium metal (99.999% pure) was cut up, cleaned in dilute nitric acid, and placed in a pyrex growth boat. The boat and its charge were then placed in an evacuated tube and the metal melted down into the boat using the zone leveller's heater. The metal was then allowed to refreeze. The zone refining process described previously was then employed, allowing the travelling furnace to traverse the sample a number of times, always in the same direction. Satisfactory results were obtained with a zone traverse speed of about 3mm/hr, and a molten zone of about one fifth the length of the ingot.

After some passes the ingot was removed and examined. Etching in dilute nitric acid made visible any grain boundaries in the sample. If grain boundaries were apparent, the ingot was replaced and a further zone pass was made. Generally about five or six passes were sufficient to produce a good crystal.

3.1.7 SAMPLE PREPARATION

The crystal samples were orientated (to an accuracy of 0.5°) using Laue X-ray back reflection photography. Figure 3.6 shows the patterns formed by the spots on the photographs when a crystal is aligned along one of its

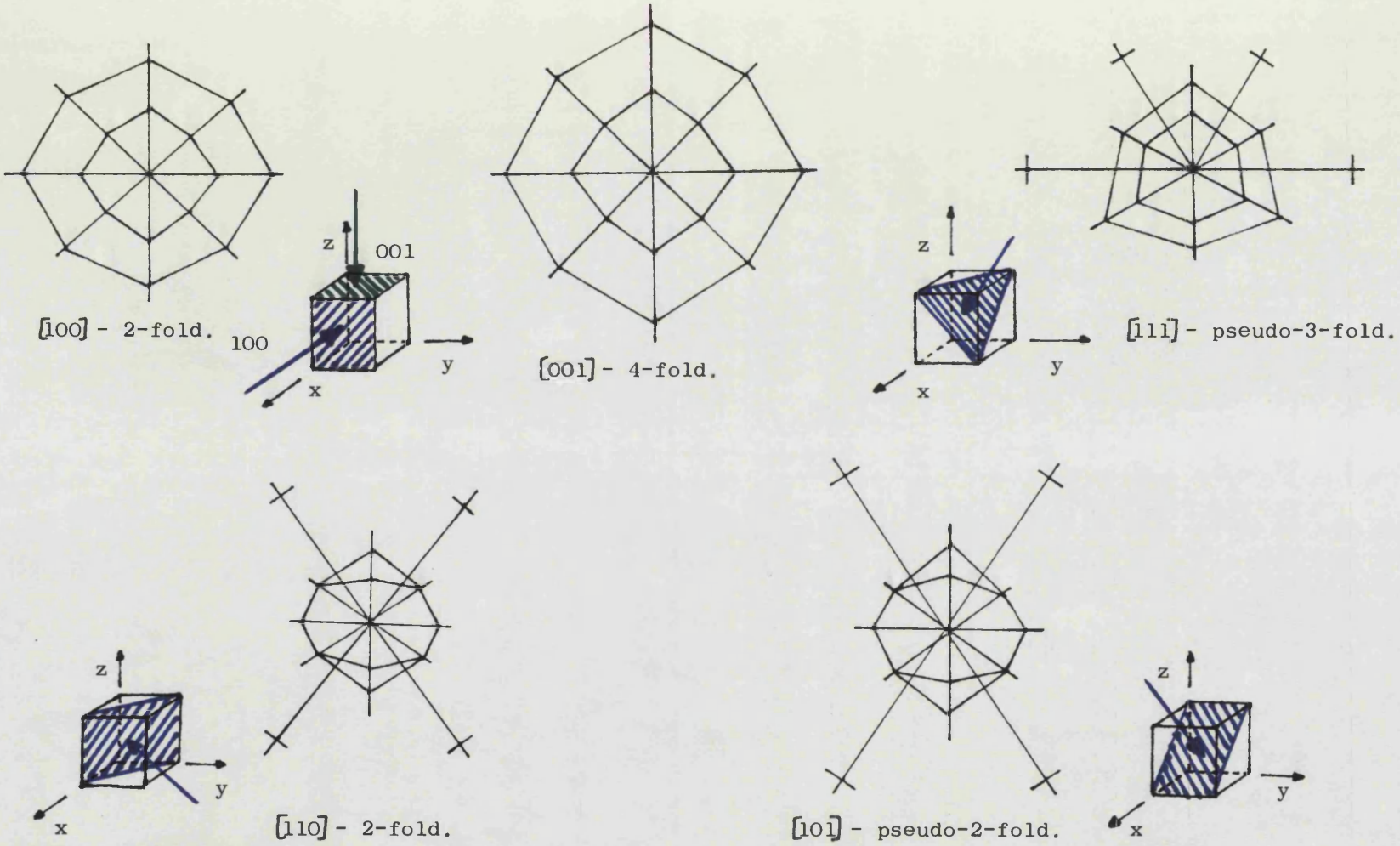

Fig 3.6 Diagram showing patterns obtained from Laue back reflection x-ray photographs, taken along various crystallographic directions in single crystal indium. Patterns are reduced to half scale from original spot patterns taken using sample-to-camera distance of 3cm.

major symmetry directions. These patterns enable one to differentiate between the two sets of 2-fold axes in the tetragonal structure (ie [100] and [110] types). The two directions may also be identified by their position relative to the psuedo-3-fold axis.

A three arc goniometer was used to align the desired crystallographic symmetry axis with the x-ray beam. The goniometer could then be transferred to a 'servomet' spark erosion machine where a spark slicing device was used to cut parallel faces perpendicular to the aligned symmetry axis. Cuts were made using 'Servomet' ranges 5 or 6 to ensure minimal surface damage. Further Laue exposures were then taken to check the orientation of the sample, which was held in a spring loaded goniometer that ensured the cut face was held perpendicular to the x-ray beam. Any small errors in alignment could then be corrected by spark planing (a sort of spark erosion polishing) with the crystal mounted on a movable table which had itself been planed (see Fig.3.5).

Samples with faces flat to surface irregularities of 2 or 3μm, and parallel to better than 10^{-3}rad were obtained using this method.

3.2 ULTRASONIC WAVE VELOCITY MEASUREMENT

3.2.1 INTRODUCTION

Mason and McSkimin [1947] and Arenberg [1950] were among the early developers of ultrasonic pulse-echo techniques, and since then many variations on the basic methods have been developed. The method used here has been an ultrasonic pulse-echo overlap technique (Papadakis [1967]) which is well suited to the measurement of stress derivatives of ultrasonic wave velocities in indium.

3.2.2 TRANSDUCERS

Pulses of ultrasound of 1to 2μsec duration were generated by applying a high voltage r.f. burst to a gold-plated piezoelectric quartz transducer. The transducers used had a fundamental frequency of 10MHz, corresponding to transducer thicknesses of 0.29mm and 0.19mm for longitudinal and transverse waves respectively. Higher frequencies would lead to increased attenuation in the indium due to frequency dependent loss mechanisms. At lower frequencies diffraction effects become more dominant.

Acoustic coupling was achieved using a suitable bonding material.'Dow' resin was used as the bond at room temperature, and ZGY couplant paste (Krautkramer GMBH Köln) was used for higher temperatures.

3.2.3 PULSE-ECHO OVERLAP

Pulses of ultrasound generated into a sample will be mostly reflected at sample faces due to a high acoustic impedance mismatch at the interface. When the reflected wave reaches the sample-transducer interface some of the acoustic energy from the ultrasound wave will be converted into electrical energy by the transducer. The initial pulse and the subsequent echo pulses, picked up by the transducer, can be displayed on an oscilloscope screen as an 'echo train' (see Fig.3.7).

The time interval (t) between successive echoes corresponds to the time taken for the ultrasound wave to cover a distance equal to twice the crystal thickness L. A rough estimate of this time can be obtained from the calibrated scale on the oscilloscope screen, and an approximate value for the wave velocity (v) may be calculated using:

$$v=2L/t$$

where L = crystal thickness and t = transit time

In the system used (see Fig.3.9) a high resolution frequency source triggered the oscilloscope at a frequency equal to the inverse of the measured transit time. This caused all the echoes to appear on the screen roughly superimposed on one another. A strobe device was then used to pick out just two successive echoes, which could be exactly overlapped (Fig.3.8) by fine adjustment

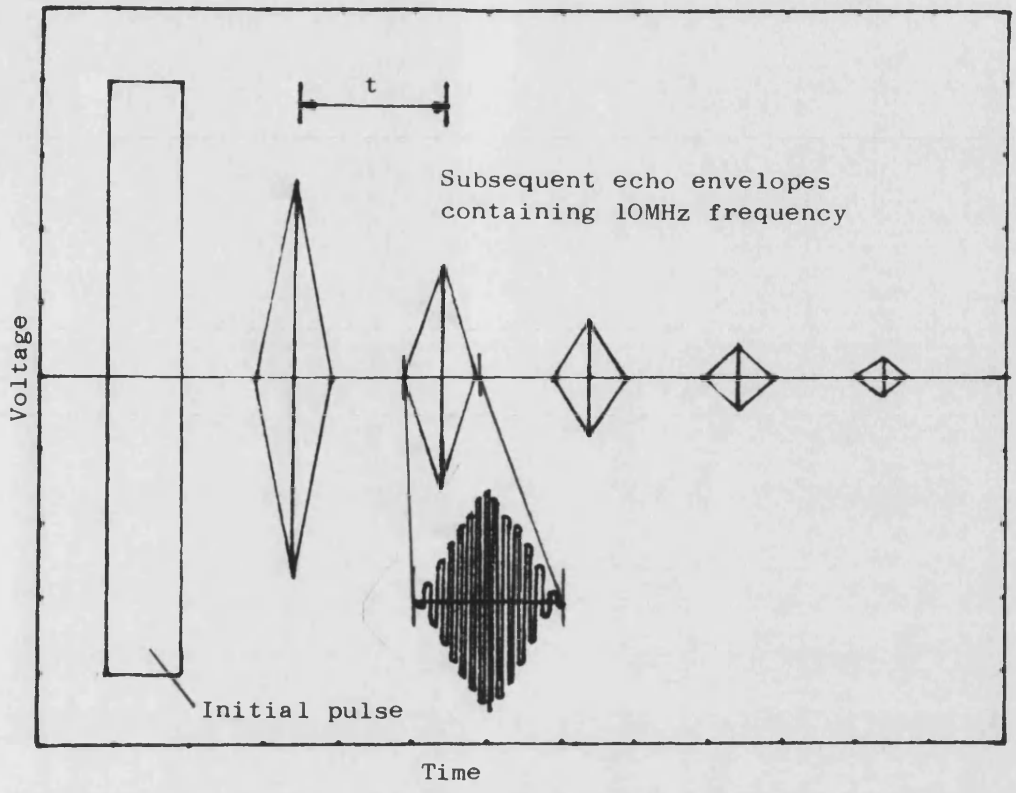

Fig. 3.7 Diagram showing oscilloscope display of ultrasonic echo train.

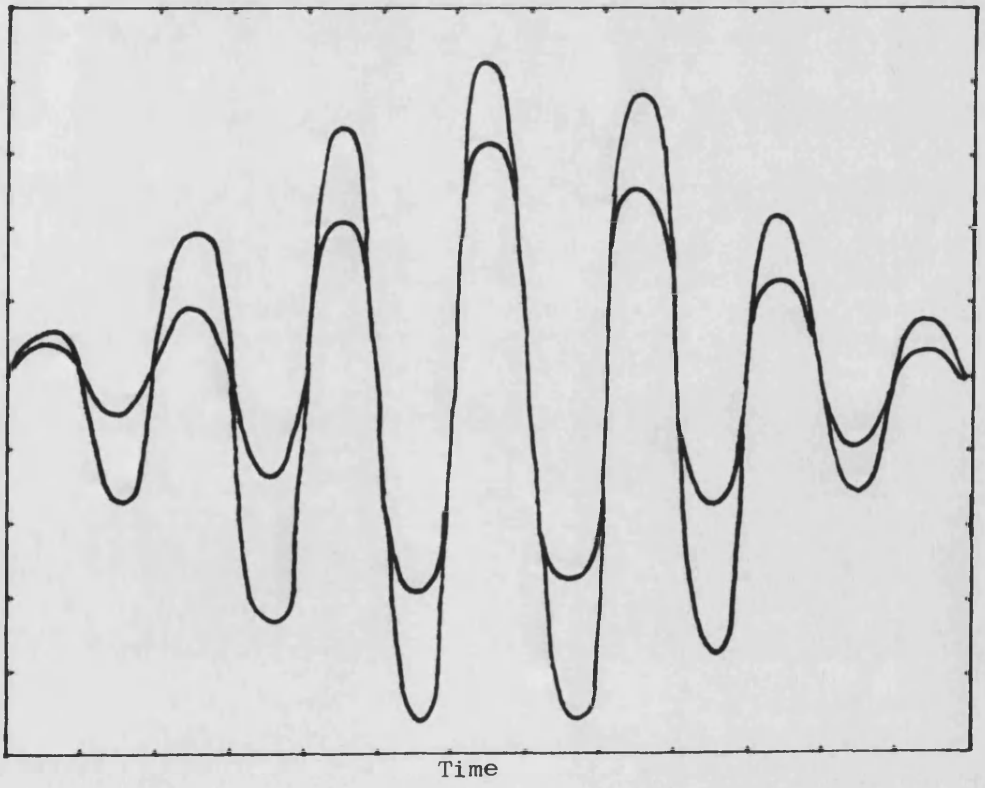

Fig. 3.8 Diagram showing two overlapped echos.

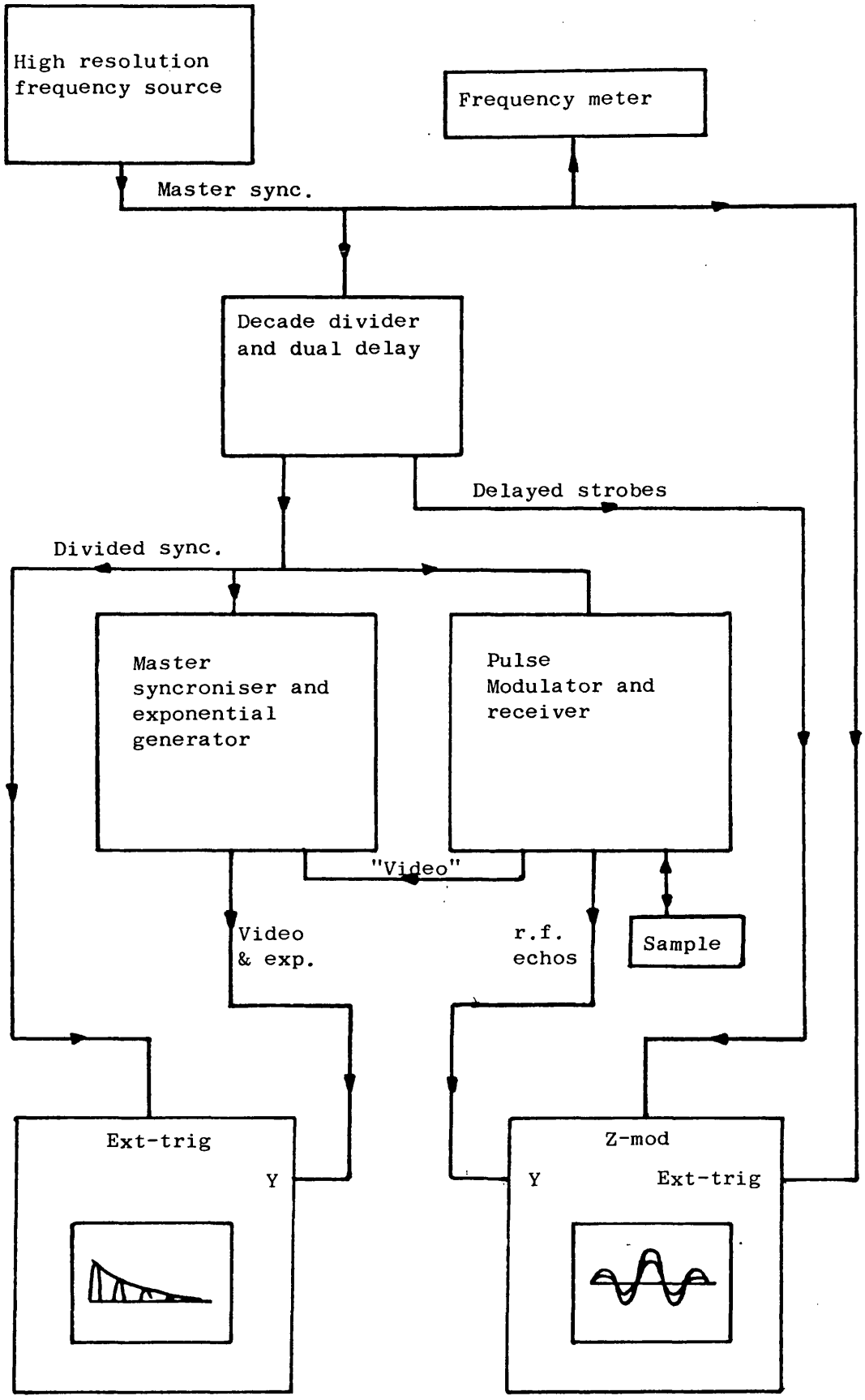

Fig. 3.9 Block diagram of pulse-echo overlap system.

of the frequency source. The frequency required to overlap exactly two successive echoes is a sensitive measure of the transit time (accurate to about 1 part in 10^4).

The system also incorporated an exponential generator, used to fit an exponential curve to the peaks of the echo train. This could be used to measure the attenuation through the sample if required. It was also used as a check of sample preparation, as an exponentially decaying echo train is a good indication that the sample has flat and parallel sides.

3.3 APPLICATION OF PRESSURE

Much of the equipment used for this work has already been described by Brassington [1982], and more general information on design and construction is given by Bradley [1969].

3.3.1 PRESSURE CELL

The application of hydrostatic pressure was achieved using a simple piston-cylinder arrangement (see Fig.3.10). The specimen was mounted in a sample holder on top of the lower piston, and connections to the outside made via beryllium-copper plugs set into the top of the piston. Castor oil was used as the pressure transmitting medium at room temperature, and silicon fluid used at higher temperatures. The pressure cell was sealed with rubber O-rings (nitrile for low temperature and viton for high temperature) and a hydraulic press

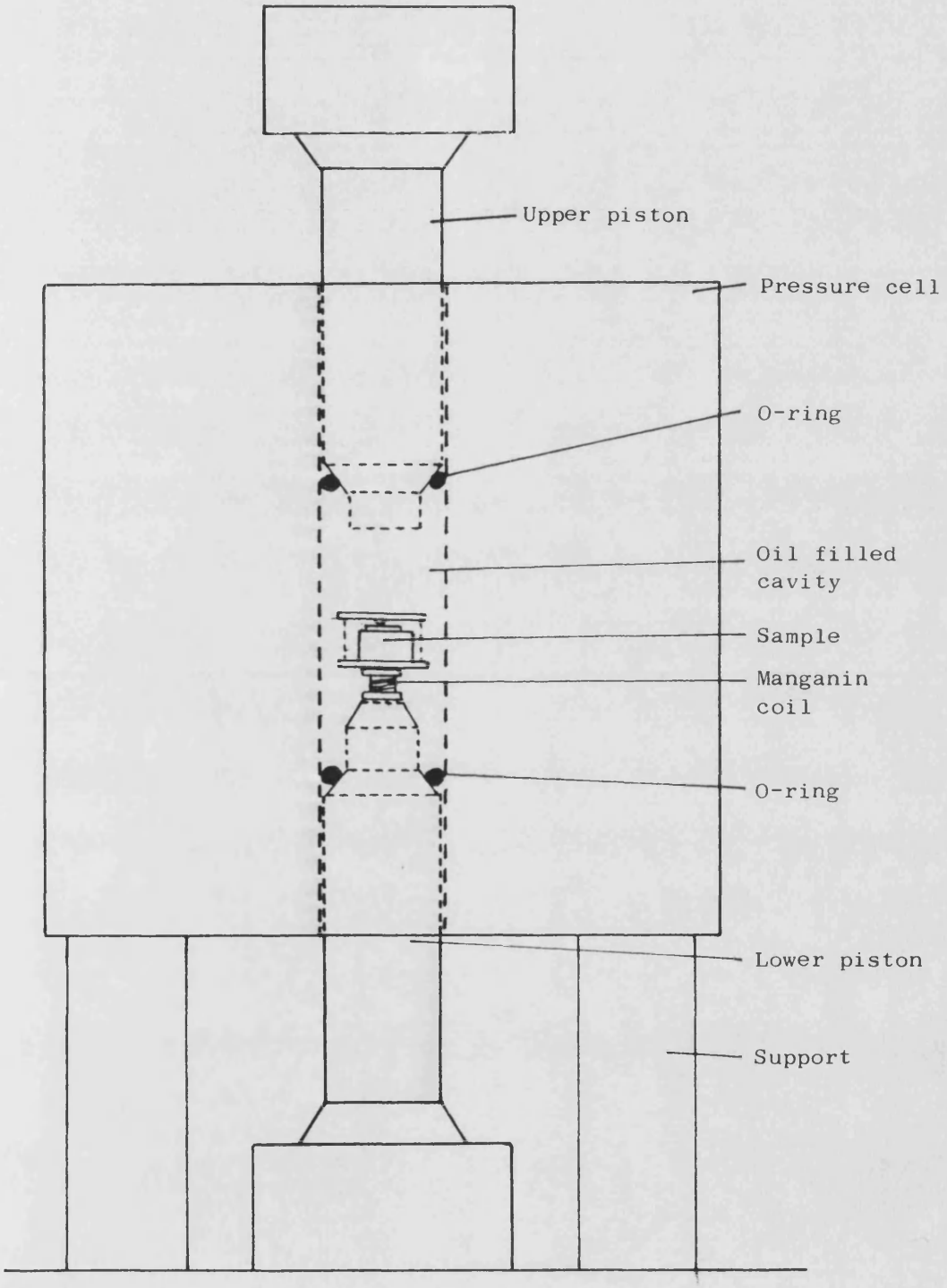

Fig. 3.10 Diagram of hydrostatic pressure cell.

was used to apply the pressure. The rise in temperature due to the pressurisation was measured using a NiCr/NiAl thermocouple mounted on the sample holder, and readings were only taken when the temperature inside the cell had returned to its initial value. The pressure inside the cell was calculated from the relative change of the resistance of a manganin coil, and the system was heated by means of a heater jacket placed around the pressure cylinder, controlled by a Eurotherm temperature controller. The whole apparatus was enclosed inside a steel cabinet for safety reasons.

With a suitable choice of O-rings this system was capable of applying pressures up to about 10kbar, but for this work it was only used up to about 1.5kbar. Note that before starting a measurement run the equipment was pressurised and left for a while to check the seals and ensure good transducer bonding.

3.3.2 MANGANIN RESISTANCE COIL

Pressure measurements were made by measuring the change in resistance of a coil of manganin wire (an alloy of Cu-Mn-Ni), within the pressure cell. This method has long been used (Bridgman [1911]) because manganin has been found to have a very nearly linear change of resistance with pressure, and a fairly low sensitivity to temperature. More recently it has been found (Chi-Yuen Wang [1966]) that the resistance-pressure response of manganin remains almost linear at elevated temperatures, and that the pressure

coefficient changes only slightly right up to 200°C. For this work the pressure coefficient of manganin wire has been taken as that obtained by Chi-Yuen Wang [1966], ie 2.4×10^{-3} Kbar^{-1} (1Kbar = 10^8 Pa). Hence pressure (P) is given by

$$P = (R_p - R_a)/(R_a \times 2.4 \times 10^{-3})$$

where R_a = atmospheric resistance and R_p = resistance at pressure P.

The pressure gauge was made by winding silk insulated manganin wire non-inductively on a PTFE bobbin. The coil was then put through a cycling process to relieve localised strain regions and improve uniformity. This entailed heating the coil to about 150°C for several hours followed by quenching in liquid nitrogen. This was repeated a number of times. To complete the seasoning the coil was then pressurised for several hours up to the maximum pressure to be used.

3.4 TEMPERATURE CONTROL

Temperatures of up to 157°C were reached within the pressure cell by using a heating element that fitted snugly around the outside cylinder. The temperature of the outside of the pressure cell was controlled to better than 0.2°C using a 'Eurotherm' PID temperature controller. All temperature measurements were made using NiCr/NiAl thermocouples connected to 'Digitron' digital thermometers.

It was important that during pressure runs the temperature was kept constant, or that readings were

always made at the same temperature. This was because the ultrasonic wave velocities, particularly of some shear modes, in indium are sensitive to temperature changes. Also, although manganin has a constant pressure coefficient with temperature, its actual resistance changes measurably with relatively small temperature variations.

3.5 DATA COLLECTION AND ANALYSIS

This section briefly describes how actual readings, taken using the above equipment, are used to calculate SOEC's and their pressure derivatives.

Figure 3.10 shows a typical frequency versus pressure response obtained for a longitudinal elastic wave propagating down the [001] direction in a single crystal of indium. A least squares fit is used to find the best straight line through the data, giving the intercept on the frequency axis and the slope of the response (f and f' (=df/dP) on Fig 3.10). The frequency intercept gives the pulse overlap frequency at zero pressure (f) from which the mode elastic wave velocity (V_o) may be calculated. The slope of the graph gives the frequency gradient at zero pressure(f'), assuming the response is a straight line.

To calculate the mode elastic constant and it's pressure derivative at any particular temperature (T), it is necessary to find the density (p), the bulk modulus (B), and the linear compressibility (S), at that temperature. The equation for the elastic constant pressure derivative is given by Thurston [1965], and in section 2.2 as :

$$(pV^2)' = pV_o^2((2f'/f) + (1/B) - 2S)$$

where pV_o^2 is the mode elastic constant.

For this work the variation of sample density and path length with temperature was calculated from thermal expansion results published by Graham et al [1955]. To

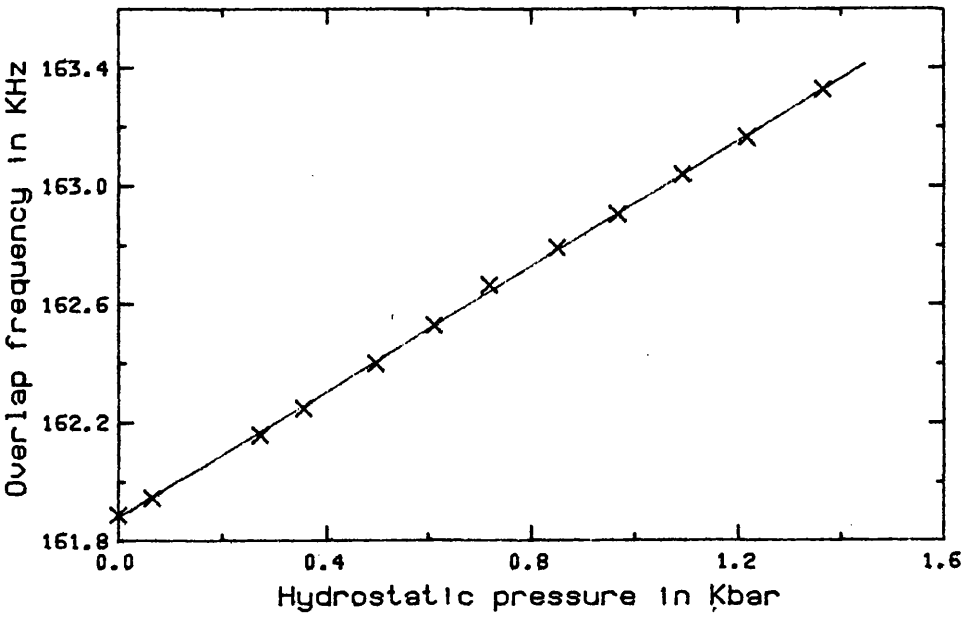

Least squares fit to data gives :

Gradient (f') = 1.06 KHz/Kbar ($x10^{-5}$Hz/Pa)
Intercept (f) = 161.88 KHz

Data at 300K :

Density (ρ) = 7284 Kg/m^3
Sample thickness (L) = 7.456 mm
Bulk modulus (B) = 4.16 $x10^{10}$Pa
Linear compressibility (S) = 9.50 $x10^{-12}Pa^{-1}$

Velocity ($V = 2fL$) = 2414 m/sec
Corrected velocity (see section 3.6.(ii)) = 2448 m/sec
Elastic constant ($C_{33} = \rho V^2$) = 4.37 $x10^{10}$Pa
Pressure derivative $(\rho V^2)' = \rho V^2(2f'/f + 1/B - 2S)$
= 5.94

Fig 3.10 Typical overlap frequency vs pressure response for indium, to illustrate how elastic constant and pressure derivative data are calculated from experimental data. (In this case the data shown is for the longitudinal mode in the [001] direction in indium at 300K)

begin with, values of bulk modulus and linear compressibity were calculated from data for the temperature dependences of elastic constants of indium, published by Vold et al [1976]. Then, once enough data had been obtained, our own results were used.

The data (temperature, intercept, and gradient) for each pressure run on a particular mode was fed into a program on a BBC microcomputer (see Appendix A). This program first worked out the zero pressure elastic wave velocity (V_0) for each run, applying a correction for multiple internal reflections at the sample-transducer interface (see section 3.6.(ii), Kittinger [1977]), and allowing for thermal expansion. It then calculated values of density, bulk modulus, and linear compressibility, at the appropriate temperature, and finally worked out the pressure derivative. The data was stored to disc so that it could be retrieved to be displayed on a graph and have a curve fitted through it (program in Appendix B).

Once the temperature responses for mode elastic constants and pressure derivatives had been obtained, for all modes at temperatures up to the melting point, values for the six SOEC's of indium and their pressure derivatives could be calculated at any desired temperature. These values were then used to obtain mode Gruneisen parameters at various temperatures, by feeding them into an adaptation of a program used by Tu Hailing [1983] (using thermodynamic pressure derivatives, see section 2.3)

3.6 EXPERIMENTAL ERRORS AND CORRECTIONS

The precision with which elastic constants and their pressure derivatives may be determined, depends upon the accuracy of measurements of absolute velocities, and the relative pressure induced changes of those velocities. There are several possible sources of error.

(i) Measurement of path length

A More and Wright 'micro 2000' digital micrometer was used to measure sample thicknesses to an accuracy of 2μm. Generally a number of readings were taken over the crystal face, and a mean value taken for the path length. This provided a rough measure of just how flat and parallel samples actually were. Typically, the standard deviations on the measurements made on a crystal dimension were about 0.02%.

(ii) Transit time errors

The measurement of absolute transit time through a sample is probably the largest single source of error in the values of elastic constants. There is a relatively large error (1 to 2%) due to multiple internal reflections within the transducer. However, this error can be estimated and a correction applied. The correction was calculated using a program called 'TRANS-CORR' (Brassington [1982]), based on computations made by Kittinger [1977].

(iii) Misorientation errors

A transducer is generally regarded as a piston source generating plane ultrasonic waves. However transducers are finite in extent and have diffraction fields which can cause errors in transit time measurements. Truell et al [1959] have calculated that as long as the crystal is orientated to an accuracy of about 0.5° and the area of the transducer is smaller than that of the sample, then the estimated error in velocity is about 0.01%.

(iv) Temperature control

The temperature of the heater jacket was generally held to within 0.2°C by a 'Eurotherm' temperature controller, and the temperature inside the pressure cell measured to 0.1°C, using a 'Digitron' digital thermometer. During a pressure run the readings were always taken at the same temperature to minimise errors due to temperature induced velocity changes. For some shear modes the velocity change due to a change in temperature of 1°C can be equivalent to the change induced by a pressure change of about 0.5kbar.

(v) Density corrections

The value of the density of indium at room temperature has been taken from the literature as 7290Kg/m^3. This agreed well with x-ray lattice parameter measurements. For high temperature work corrections to the room temperature value were made using thermal expansion data from Graham et al [1955].

(vi) Temperature corrections

Sample path length corrections at elevated temperatures were made using the same thermal expansion data. To make the necessary corrections to the pressure derivatives, due to changes in path length and density with pressure (Thurston [1965]), the values of the sample's bulk modulus and linear compressibility must be known. This requires a knowledge of the second order elastic constants, which are temperature dependent. At elevated temperatures the appropriate corrections were made using temperature coefficient values given by Vold et al [1976].

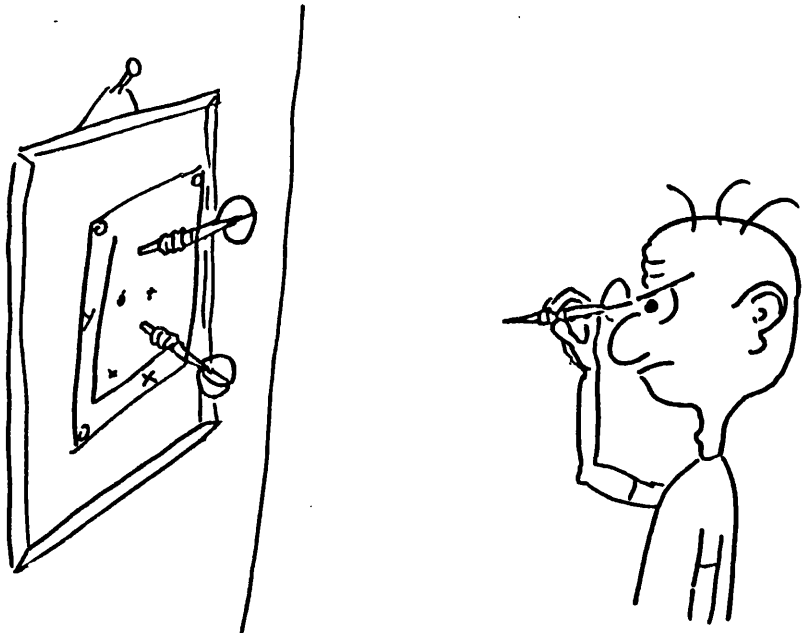

EXPERIMENTAL RESULTS

EXPERIMENTAL RESULTS

4.1 INTRODUCTION

Presented in this chapter are values of the SOEC's , and the pressure derivatives of the SOEC's , obtained experimentally for single crystal indium in the temperature range between room temperature and the melting point (429.7 deg. K) . Also included are temperature dependences of bulk modulus , compressibility and mode Grüneisen parameters for indium . These results have been obtained from measurements of ultrasound propagation velocities along various crystallographic directions , and from the observed hydrostatic pressure dependences of the mode velocities . Where possible comparisons have been made with previously published data .

4.2 ULTRASONIC PROPAGATION VELOCITIES

The ultrasonic propagation velocities , for various crystallographic directions in single crystal indium , were determined by measuring the time taken for pulses of ultrasound to traverse suitably orientated samples of known thicknesses (see section 3.2) .

The sample path lengths were measured at room temperature using a digital micrometer and corrected at higher temperatures using thermal expansion data published by Graham et al [1955] . The equations given by these

workers for the temperature dependence of thermal expansion for indium are shown in Table 4.1 . It should be noted that their data only goes up to 135 deg.C . In this work extrapolated values have been used in the absence of any other published thermal expansion data near the melting point . Since the analysis of the data given here some thermal expansion measurements have been made at high temperatures for indium (Prof. G.A.Saunders , Bath University , private communication) , but these results do not differ greatly from the extrapolated values used . Figures 4.1 , 4.2 , and 4.3 show lattice spacing variations with temperature , calculated from the equations in Table 4.1 , in the range 10 deg.C to 156 deg.C .

All velocity values given here have been corrected to allow for effects due to multiple internal reflections at the sample-transducer interface (Kittinger [1977]) .

Table 4.2 shows values for ultrasonic propagation velocities through single crystal indium at room temperature . The choice of the various propagation and polarisation directions was made so that enough information would be available to calculate the complete set of six SOEC's associated with the tetragonal structure . Table 4.2 also shows the various combinations of SOEC's associated with each measured propagation mode (ie mode elastic contants) , and gives their experimental values . Once the SOEC's have been calculated from these

TABLE 4.1 Thermal expansion data for indium [-183 deg.C to 135 deg.C] (Graham et al [1955])

The lattice parameters for indium may be obtained using the following expressions:

$$a = 4.5422(1 + 2.59 \times 10^{-5} T + 1.15 \times 10^{-10} T^3)$$

$$c = 4.9141(1 + 2.59 \times 10^{-5} T - 1.15 \times 10^{-10} T^3)$$

$$c/a = 1.0819(1 - 2.30 \times 10^{-10} T^3)$$

where the temperature is expressed in K.

The thermal expansion coefficients are obtained by differentiation and are given by:

$$\alpha_a = 2.59 \times 10^{-5} + 3.45 \times 10^{-10} T^2$$

$$\alpha_c = 2.59 \times 10^{-5} - 3.45 \times 10^{-10} T^2$$

which gives a volume coefficient of expansion of:

$$\alpha = 7.77 \times 10^{-5} + 3.45 \times 10^{-10} T^2$$

Fig.4.1 Thermal expansion of indium
(Graham et al [1955])

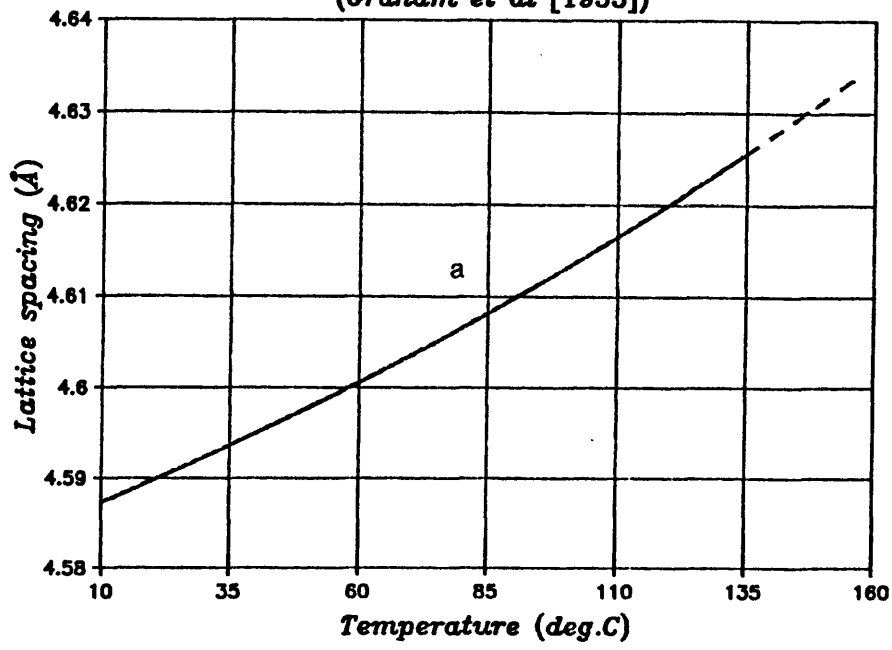

Fig. 4.2 Thermal expansion of indium
(Graham et al [1955])

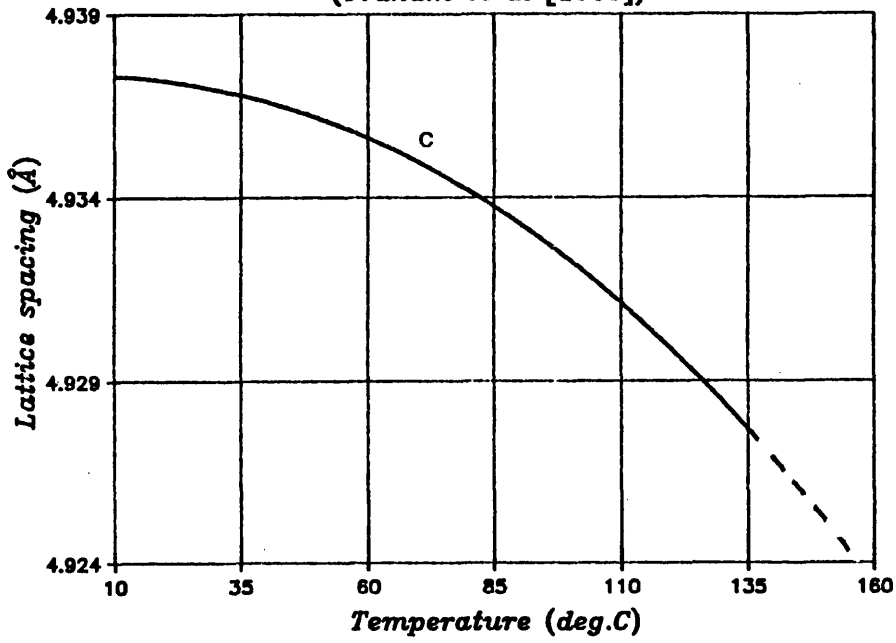

Fig. 4.3 Thermal expansion of indium
(Graham et al [1955])

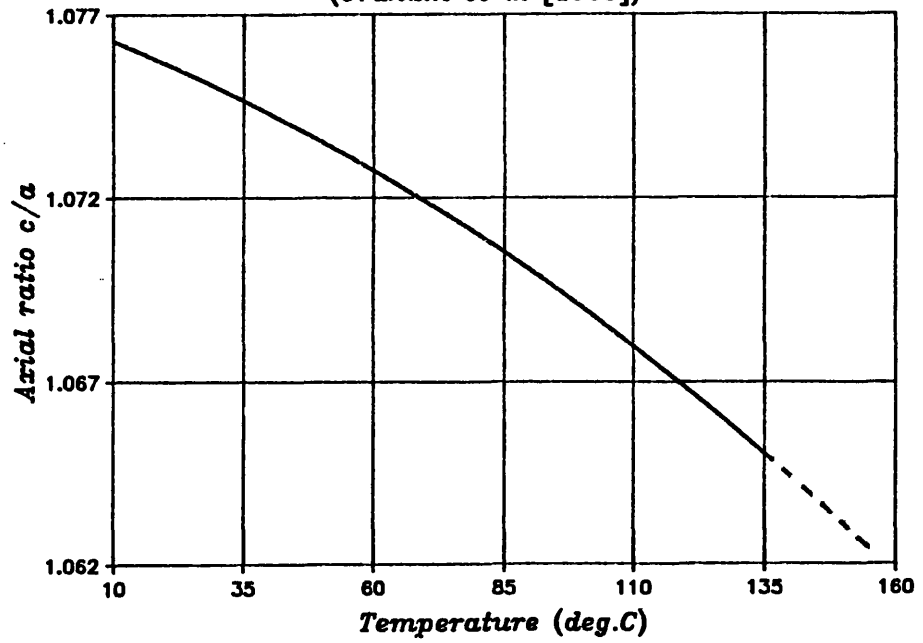

Propagation direction	Polarisation direction	Mode elastic constant	Velocity (m/sec)	ρV^2 ($\times 10^{10}$ Pa)	$(\rho V^2)'$
k	e				
[100]	[100]	$\rho V^2 = C_{11}$	2486	4.50	5.56
[100]	[010]	C_{66}	1277	1.19	2.02
[001]	[001]	C_{33}	2448	4.37	5.56
[001]	xy plane	C_{44}	946	0.65	0.99
[110]	$[1\bar{1}0]$	$\frac{1}{2}(C_{11}-C_{12})$	589	0.25	0.60
[011]	$[\varphi]$	$\frac{1}{2}(A+(A^2-B+C^2)^{1/2})$	529	0.20	0.54

Table 4.2 Mode velocities and pressure derivatives for pure indium at 300K.

relations it is possible to work out the ultrasonic propagation velocities for any direction through the crystal . These values are obtained as the eigenvalues of the Christoffel equations and have to be calculated in order to be able to determine values of mode Grüneisen parameters for any direction (see section 2.5) .

The directional dependences of the mode velocities obtained at room temperature and at 427 K are presented as velocity surface plots in Fig. 4.4 . In each case the [101] slow shear mode is seen to be the slowest propagation mode , and the [110] longitudinal mode the fastest . It should be noted that all propagation velocities decrease with an increase in temperature.

The results for the change in velocity with temperature for each of the six modes measured are shown graphically in figures 4.5 to 4.10 . In general the graphs show quite smooth responses with little scatter . The scatter that there is tends to suggest that the maximum spread of results for most plots is rather less than 1% . The smoothness of the plots is due to the fact that the runs usually started at room temperature after which the temperature was steadily incremented towards the melting point , making it easier for the operator to follow the correct overlap frequency .

However , it should be noted that for most runs the sample was not changed during a run , and to get a true idea of the accuracy of results comparison should be made

Fig. 4.4 Mode Velocities plotted .

against Propagation Direction

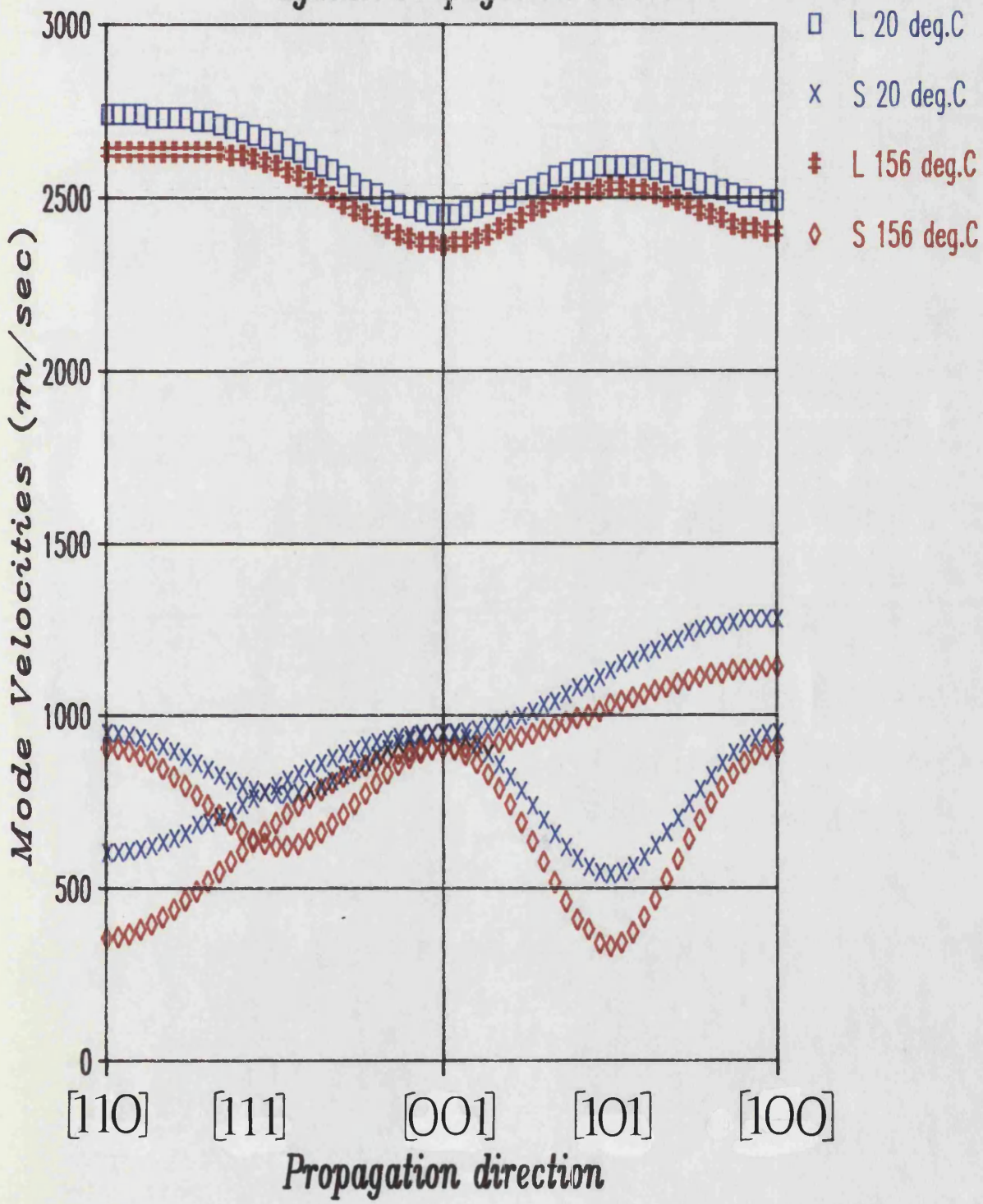

Fig4.5 Propagation velocity vs temperature

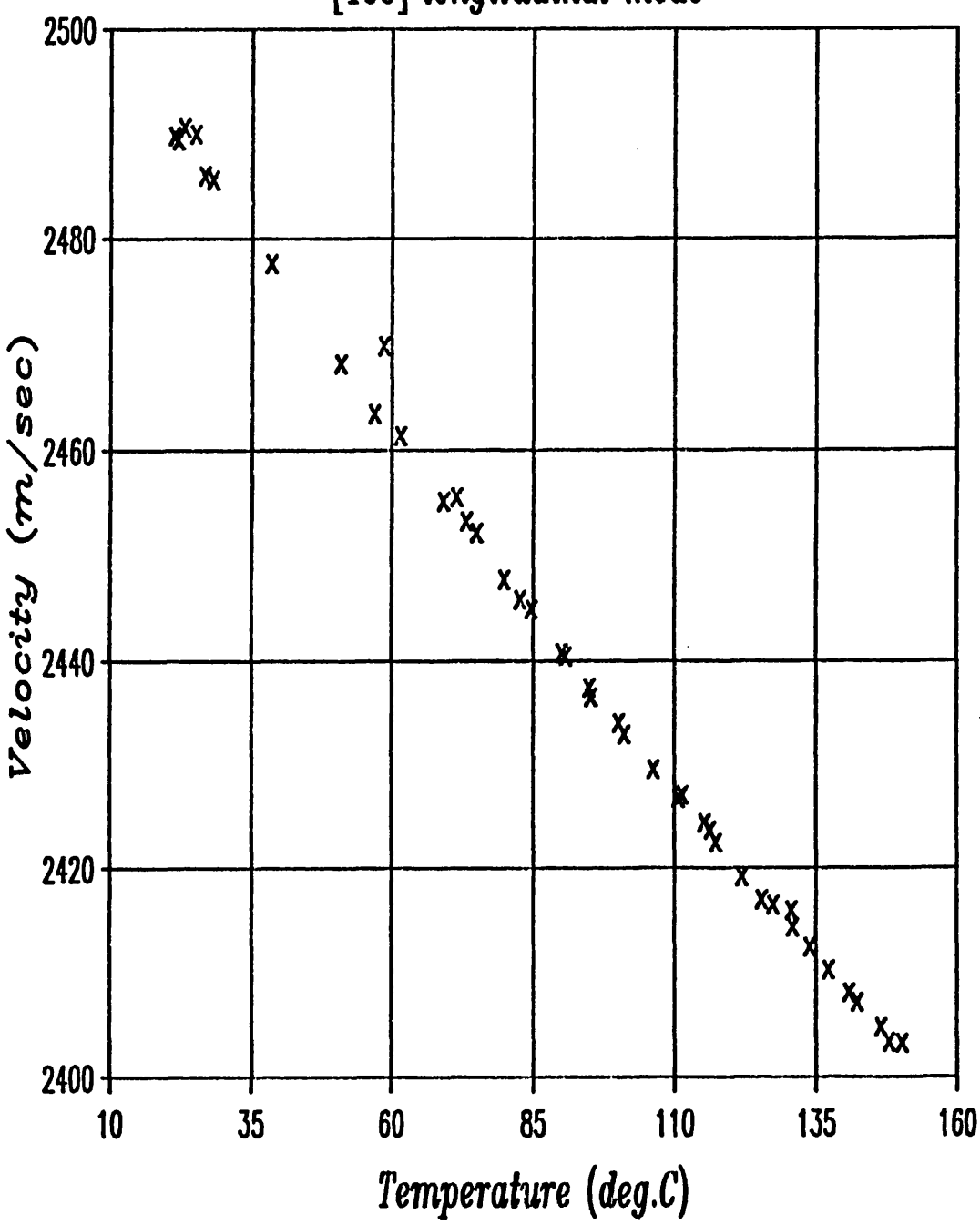

Fig.4.6 Propagation velocity vs temperature

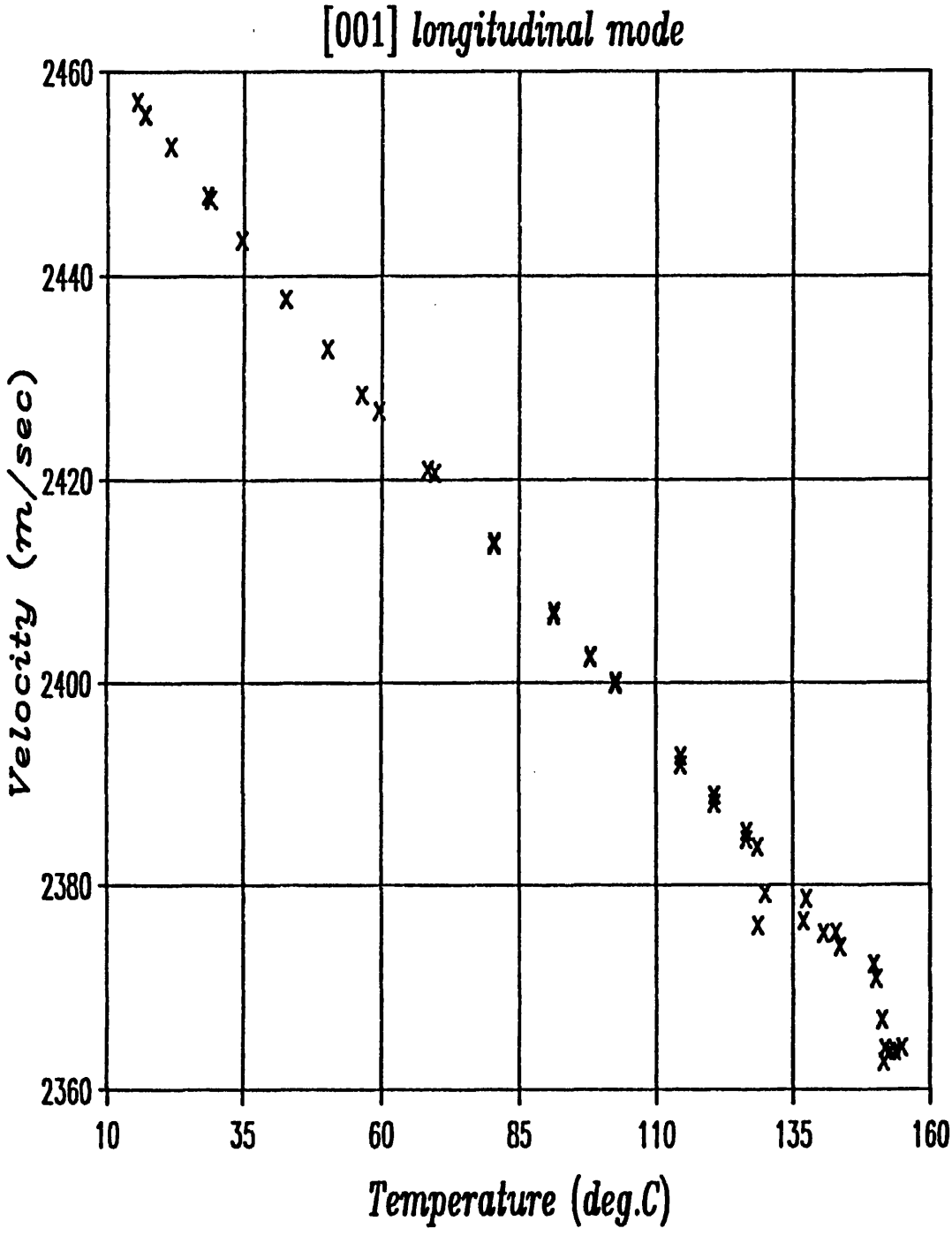

Fig4.7 Propagation velocity vs temperature

[100]q//[010] shear mode

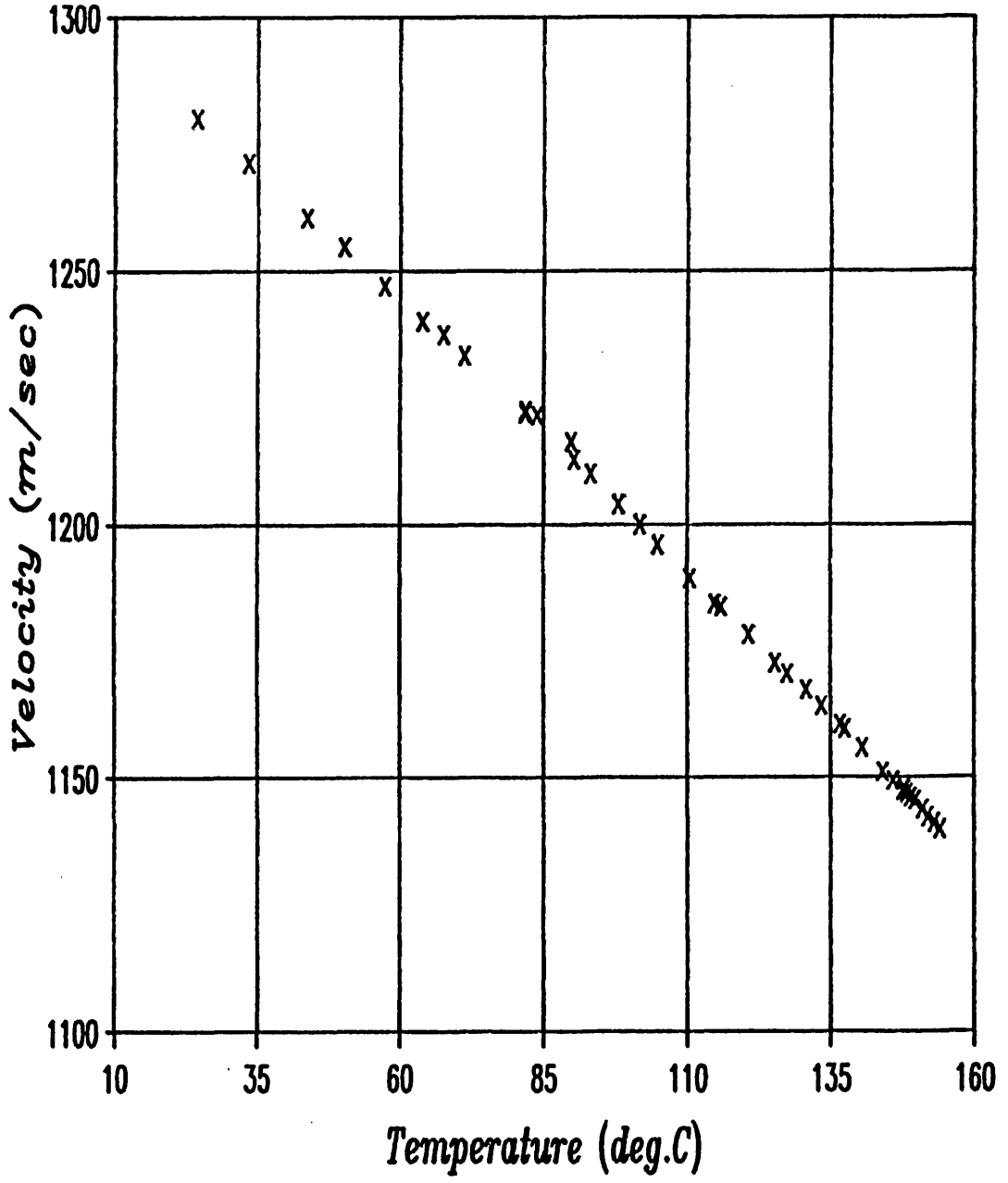

Fig4.8 Propagation velocity vs temperature

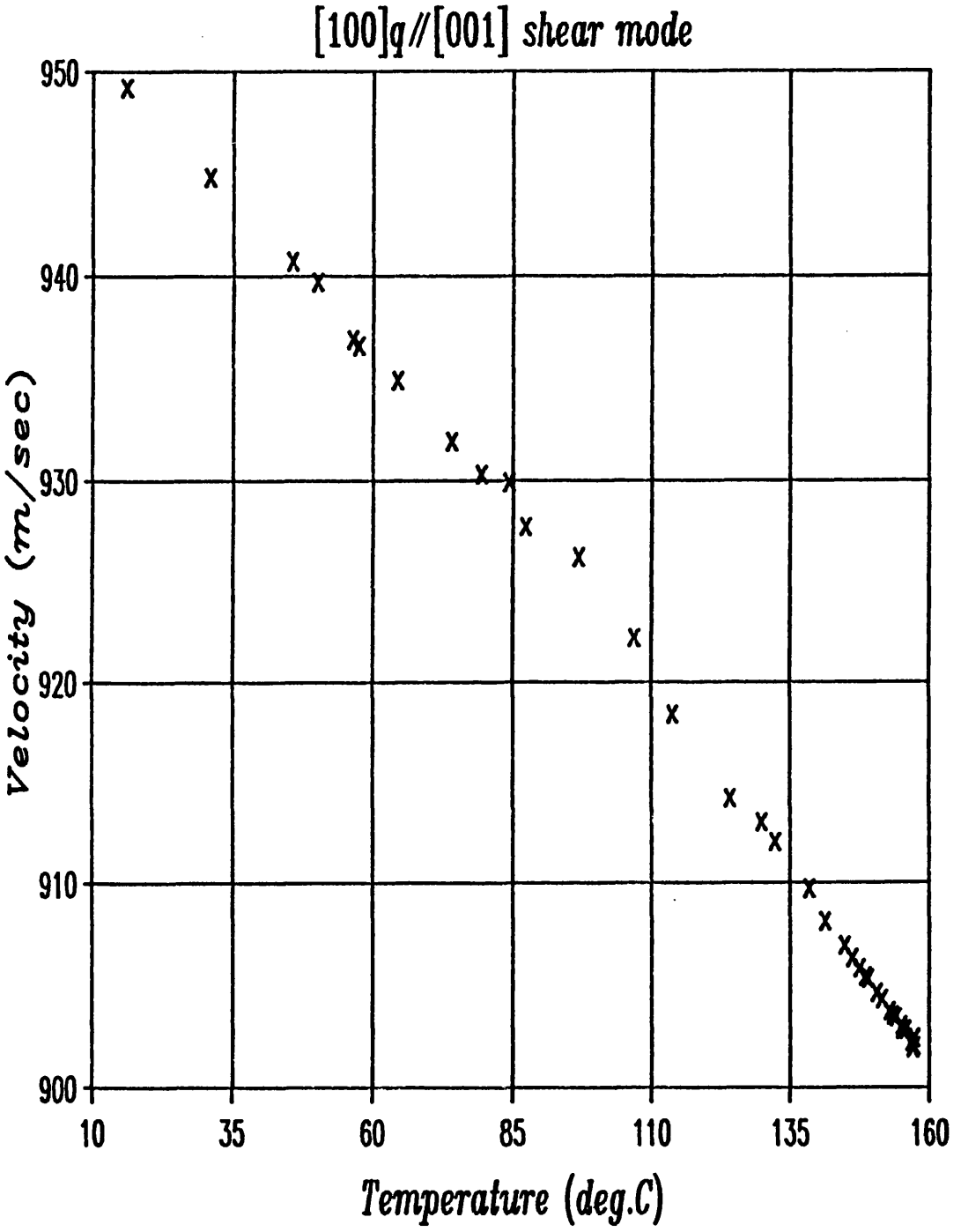

Fig.4.9 Propagation velocity vs temperature

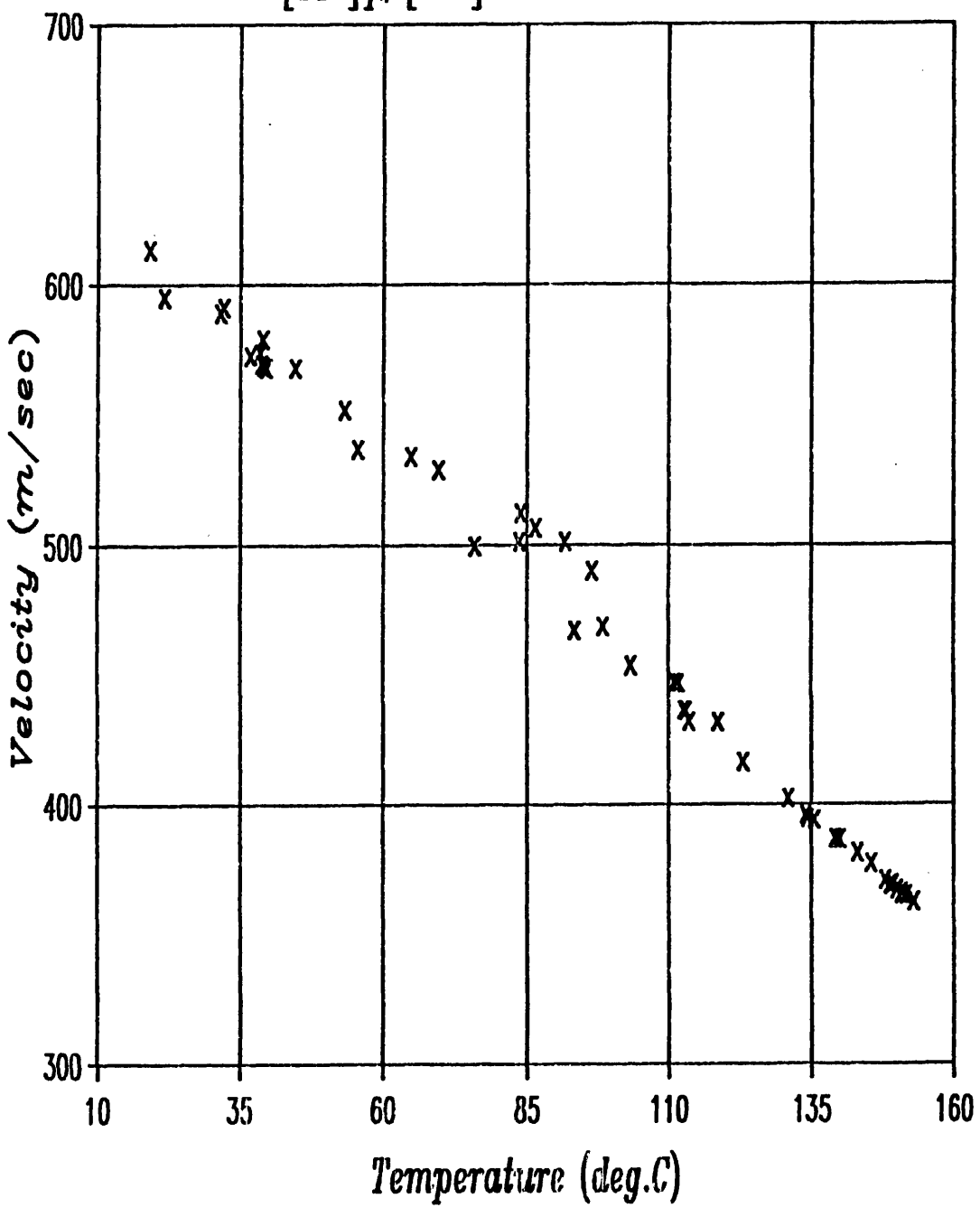

Fig.4.10 Propagation velocity vs temperature

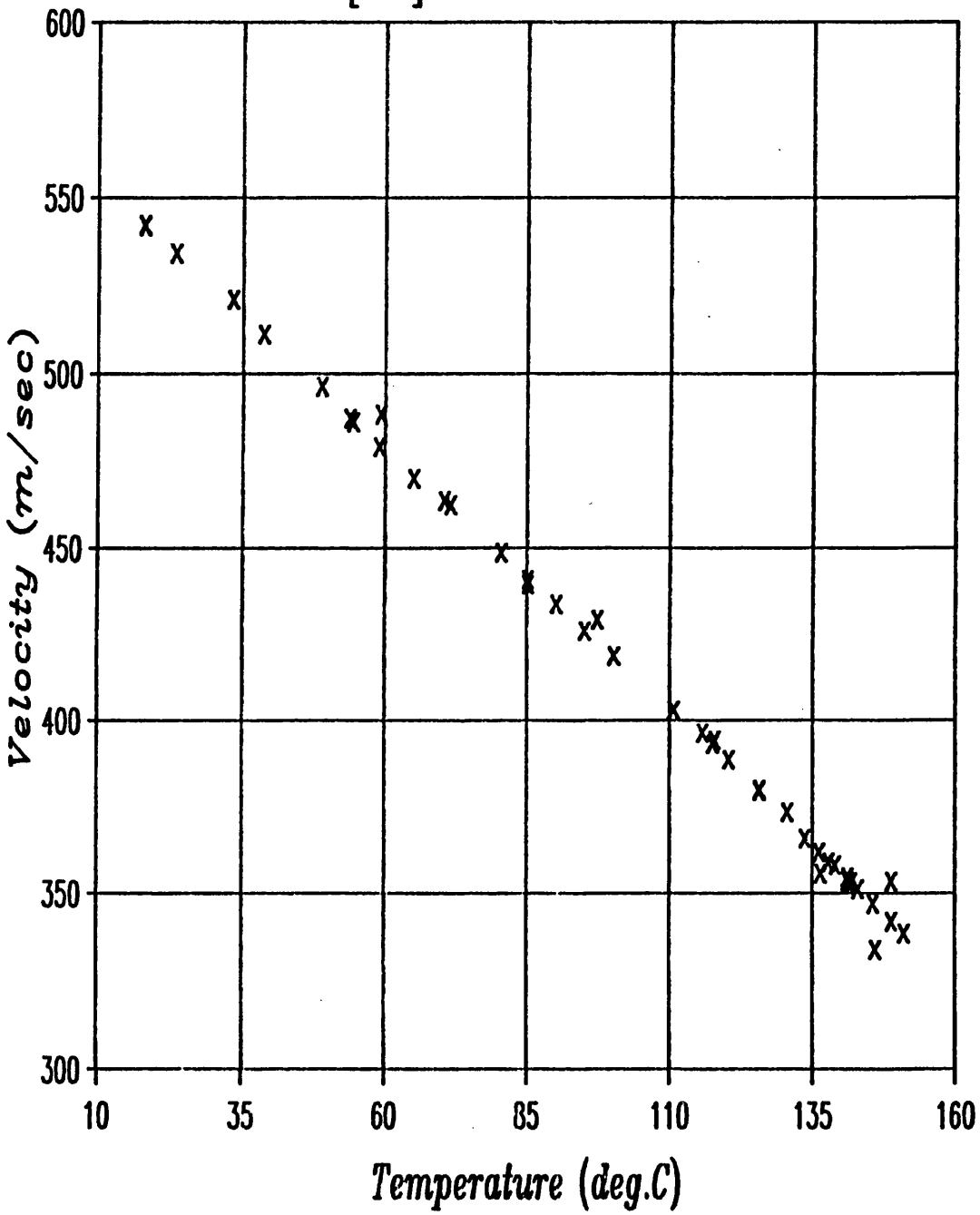

between runs on different samples . The graph of velocity versus temperature for the [110] slow shear mode (Fig 4.9) shows a combined set of results from three separate runs , and displays a spread of values of more like 2-3% . Other comparisons for different modes at various temperatures tended to show that results were reproducible to better than $\pm$ 1% .

4.3 SECOND ORDER ELASTIC CONSTANTS

The values of the six second order elastic constants (SOECs) for indium can be calculated knowing its density ρ_o , and the velocity of propagation of ultrasound along appropriately selected crystallographic directions (see section 2.3) . The velocity data presented in the previous section covers enough modes of propagation to allow a full set of SOECs to be calculated . For this work the value for the density , ρ, of indium was taken from the literature as 7290 Kg/m^3 at 20 deg.C , which agreed well with lattice parameter measurements made using an X-ray powder camera . The density was calculated for higher temperatures using thermal expansion data published by Graham et al [1955] .

Table 4.3 shows the results obtained for the SOECs of indium at 300 deg.K , and compares them with previously published data (Chung et al [1976] , Vold et al [1977] , and Winder and Smith [1958]) . It can be seen that there is generally good agreement at this temperature .

Figures 4.11 to 4.16 show the measured change of mode elastic constant with temperature for the six modes studied . These mode parameters can be a combination of two or more SOECs (see table 2.1) . Parabolas were fitted through the data , using a least squares method , allowing mode parameters and the SOECs to be calculated at

Elastic constant	Present work	Chung et al.	Vold et al.	Winder & Smith
C_{11}	4.50 ± 0.02	4.57	4.51	4.44
C_{33}	4.37 ± 0.02	4.46	4.53	4.43
C_{44}	0.65 ± 0.01	0.65	0.65	0.65
C_{66}	1.19 ± 0.01	1.20	1.19	1.22
C_{12}	4.00 ± 0.04	4.07	3.97	3.94
C_{13}	4.03 ± 0.08	4.16	4.11	4.04
				($\times 10^{10}$ Pa)

Table 4.3 Comparison of elastic constants for indium at 300K

Elastic constant	a	b	c
C_{11}	-3.318×10^{7}	17677	4.591×10^{10}
C_{33}	-2.744×10^{7}	-6630	4.442×10^{10}
C_{44}	-3.936×10^{6}	-7778	6.629×10^{9}
C_{66}	-1.893×10^{7}	-8473	1.241×10^{10}
C_{12}	65970	-27101	4.000×10^{10}
C_{13}	-5.695×10^{6}	-22181	4.044×10^{10}
$\frac{1}{2}(C_{11}-C_{12})$	-1.664×10^{7}	22426	2.956×10^{9}
ρV^2 011 slow shear	-1.228×10^{7}	13761	2.358×10^{9}

Table 4.4 Temperature dependences of elastic constants of indium in temperature range 10 - 156 deg.C. The results are least squares fitted parabolas; $C = aT + bT^2 + c$

Fig4.11Mode elastic constant vs temperature

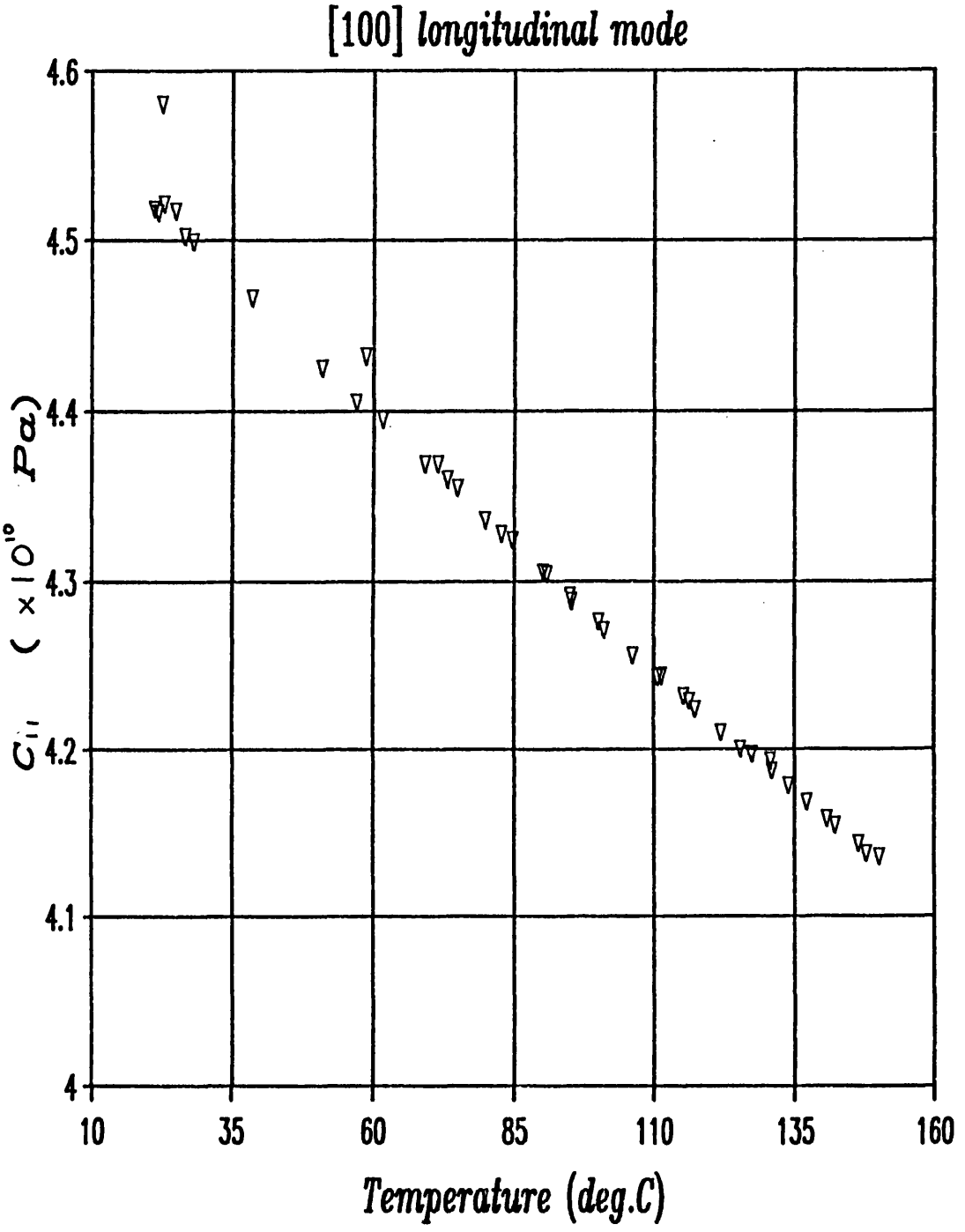

Fig.4.12 Mode elastic constant vs temperature

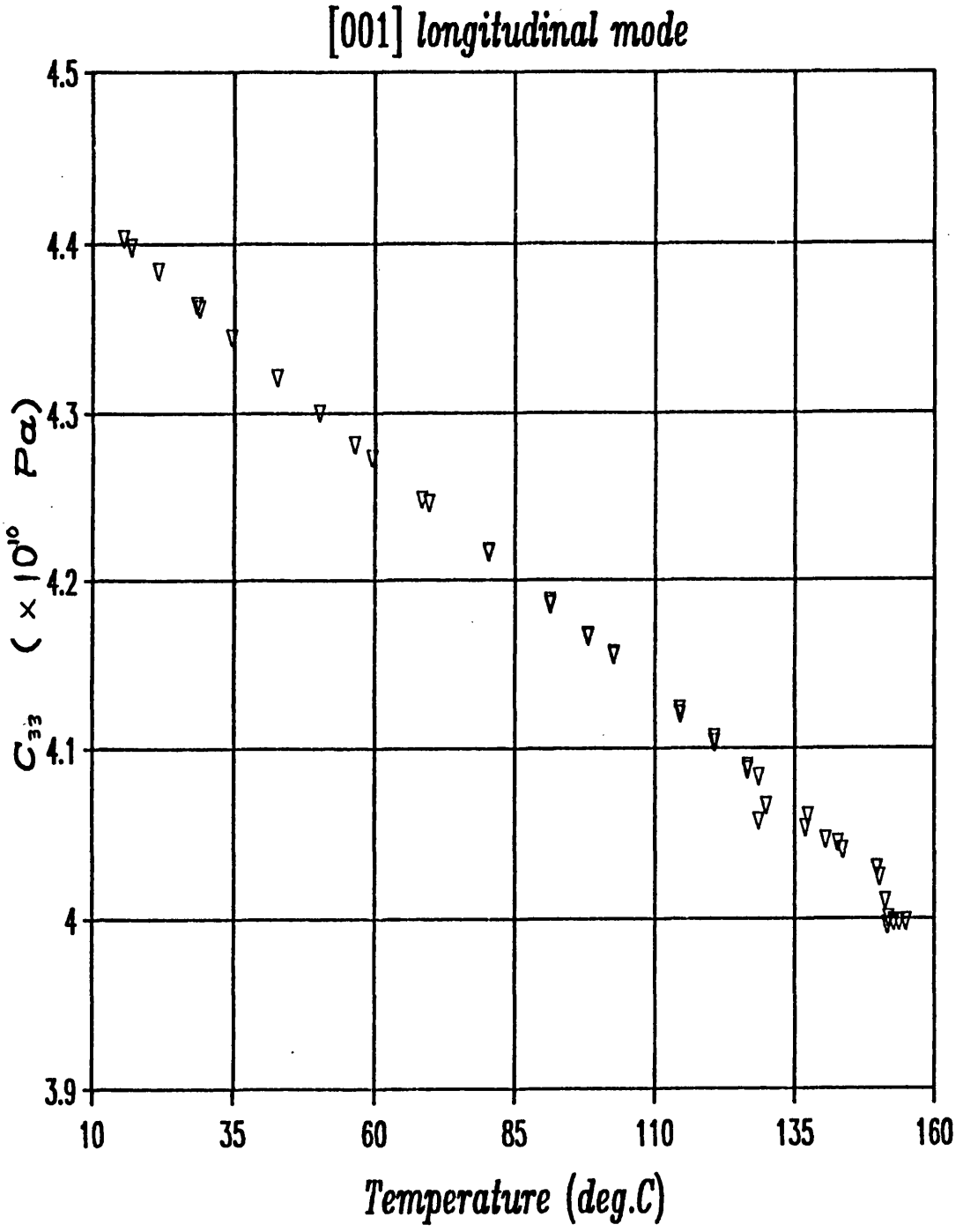

Fig.4.13 Mode elastic constant vs temperature

[100]q//[010] shear mode

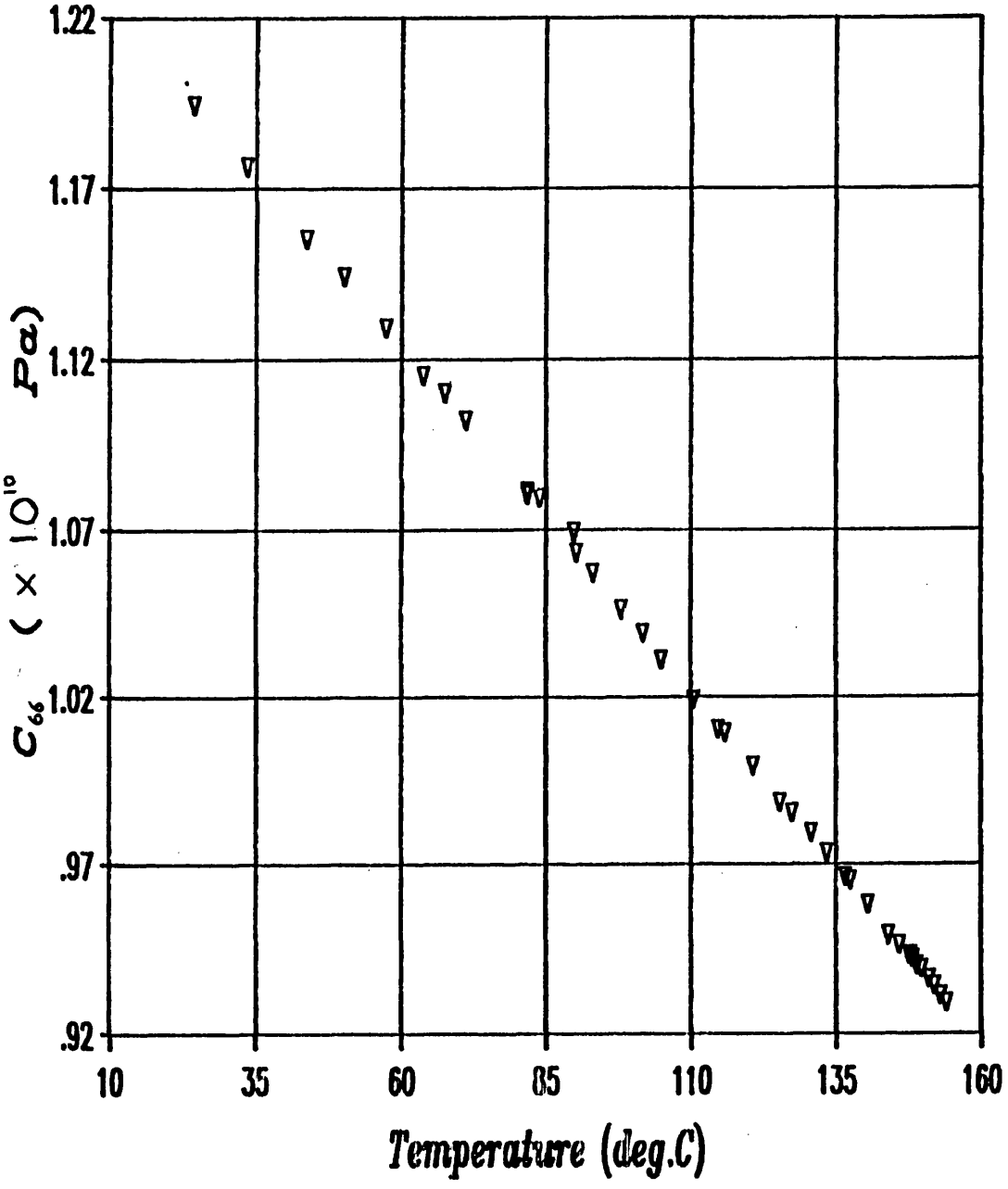

Fig.4.14 Mode elastic constant vs temperature

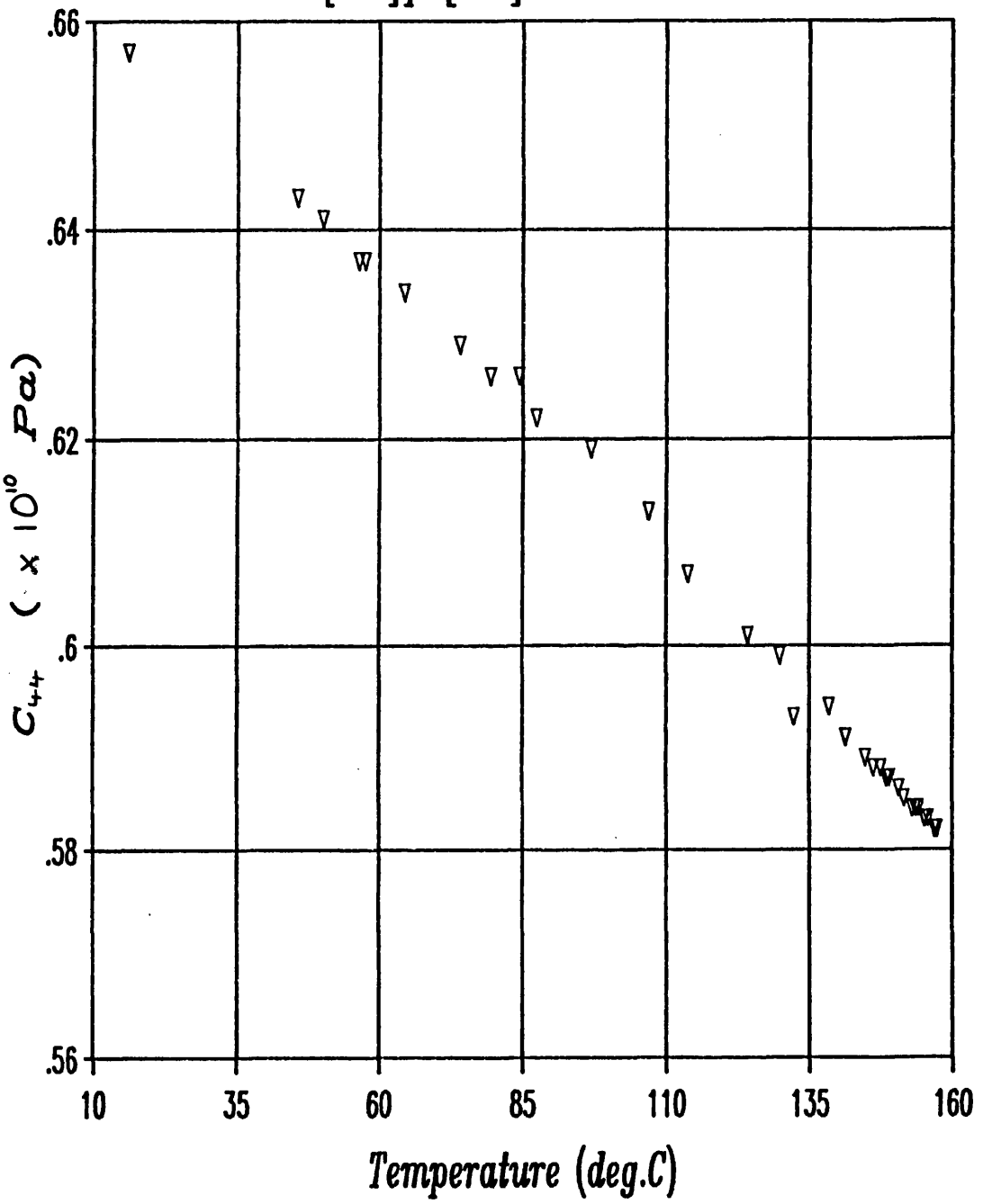

Fig.4.15 Mode elastic constant vs temperature

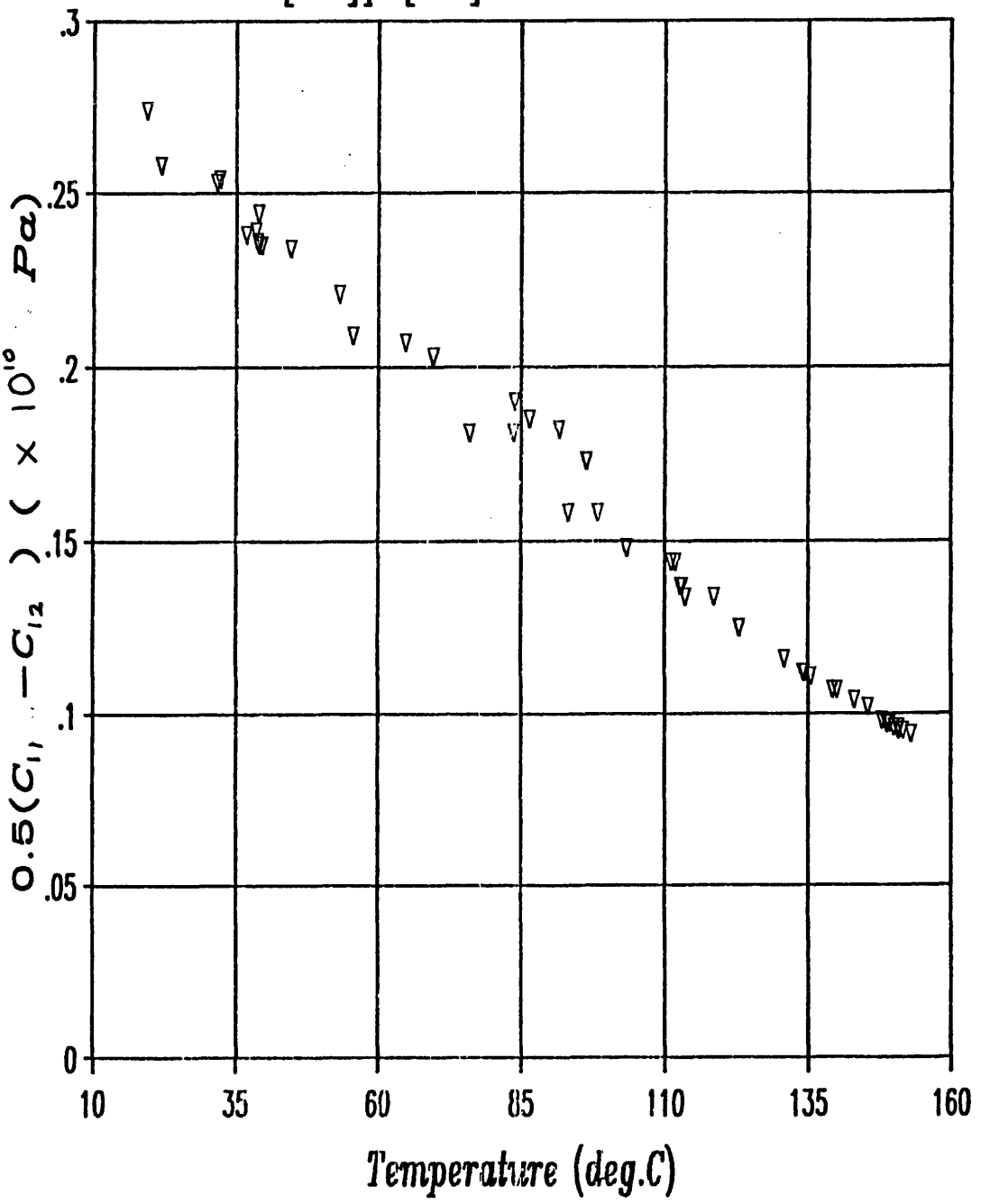

Fig.416 Mode elastic constant vs temperature

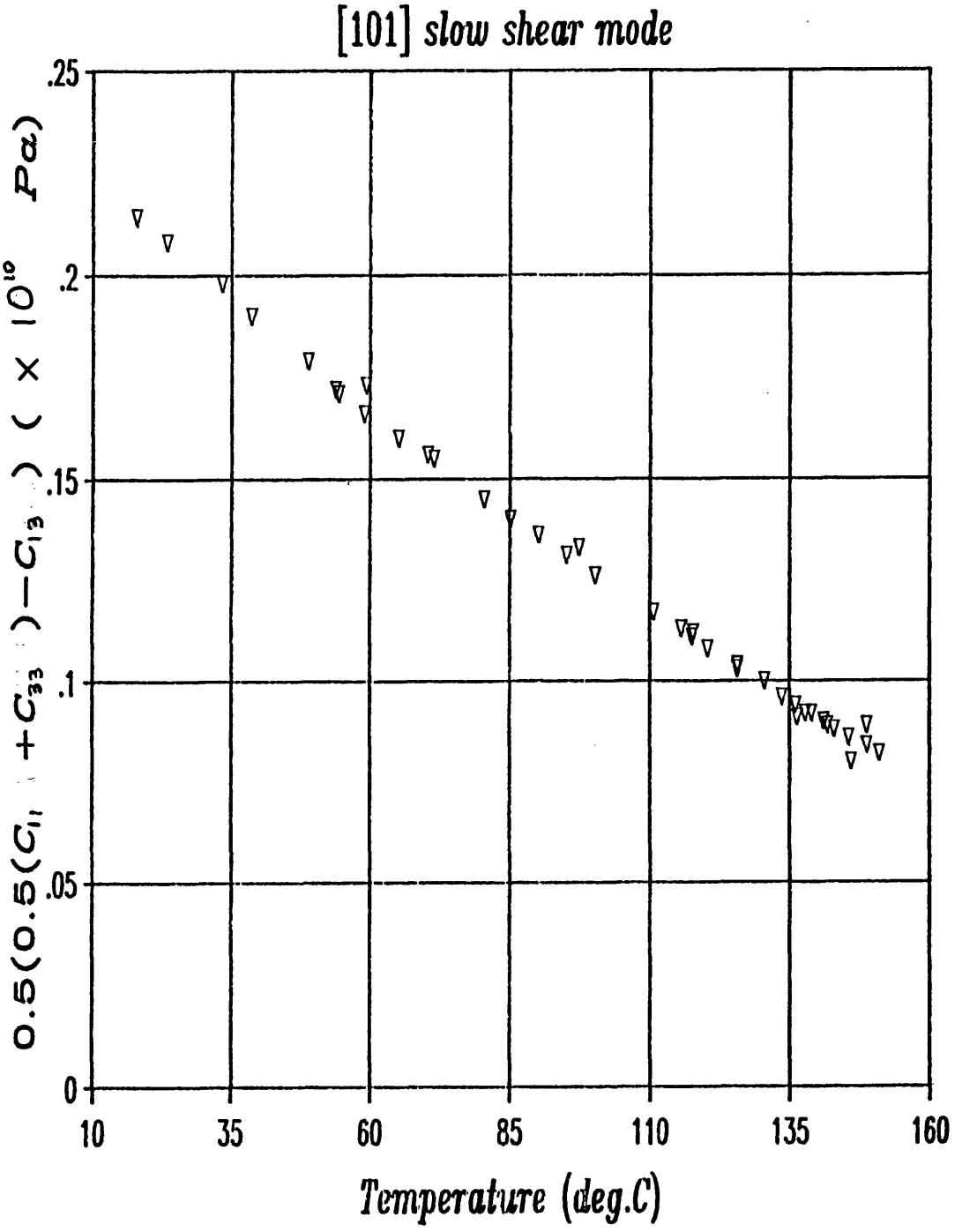

any temperature in the range . Table 4.4 presents the temperature coefficients found for all six SOECs . The temperature responses for the SOECs are shown graphically in figures 4.17 and 4.18 , and comparison is made with previously published data (Vold et al [1977]) . The two sets of results compare well with close agreement for most constants . The only real differences observed are for the C_{33} and C_{13} values which disagree by only about 4% . It is interesting to note that Vold et al found very similar values for C_{11} and C_{33} over the whole temperature range and that the apparant equality of these two constants could account for the observed difference between their results for C_{13} and those presented here . Reliable measurement of C_{11} and C_{33} is quite difficult as crystallographically the two directions are difficult to tell apart on a near cubic material such as indium .

The value of C_{13} may be quickly , but quite accurately, calculated for indium , from data for the slow shear mode propagated ($\underline{k}$) in the [101] direction and polarised ($\underline{e}$) along $\varnothing$ (close to $[10\bar{1}]$) using the equation;

$$\rho V^2 = ((C_{11} + C_{33})/2 - C_{13})/2$$

This assumes that the value of $A^2 - B$ is negligibly small compared to C^2 in the mode constant equation (Table 2) , ie that $(C_{11} - C_{33})^2/4$ is negligibly small compared to $(C_{13} + C_{44})^2$ which is true for indium with its near cubic

Fig.4.17 SOEC's vs Temperature

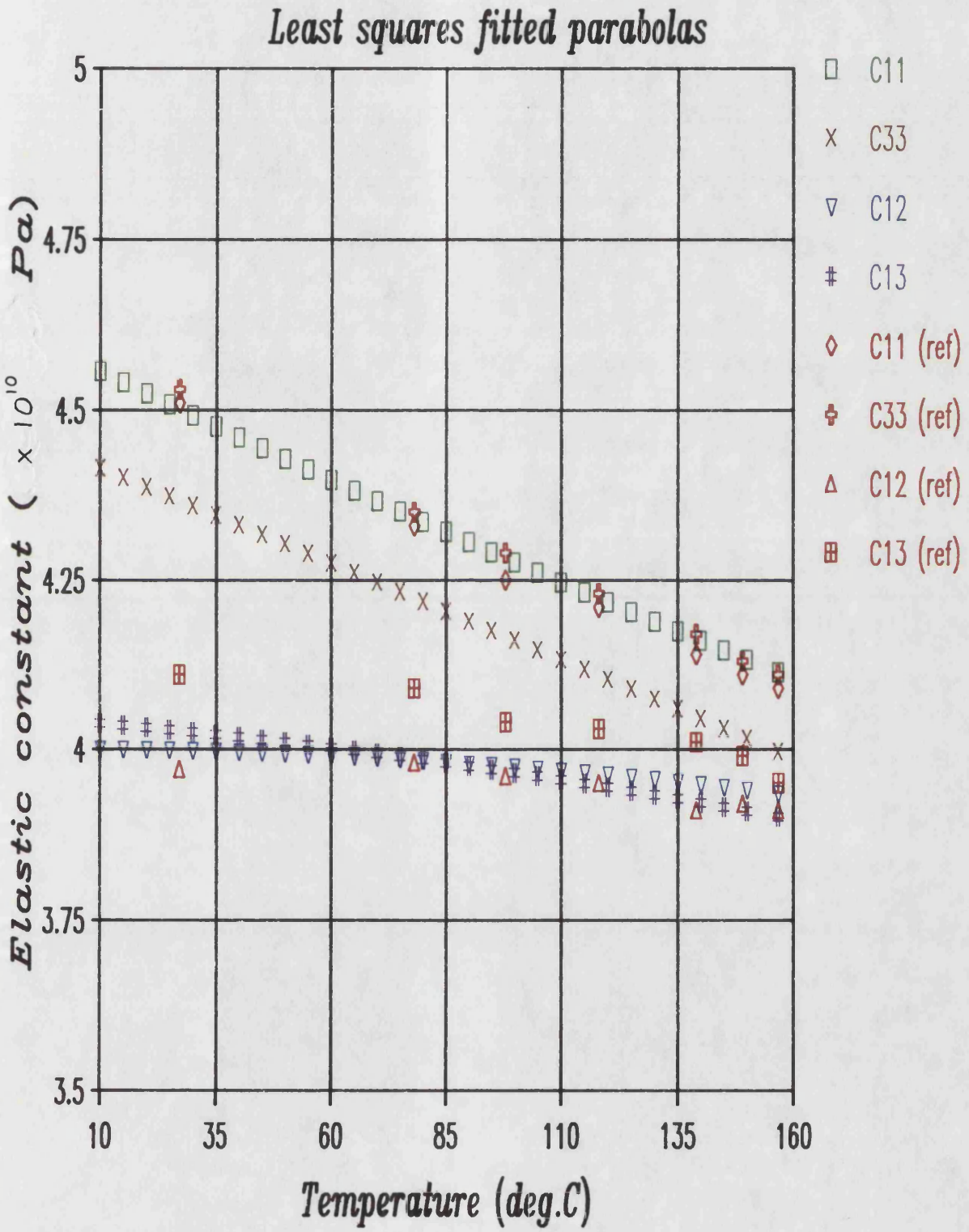

Fig.4.18 SOEC's vs Temperature

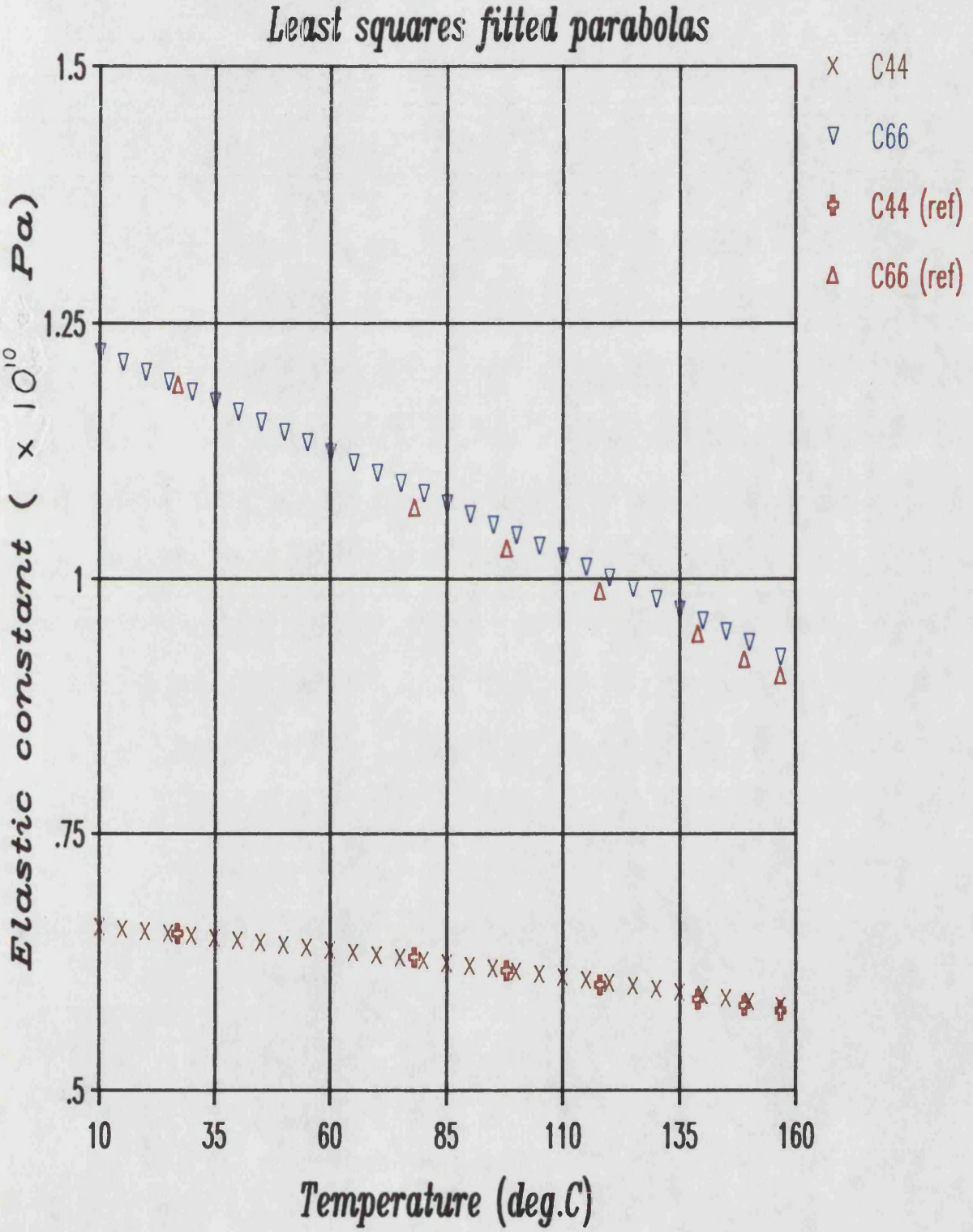

structure . If indium were cubic the above equation would reduce to the more familiar expression ;

$$\rho V^2 = (C_{11} - C_{12})/2$$

Figures 4.19 and 4.20 show the temperature dependences of the bulk modulus , B^S, and volume compressibility , χ^S, of indium within the measured temperature range . These values were calculated from values of second order elastic compliances , S_{ij} , obtained by inverting the second order elastic constant matrix , ie

$$= 2S_{11} + S_{33} + 2(S_{12} + 2S_{13})$$

and $$B^S = 1/\chi^S$$

Fig.4.19 Plot of Bulk Modulus vs temperature

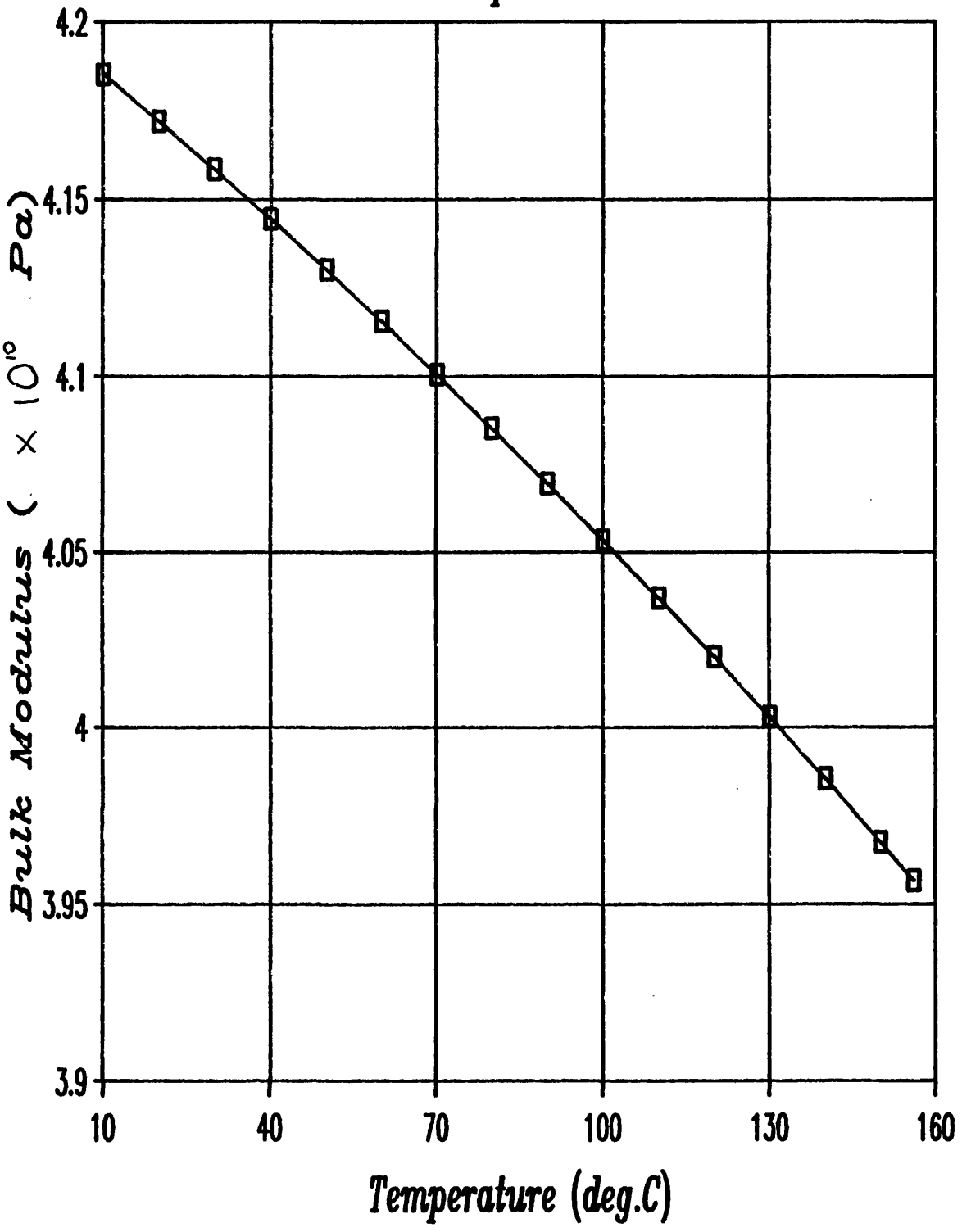

Fig.420 Plot of Volume Compressibility vs temperature

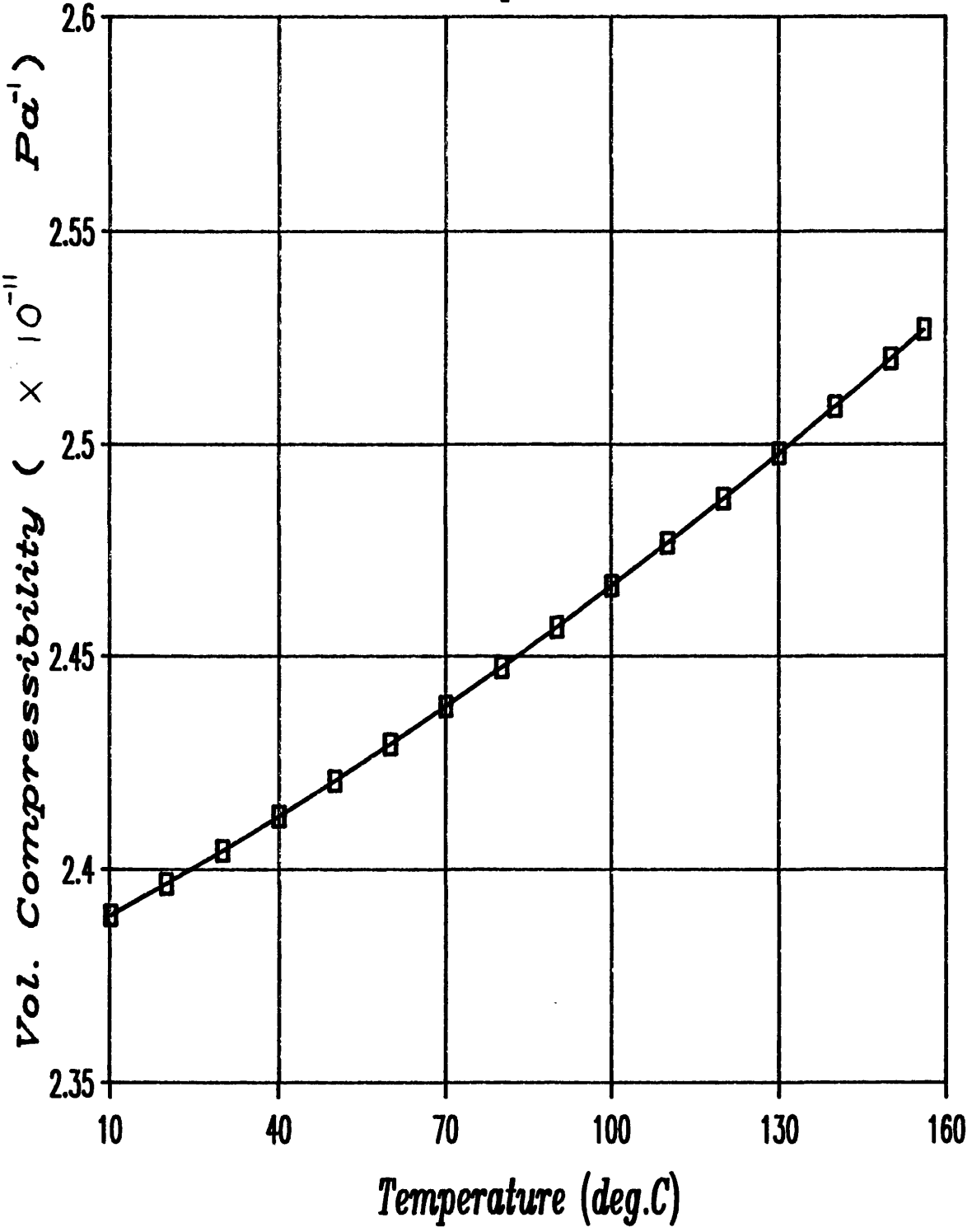

4.4 PRESSURE DERIVATIVES OF SOECs

The hydrostatic pressure derivatives of the SOECs of indium have been calculated from the pressure responses of ultrasonic propagation velocities using equations given in section 2.4 (Thurston [1965]) . Pressure derivative values at room temperature are given in table 4.5 where they are compared with values obtained for an In - 3.4 at% Cd alloy (Madhava and Saunders [1977] , Dr. Y.K.Yogurtcu [private communication]) . This alloy was face centred tetragonal in structure and had a c/a ratio of about 1.05. There is a progressive reduction in c/a ratio from the value of 1.08 for pure indium with increasing Cd content in the alloy , and by the time more than about 4-5 at% Cd has been added the alloy is cubic , (Madhava and Saunders [1977]).

The first thing to note is that all pressure derivative values measured were positive , indicating that application of pressure tends to stabilize the tetragonal phase , ie it stiffens as you press it . It has been shown previously (Gunton and Saunders [1976]) that this is true also for a fct indium-thallium alloy , while pressure tends to drive the fcc alloys (with some negative pressure derivatives) towards a shear assisted displacive phase transition .

All of the mode pressure derivatives for indium continue

TABLE 4.5

Comparison between elastic constant data for indium (present study) and In-3.4 at % Cd (Madhava [1977] and Y.K.Yorgurtcu [private communication]) at room temperature.

	In	In-3.4 at % Cd	
C_{11}	4.50	4.48	($\times 10^{10}$ Pa)
C_{33}	4.37	4.41	"
C_{44}	0.65	0.68	"
C_{66}	1.19	1.12	"
C_{12}	4.00	4.10	"
C_{13}	4.03	4.05	"
$(C_{11}-C_{12})/2$	0.25	0.19	"
B	4.16	4.17	"
$\partial C_{11}/\partial P$	5.56 ($\pm$ 0.10)	7.39	
$\partial C_{33}/\partial P$	5.56 ($\pm$ 0.10)	5.98	
$\partial C_{44}/\partial P$	0.99 ($\pm$ 0.02)	1.10	
$\partial C_{66}/\partial P$	2.02 ($\pm$ 0.04)	1.96	
$\partial C_{12}/\partial P$	4.37 ($\pm$ 0.20)	6.30	
$\partial C_{13}/\partial P$	4.48 ($\pm$ 0.40)	4.91	
$\partial((C_{11}-C_{12})/2)/\partial P$	0.59 ($\pm$ 0.02)	0.54	

to be positive as the temperature is increased , as shown by the experimental results displayed in figures 4.21 to 4.26 . Figures 4.27 and 4.28 show the temperature dependences of the pressure derivatives of all six SOECs , which are also seen to remain positive within the temperature range studied . The values plotted on these graphs were calculated from the equations of curves fitted to experimental data . Table 4.6 gives the best fits to an equation of the form $C = aT + bT^2 + c$.

It is interesting to note that most of the hydrostatic pressure derivative plots (other than those for the slow shear modes) show an upward trend as the melting point is approached . This shows that as the temperature increases and the SOECs decrease , the application of hydrostatic pressure becomes ever more effective as a means of stiffening the structure .

The pressure derivatives for the two slow shear modes measured ($\underline{k}[110],\underline{e}[1\bar{1}0]$ and $\underline{k}[101],\underline{e}[\emptyset]$) tended to show a flat temperature response from room temperature right up to near the melting point (figs 4.25 and 4.26) . However, there was some indication of a substantial fall in value of pressure derivative for the $\underline{k}[110],\underline{e}[1\bar{1}0]$ mode just before melting. Unfortunately this particular effect was only observed on one set of measurements (other runs on this mode and the $\underline{k}[101],\underline{e}[\emptyset]$ mode did not achieve the same temperature) . This , combined with the fact that results taken going back down in temperature did not agree

Pressure derivative	a	b	c
C_{11}'	-6.094×10^{-3}	6.207×10^{-5}	5.681
C_{33}'	-1.660×10^{-2}	1.236×10^{-4}	5.900
C_{44}'	-1.333×10^{-3}	1.658×10^{-5}	1.017
C_{66}'	-2.474×10^{-3}	2.192×10^{-5}	2.067
C_{12}'	-6.739×10^{-3}	7.988×10^{-5}	4.491
C_{13}'	-1.186×10^{-2}	1.010×10^{-4}	4.718
$\frac{1}{2}(C_{11}'-C_{12}')$	3.275×10^{-4}	-8.932×10^{-6}	0.595
$(\rho V^2)'$ 011 slow shear	2.214×10^{-4}	-3.859×10^{-6}	0.537

Table 4.6 Temperature dependences of the pressure derivatives of the elastic constants of indium, in temperature range 10 - 156 deg.C. Obtained by fitting least squares parabola to experimental data; $C' = aT + bT^2 + c$

Fig.4.21 Pressure derivative vs temperature

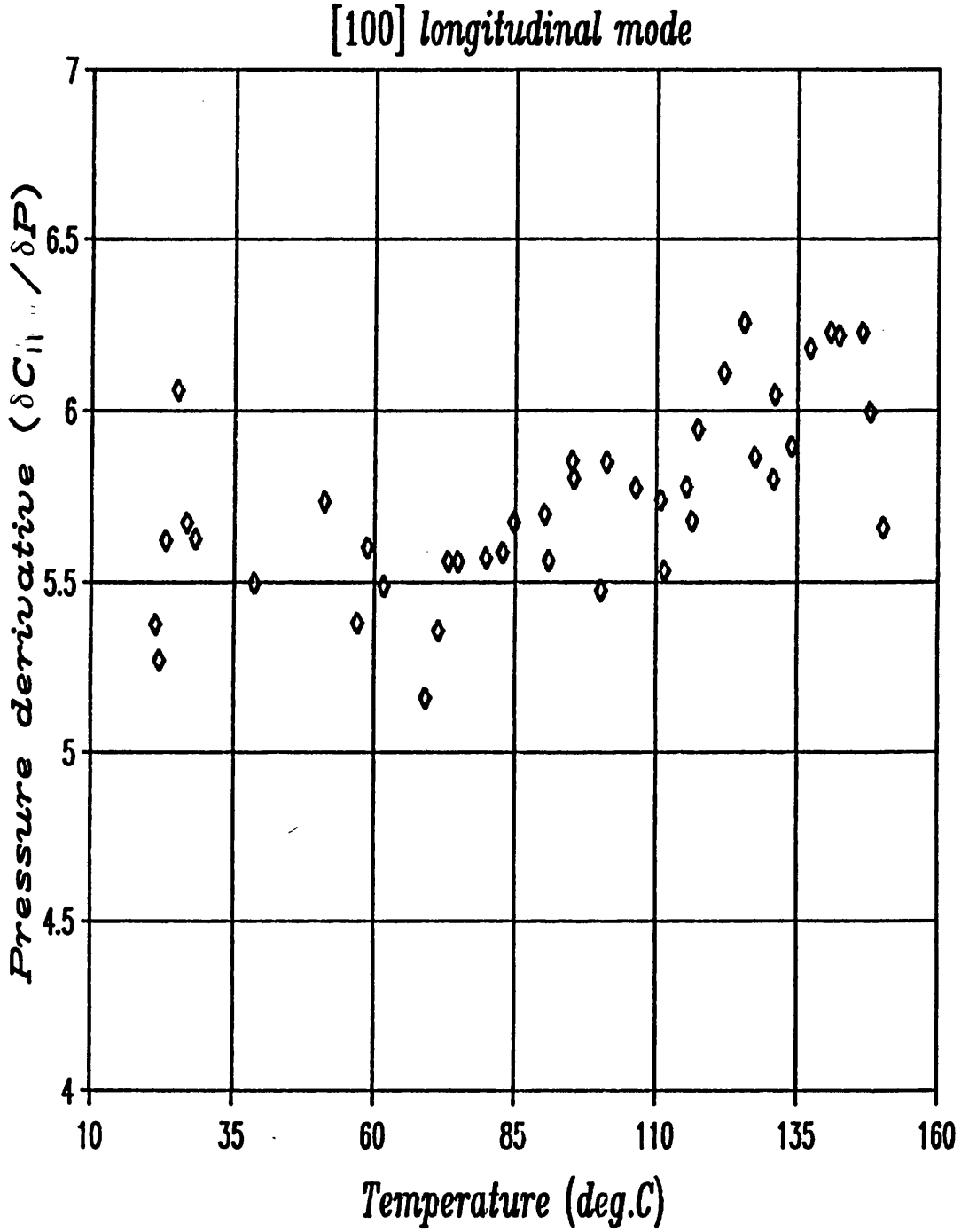

Fig 4.22 Pressure derivative vs temperature

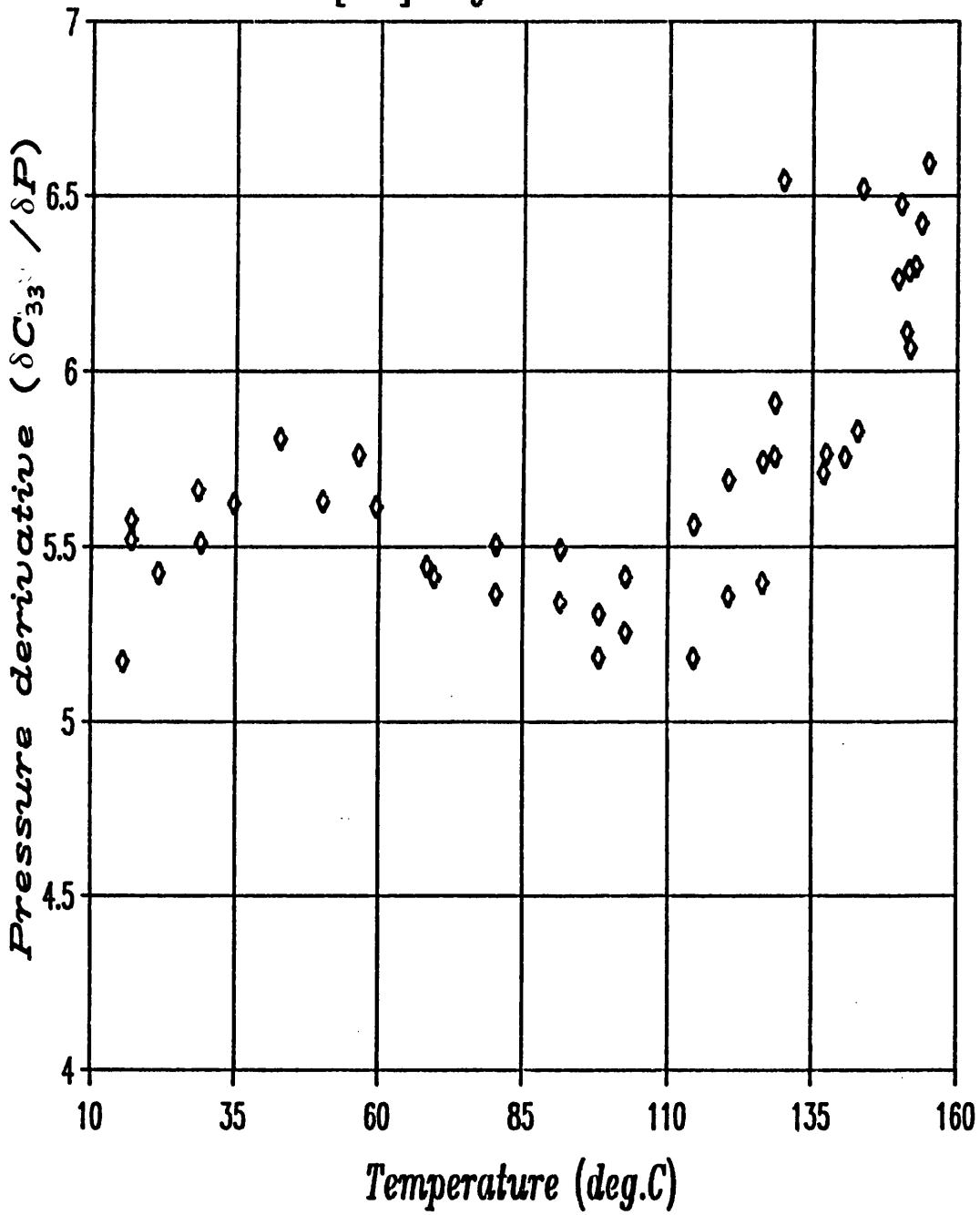

Fig 4.23 Pressure derivative vs temperature

[100]q//[010] shear mode

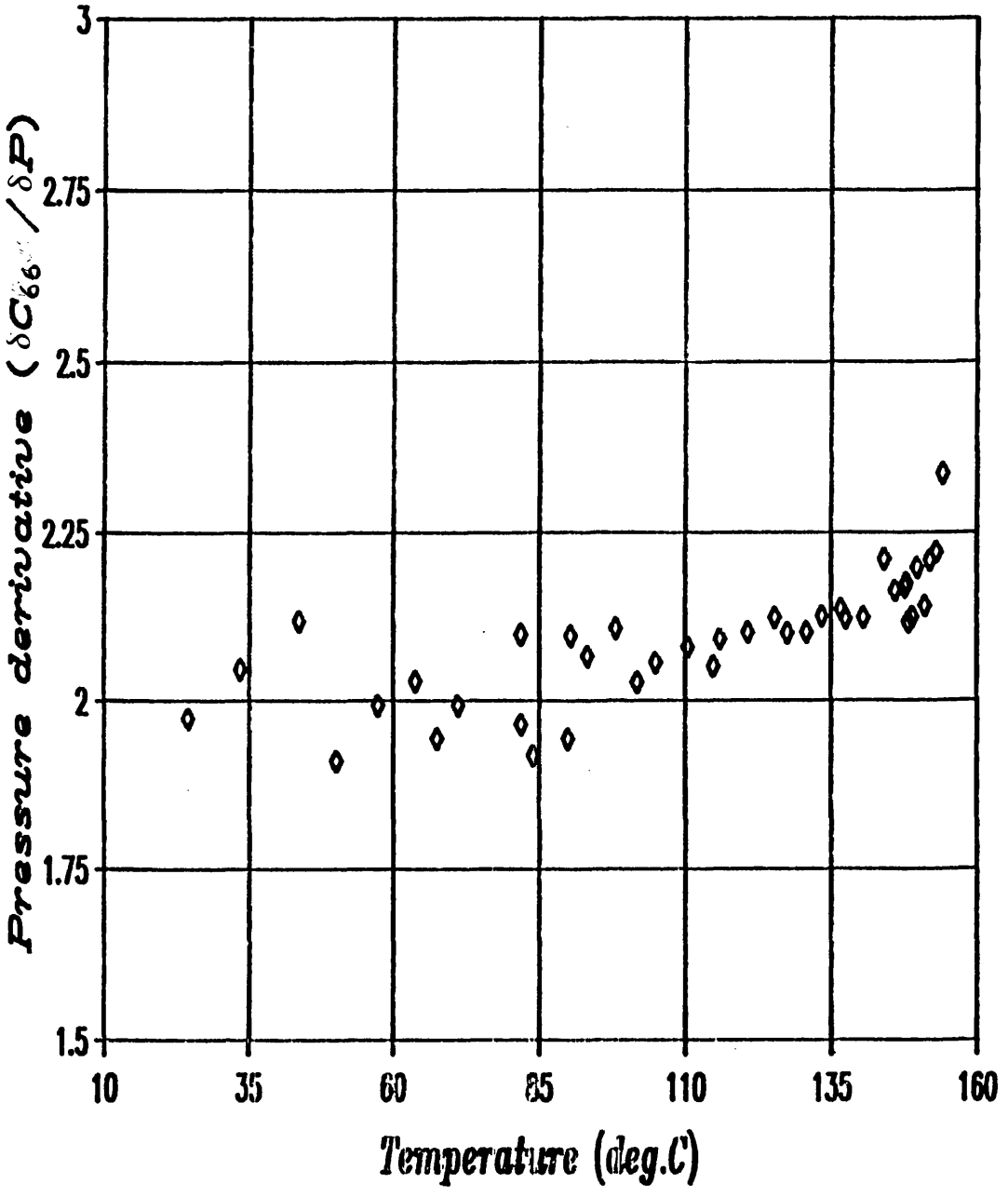

Fig 4.24 Pressure derivative vs temperature

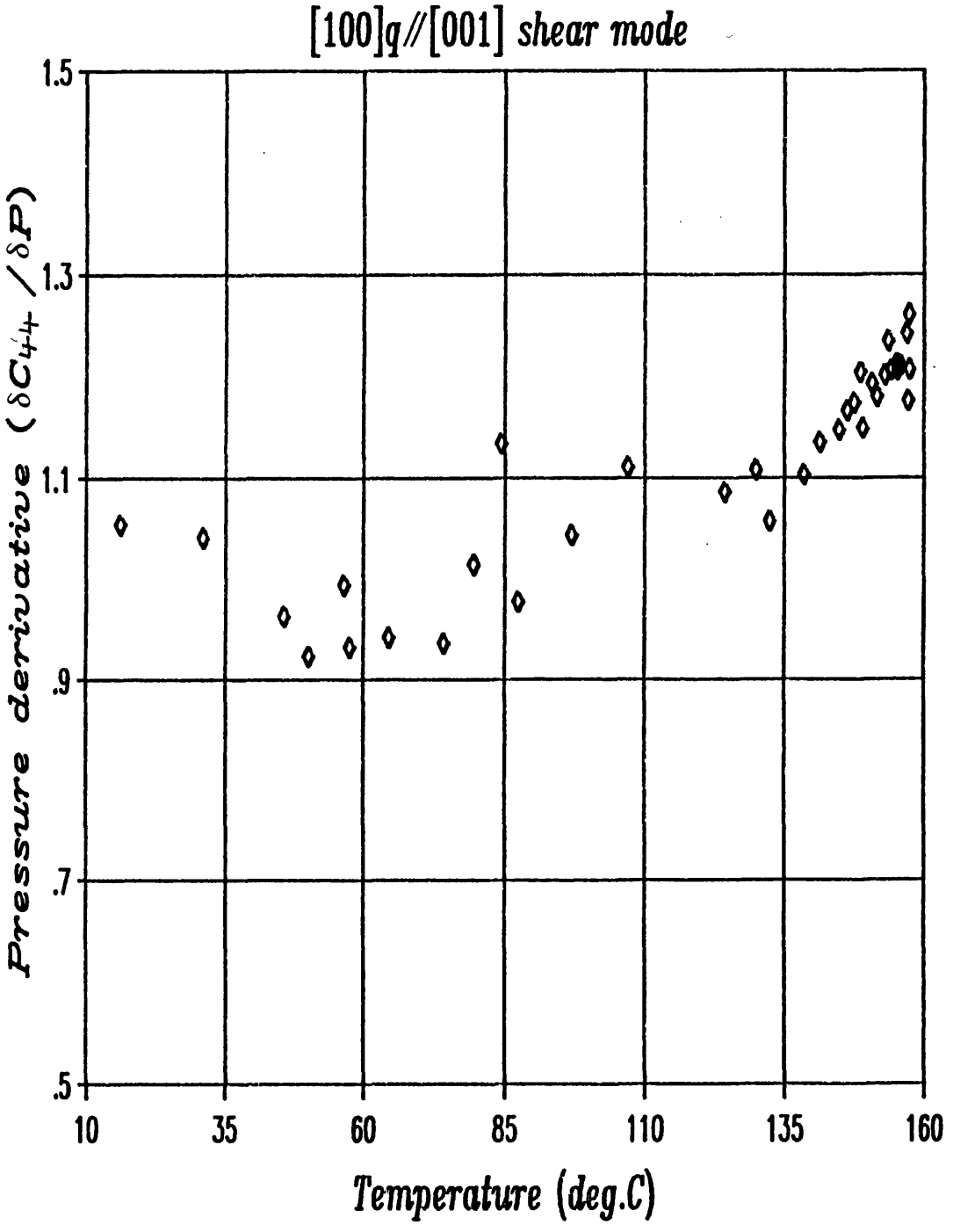

Fig 4.25 Pressure derivative vs temperature

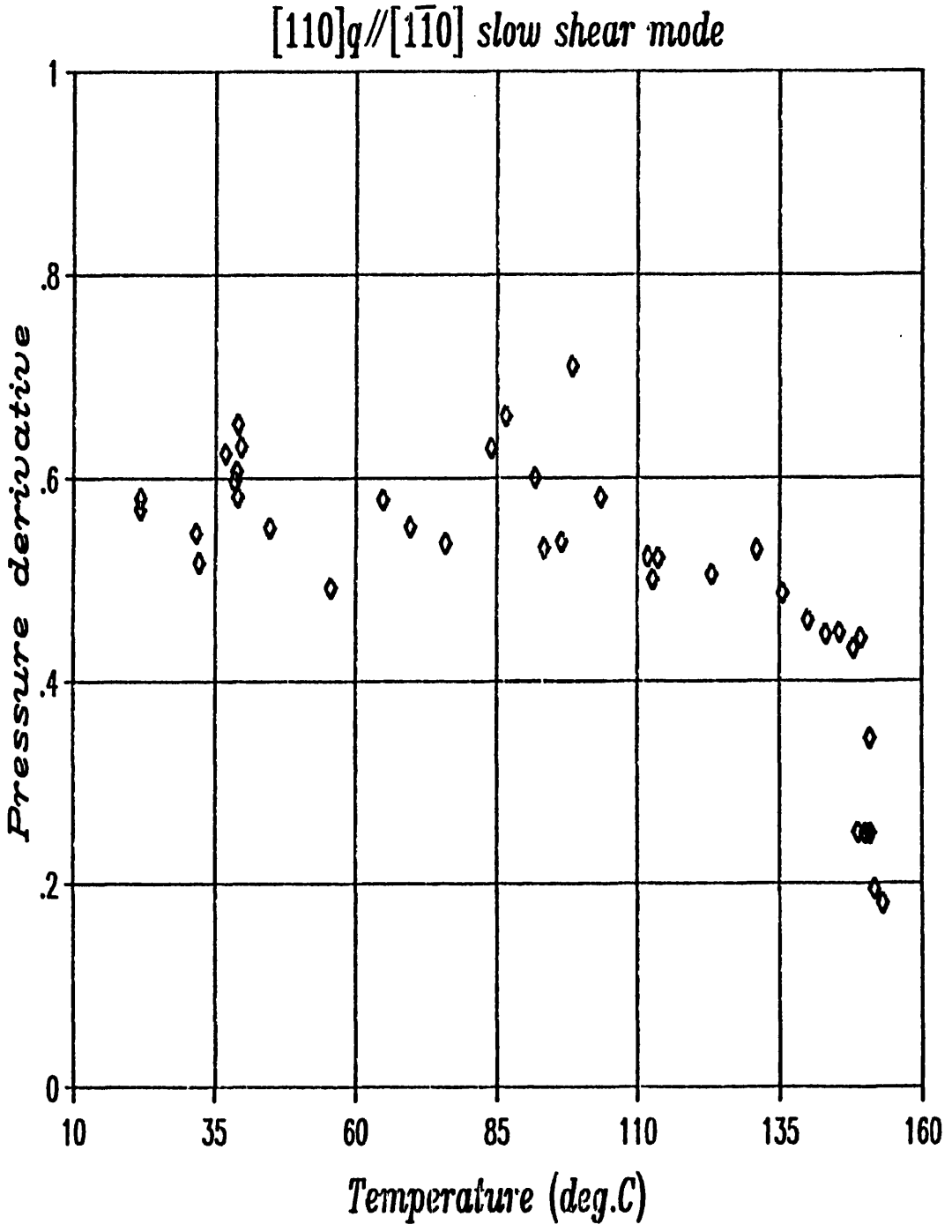

Fig 4.26 Pressure derivative vs temperature

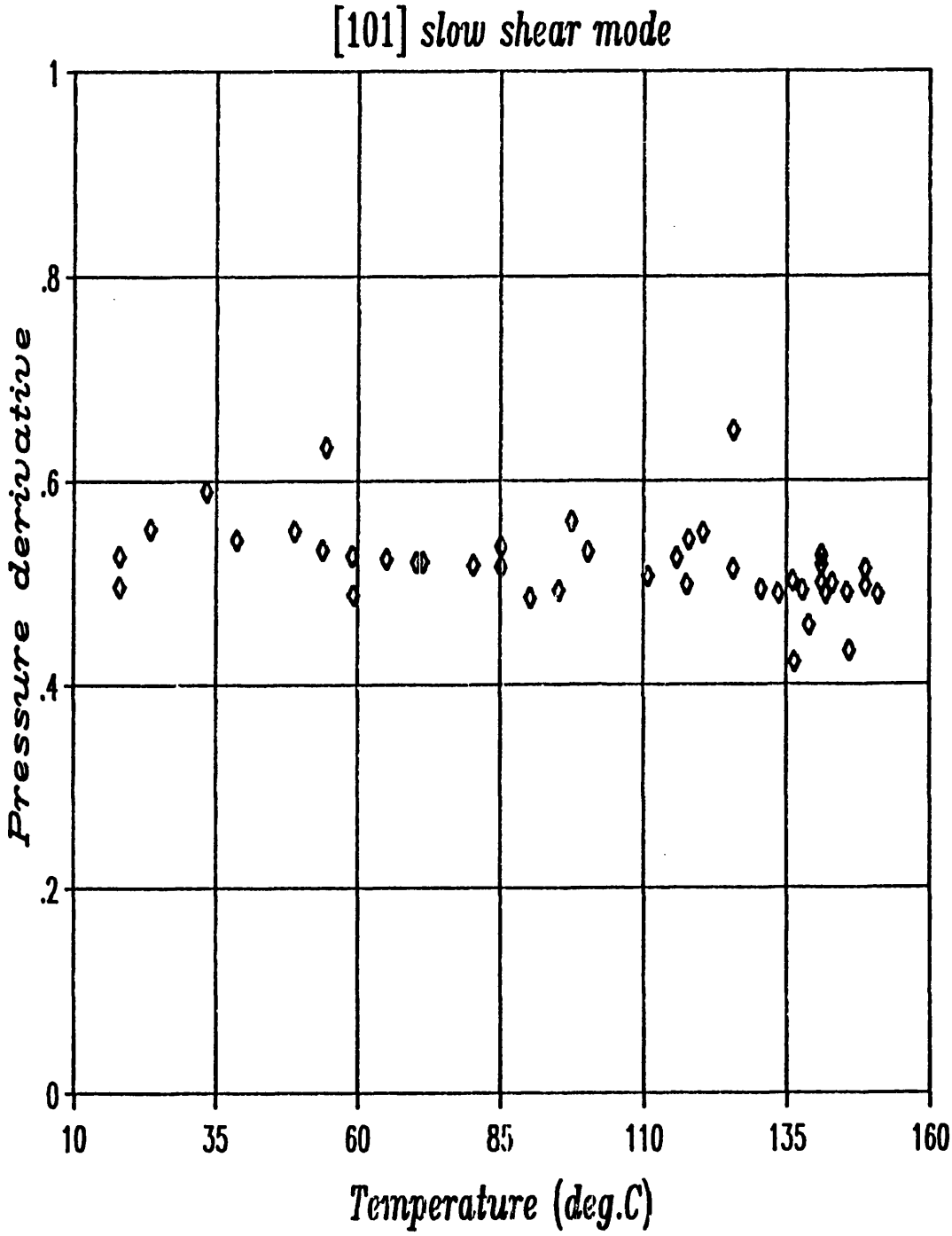

Fig 4.27 Pressure derivatives of SOECs vs temperature

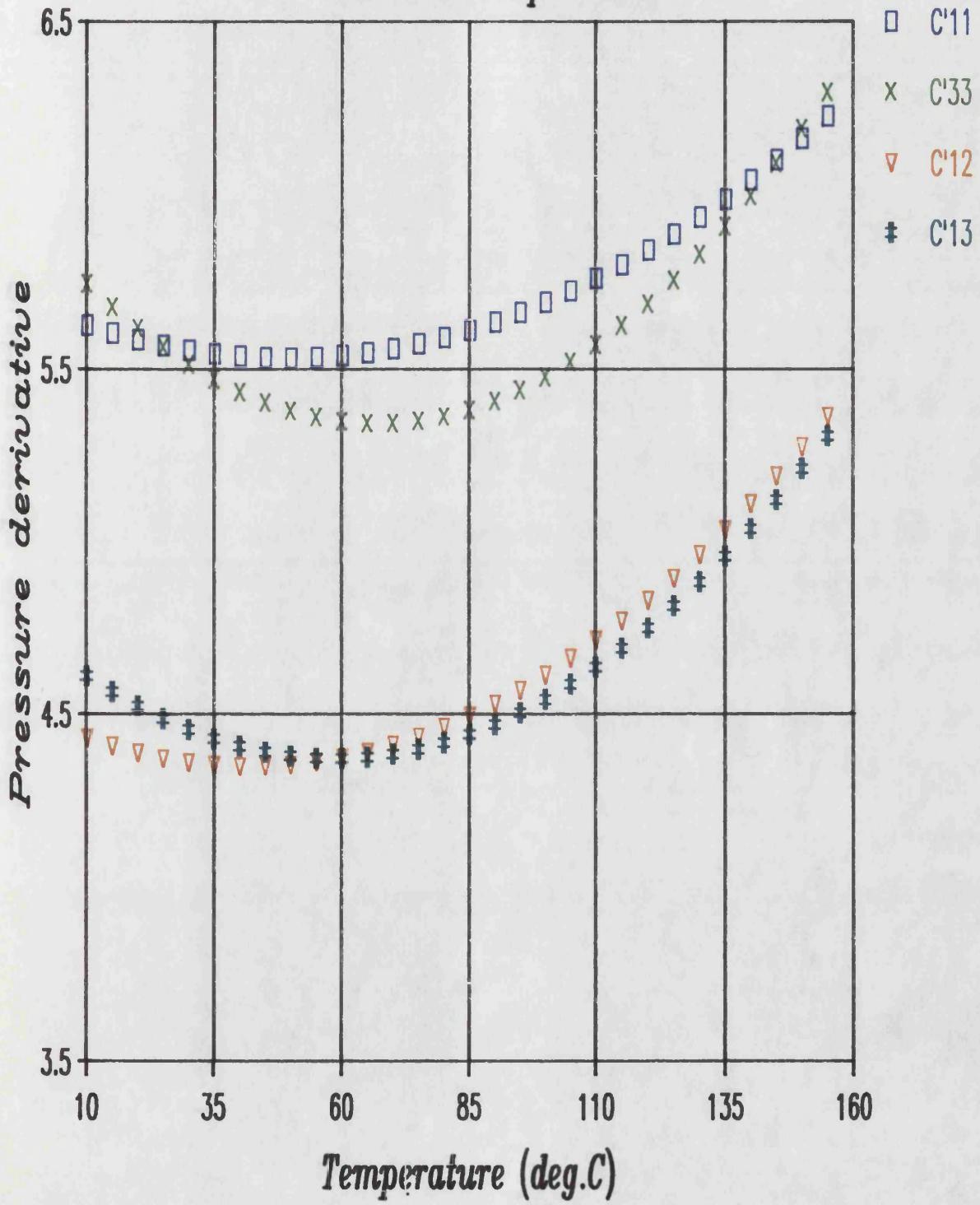

Fig 4.28 Pressure derivatives of SOECs vs temperature

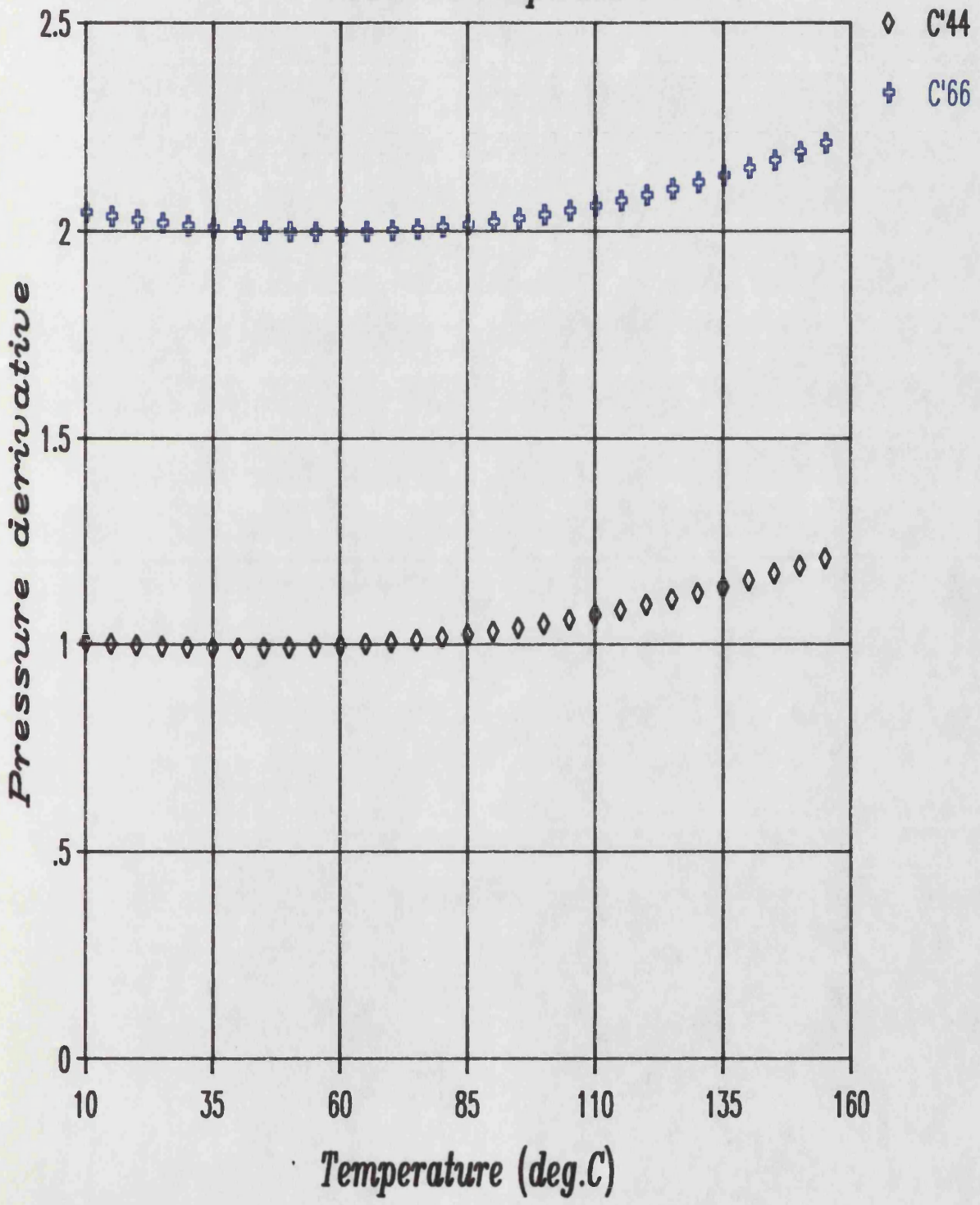

with results taken going up tends to suggest that some irreversible change had taken place near the melting point , and that the validity of these results may be in some doubt . Indeed when the run was finished and the apparatus dismantled it was found that the upper piston had pressed on the sample holder cracking the quartz transducer and denting the sample . The only reason that these results are included here is that while there was not agreement in pressure derivative results going up and coming down in temperature the values obtained for SOECs matched very well , possibly lending some plausibility to the high temperature data .

In general results for most modes were reproducable from run to run , both with increasing and decreasing temperature .

4.5 GRUNEISEN PARAMETERS

Values of acoustic mode Grüneisen parameters have been obtained from the thermodynamic pressure derivatives of SOECs . The relationship between 'effective' pressure derivatives (as measured here) and thermodynamic pressure derivatives is given by Thurston [1965] , and the particular relations for a tetragonal (4/mmm) structure are listed by Tu Hailing [1982] , and also shown in section 2.5 . The calculations that needed to be done to convert to the appropriate values were carried out within the analysis program listed in appendix A .

To be able to calculate mode Grüneisen parameters in any direction in the indium structure data on the pressure responses of all six independent SOECs was required . The data presented in the preceding section provided enough information for values of all six thermodynamic pressure derivatives to be calculated at any temperature between room temperature and about 156 deg.C .

Figure 4.29 compares the acoustic mode Grüneisen parameter values obtained for indium at room temperature with those found at 156 deg.C .

Values of Grüneisen parameters have been calculated here using the measured adiabatic elastic constant data rather than the required isothermal values (Thurston [1967]) .

Fig. 4.29 Plot of Mode Gruneisen Parameters against Propagation Direction

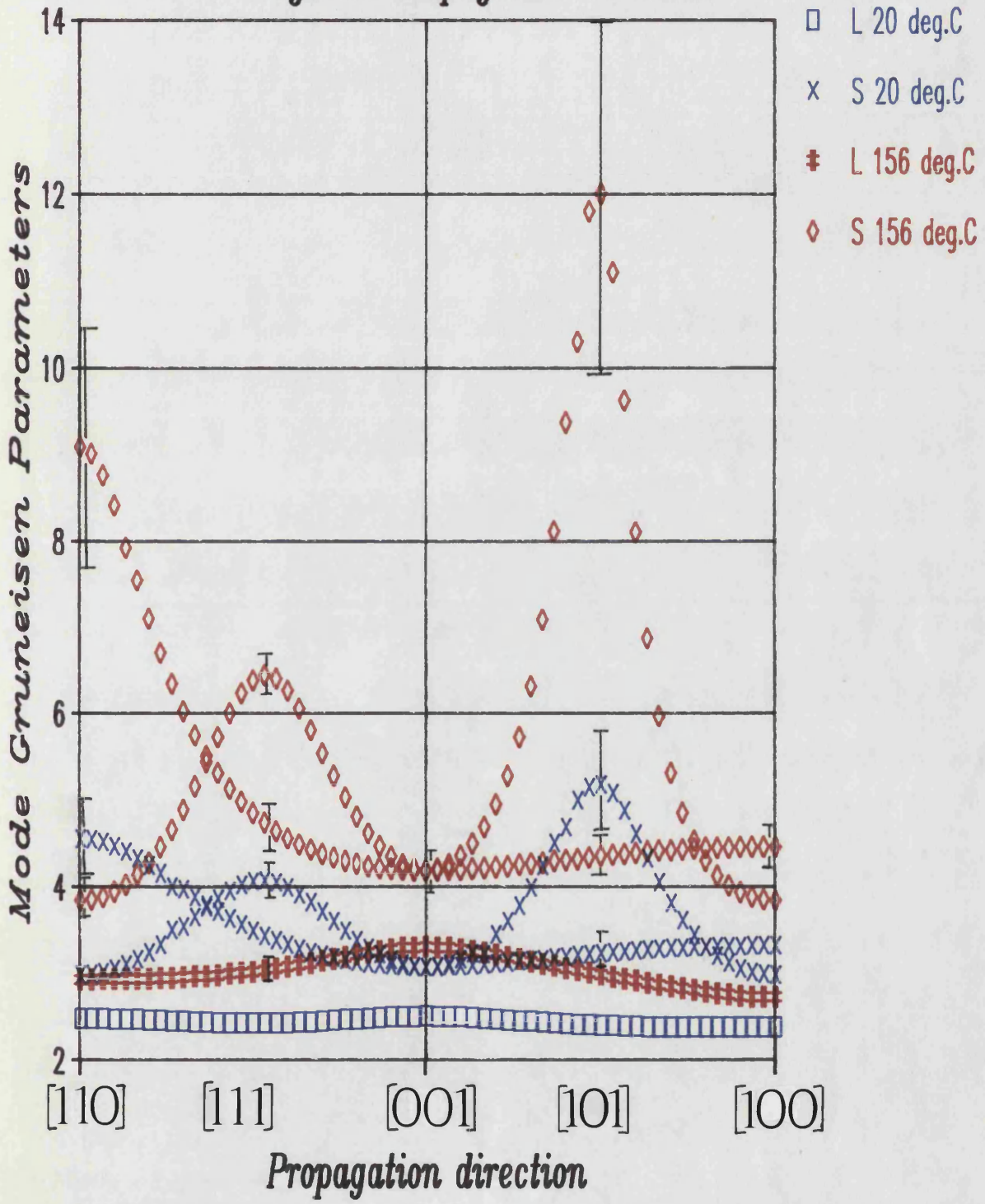

This was done partly to ease calculation , but mainly because no data had been found in the literature giving values of the specific heat of indium up to high temperature .

Calculations using the specific heat of indium at room temperature showed that , at that temperature , the differences between adiabatic and isothermal values of SOECs were small when compared with experimental errors . In the absence of high temperature data it was assumed that this was still the case at temperatures approaching the melting point. Since the original calculations were done results of measurements of the specific heat of indium up to near the melting point have been found (Kramer and Nölting [1972]). This data (shown in fig 4.30) has been used , along with thermal expansion results (Graham et al [1955]) , to show that even at temperatures near the melting point of indium there seem to be only marginal differences between adiabatic and isothermal values .

The conversion between adiabatic and isothermal values was done using a method described by Thurston [1967], and some worked examples are given as illustration of this method in appendix B .

The calculated values for the shear mode Grüneisen parameter close to the $\underline{k}[101],\underline{e}[\emptyset]$ mode are very sensitive to quite small changes in values of elastic constants . This is because the value of ω in the mode

Fig 4.30

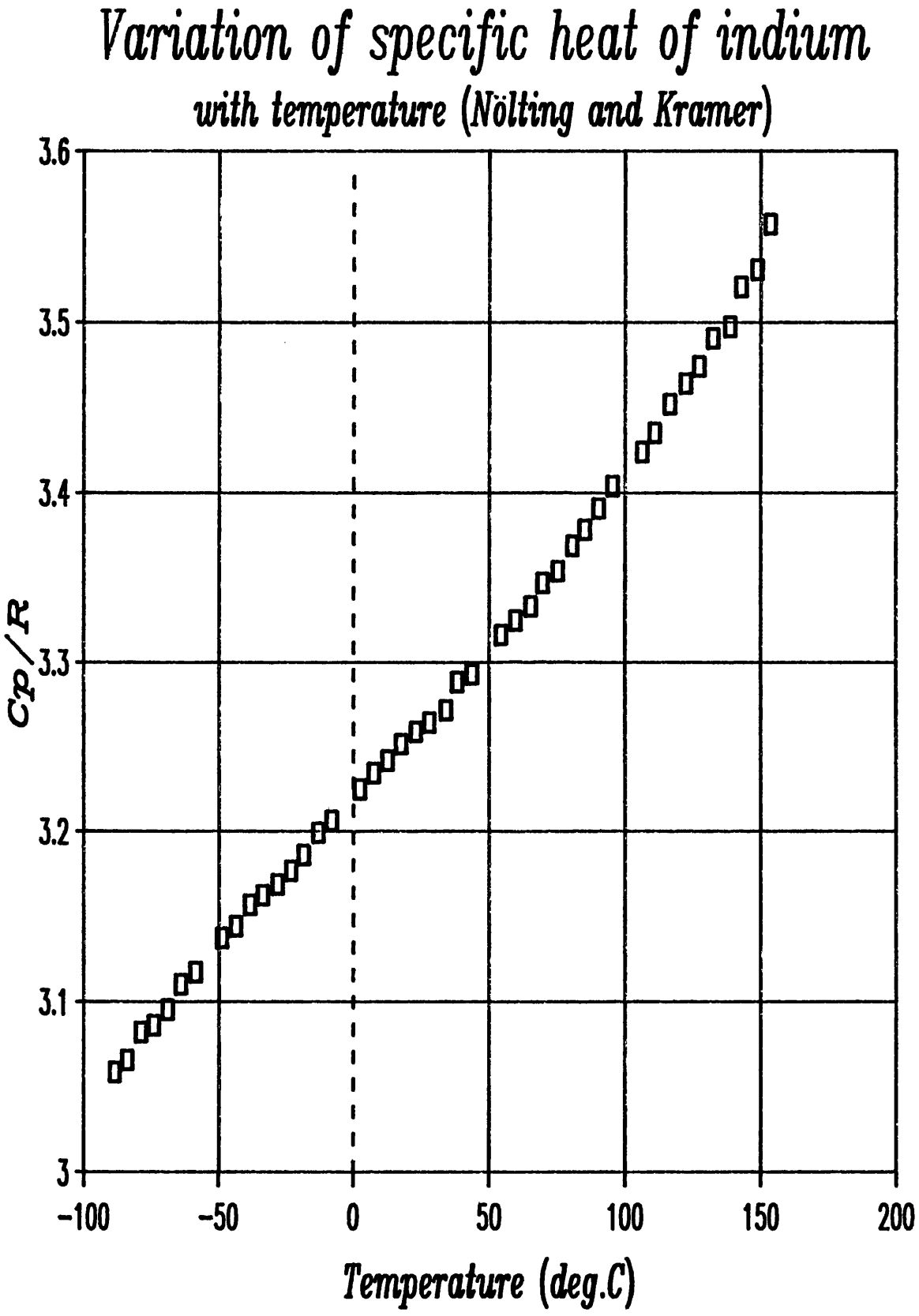
Variation of specific heat of indium
with temperature (Nölting and Kramer)
3.6
3.5
3.4
3.3
3.2
3.1
3
Cp/R
-100
-50
0
50
100
150
200
Temperature (deg.C)

Grüneisen parameter equation for this direction (section 2.5) is given by the relation ;

$$\omega = C_{11}(N_1 U_1)^2 + C_{33}(N_3 U_3)^2 + 2C_{13}(N_1 N_3 U_1 U_3)$$

As indium is nearly cubic the values of N_1 , N_3 , U_1 , and U_3 are of approximately the same size (although U_3 is negative) , and the values of C_{11} , C_{33} , and C_{13} are also very nearly the same . This means that the value of ω is essentially given by the difference between two quite similar numbers (the mode Grüneisen parameter equation is ill-conditioned for this mode) . The calculated values came out as being small but positive leading to a large positive mode Grüneisen parameter , but with some adjustment of the values of the elastic constants within their error limits (C_{13} has quite large error limits as its calculation involves a number of other elastic constants) it is possible to make ω a small negative number leading to a large negative mode Grüneisen parameter . In fact early work at room temperature (Flower et al [1985]) did suggest a negative value for this mode (see also section 5.5).

The values given here for acoustic mode Grüneisen parameters have benefitted from the large amount of data that has been collected over a wide temperature range . This allowed curves to be fitted , providing a means of calculating mode Grüneisen parameter values at any particular temperature with greater confidence . Also the

results shown for the $\underline{k}[101],\underline{e}[\emptyset]$ mode compare favourably with the results for the $\underline{k}[110],\underline{e}[1\bar{1}0]$ slow shear mode (which is less sensitive) .

The $\underline{k}[101],\underline{e}[\emptyset]$ slow shear mode shows the largest value for any mode Grüneisen parameter and it also shows the biggest increase in value between room temperature and the melting point (Fig 4.29) . A plot showing the temperature response for this mode's Grüneisen parameter , and comparing it with the results for the other mode Grüneisen gammas in the [101] direction , is included here (Fig. 4.31) to show how the slope of the response changes with temperature . The mode Grüneisen gamma for the $\underline{k}[101],\underline{e}[\emptyset]$ mode does show a steeper temperature gradient than the other modes and the gradient increases quite rapidly as the melting point is approached .

Summing over the mode Grüneisen parameters it is possible to obtain average shear and longitudinal Grüneisen parameters , and an overall mean value . This has been done over the range of temperatures between room temperature and the melting point , and the results are shown in figure 4.32 .

The data published by Kramer and Nölting [1972] for the specific heat of indium at temperatures approaching the melting point (Fig 4.30) combined with values for volume compressibility , taken from the present study , have allowed the thermal Grüneisen parameter to be

Fig 4.31 Temperature response for [101]

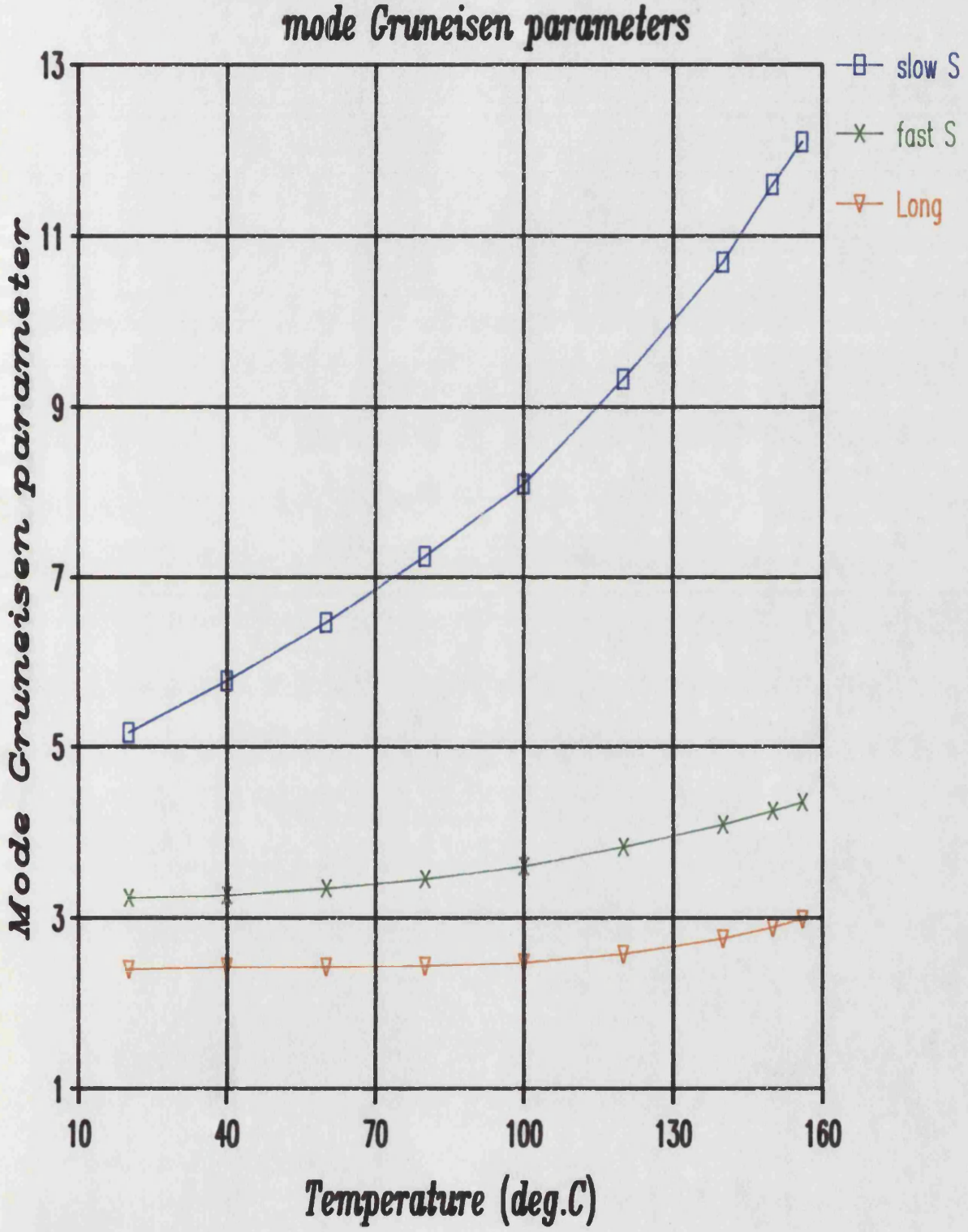

Fig 4.32 Mean Gruneisen parameters

plotted against temperature

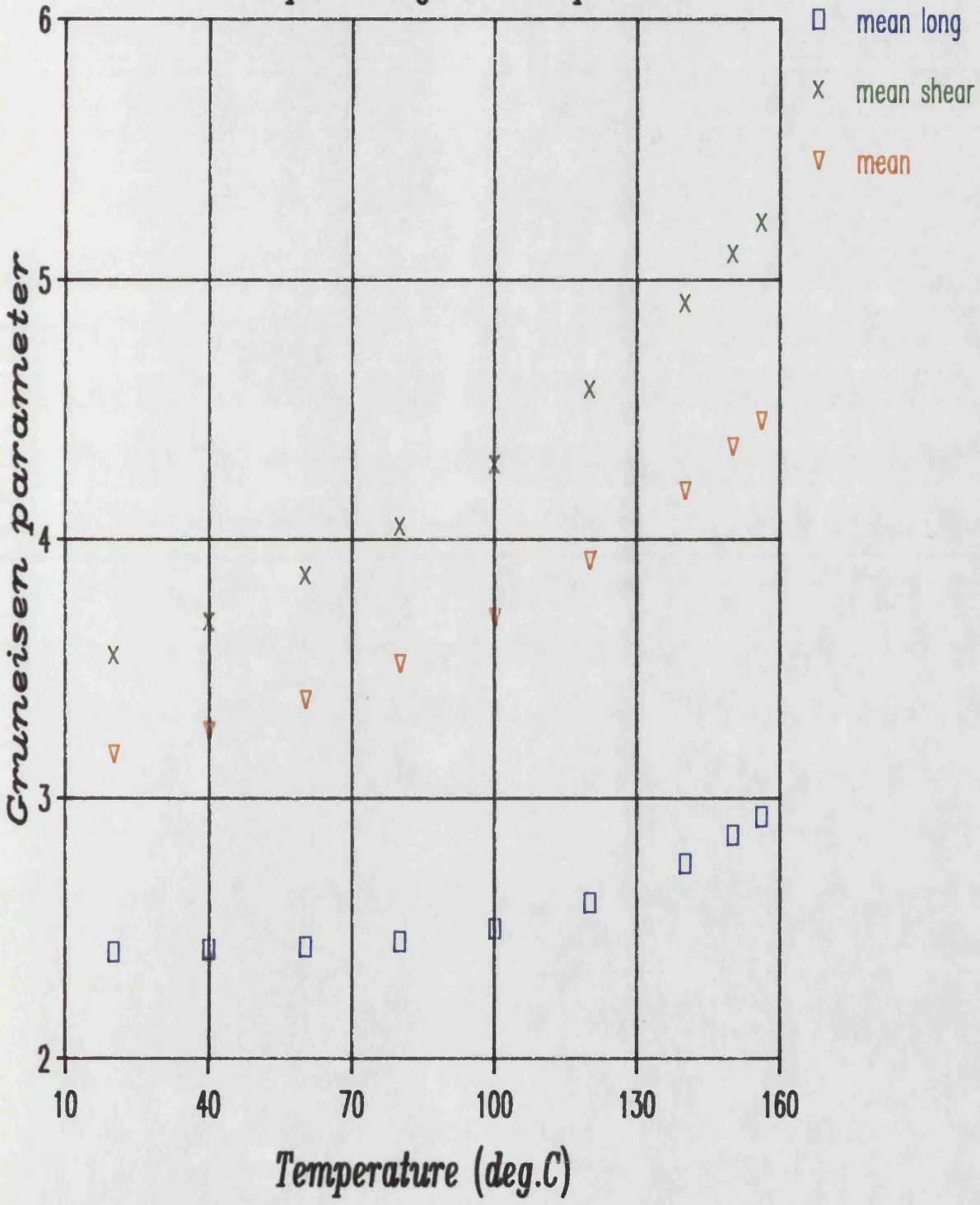

calculated at high temperatures . The values obtained are shown graphically in fig. 4.33 where they are compared with the mean mode Grüneisen parameter .

Fig 4.33 Comparison of mean and thermal

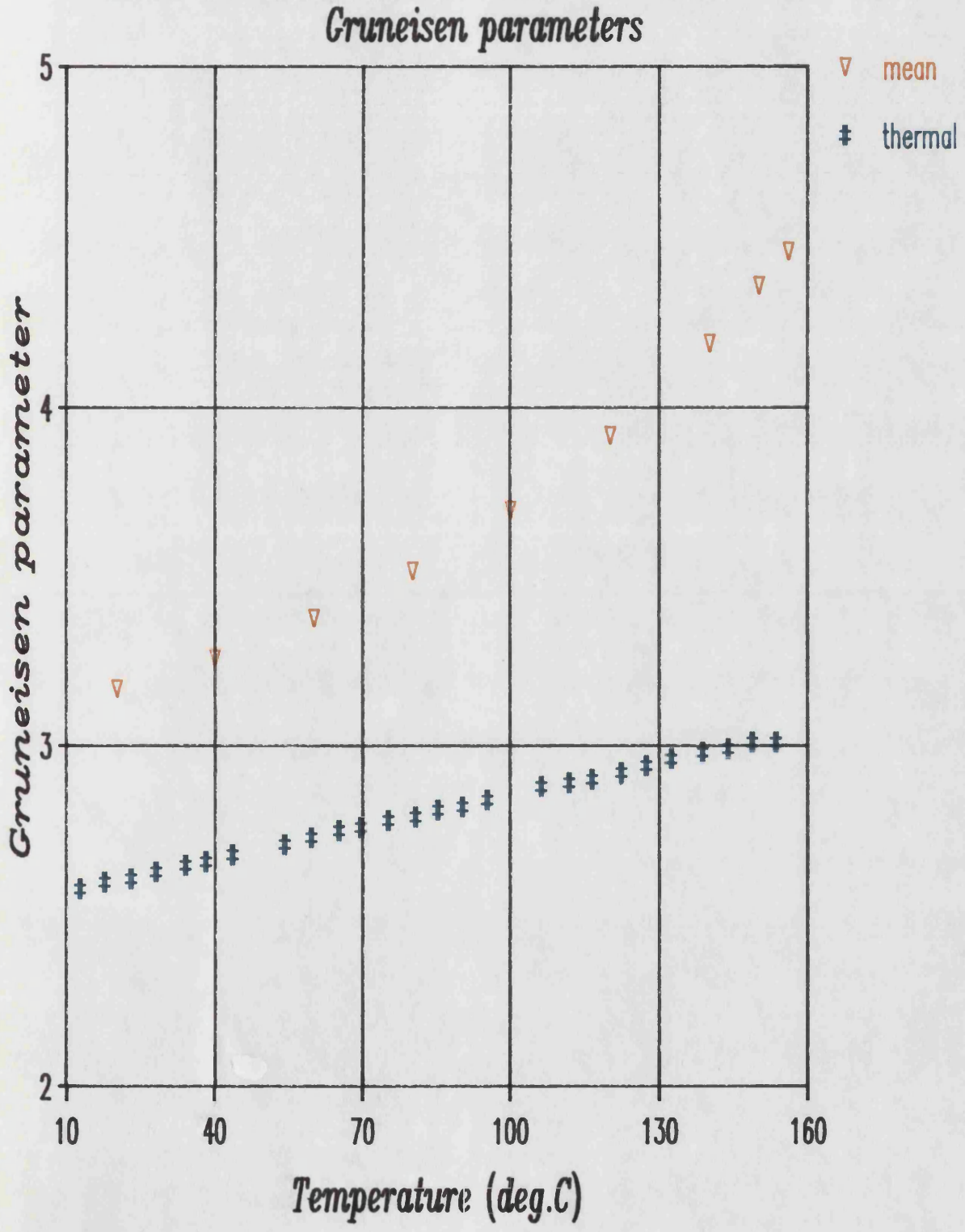

DISCUSSION

5.0 DISCUSSION

5.1 INTRODUCTION

The data obtained from this study of the elastic properties of indium has allowed the complete set of six second order elastic constants (SOECs), and their pressure derivatives , to be calculated for temperatures between room temperature and about 154 deg.C (close to the melting point of indium 156.7 deg.C) . These parameters were used to obtain values for acoustic mode Grüneisen parameters in the long wavelength limit over the same temperature range . This characterises aspects of the element's vibrationally anharmonic behaviour as the melting transition is approached . In the past many of the theories trying to relate crystal lattice instability with melting have stressed the need for more information about anharmonic behaviour near the melting point . Such information could help in gaining a better understanding of the actual mechanism of the melting process .

Where possible results are discussed in relation to previous work and compared with previously published data. Results presented here for the SOECs of indium show good agreement with previously published data , lending extra confidence to pressure derivative results and calculated mode Grüneisen parameter values (for which no previous data is available over the temperature range studied) .

5.2 PROPAGATION VELOCITIES

The values measured for ultrasonic propagation velocities through single crystal indium were in good agreement with data from previous work on indium and indium alloys (Chung et al [1976], Vold et al [1977], and Madhava [1977]) . The temperature responses for the various mode velocities were generally smooth curves showing decreasing velocities with increasing temperature. This is the normally expected behaviour and arises from vibrational anharmonicity . Sound waves generally travel more slowly through a material whose constituent atoms or molecules are more spread out and less tightly bound to one another . The velocity versus temperature curves all show a slight decrease in gradient as the temperature is increased but there are no discontinuities or unusual trends close to the melting point .

The velocity surface plots in Fig 4.4 show that for indium the slowest propagation mode is the shear mode propagated ($\underline{k}$) along the [101] direction and polarised ($\underline{e}$) along $\emptyset$ (close to the $[10\bar{1}]$ direction) which is appreciably slower than that propagated along the [110] direction and polarised $[1\bar{1}0]$. This might be expected as an atom trying to vibrate in a [101] type direction would see a greater interatomic spacing than in any other direction.

The results shown in (table 4.5) for indium - 3.4 at.% cadmium at room temperature (Madhava [1977]) give propagation velocities for the two slow shear modes which are almost identical:

$$V_{\underline{k}[110],\underline{e}[1\bar{1}0]} = ((C_{11} - C_{12})/2\rho)^{\frac{1}{2}} = 509.6 \text{ m/sec} \qquad (5.1)$$

$$V_{\underline{k}[101],\underline{e}[\emptyset]} = (\{A - (A^2 - B + C^2)^{\frac{1}{2}}\}/2\rho)^{\frac{1}{2}} \qquad (5.2)$$

$$= 519.5 \text{ m/sec} .$$

This shows that alloying with cadmium leads to an appreciable stiffening of the $\underline{k}[101],\underline{e}[\emptyset]$ shear mode whilst softening the $\underline{k}[110],\underline{e}[1\bar{1}0]$ shear mode . It is the $\underline{k}[110],\underline{e}[1\bar{1}0]$ shear mode softening that has previously been connected with structural phase transitions (Madhava and Saunders [1977] , Gunton and Saunders [1974]) . Soft modes are discussed further in section 5.3 .

The slower $\underline{k}[101],\underline{e}[\emptyset]$ mode for indium suggests that this is probably the mode of greatest interest as it is likely to be the one exhibiting the most anharmonicity . For any mode the slope of the velocity versus temperature curve reflects the anharmonicity in the binding forces appropriate to that mode . The two slow shear modes have very similar temperature dependences which are much steeper than the slopes measured for the other modes . This indicates that the atomic displacements associated with the slow shear modes are those most subject to anharmonic forces .

No mode velocities are seen to tend towards zero as the melting point is approached which would be a requirement for meeting the Born criterion for melting (Born [1939]) . Although Ida [1969] predicted that as the melting point is approached the observed velocity versus temperature response should fall measurably below the normal almost linear relationship , none of the modes measured here show any significant decrease in mode velocity close to melting .

5.3 ELASTIC CONSTANTS

The results shown in section 4.3 for the temperature responses of the SOECs of indium , in the temperature range between room temperature and near the melting point, show good agreement with previously published data (Chung et al [1976] , Vold et al [1977] and Winder and Smith [1958]) . The results also agree with previous findings (Madhava and Saunders [1977] , Chung et al [1976]) showing that while the slow shear modes in indium soften considerably as the melting point is approached , the mode elastic constants ($(C_{11} - C_{12})/2$, and $((C_{11} + C_{33})/2 - C_{13})/2$) do not approach zero.

If we were to extrapolate data above the melting point we would find that the slow shear mode elastic constants would only approach zero at a temperature of about 260 deg.C . If it did not melt first this temperature would mark the point at which indium might undergo a structural phase transition (as seen in some indium-thallium and indium-cadmium alloys Chung et al [1976]) . The work of Chung et al [1976] also notes this point and concludes that mode softening does not seem to be a prelude to melting . Their statement was further backed up when they showed that for a cubic In-Tl alloy a slow shear mode elastic constant , that was known to go to zero (within experimental error) at a martensitic phase transition below the melting point , did not decrease again as the

melting point was approached .

The results presented here do not show any vanishing elastic moduli . The temperature responses for all the mode constants show smooth curves right up to the highest temperatures measured (within a few degrees of the melting point) . Thus the elastic constants do not seem to display any precursive influences due to the impending transition . There is also no sign of any unusual changes in the value of volume compressibility as the melting temperature is approached (Fig. 4.20) , an effect observed with some alkali halides (Hunter and Seigel [1942]) .

5.3.1 SOFT MODES

A 'soft' mode is a vibrational mode whose frequency is seen to dramatically decrease with changes in pressure or temperature , and such modes are often connected with structural phase transitions (a mode of vibration whose frequency reduces to zero may simply be thought of as a translation giving rise to a change in structure) .

Previous work on In-Tl alloys (Gunton and Saunders [1973]) has shown that structural transitions can result from the instability of a crystal against a soft mode (the $(C_{11} - C_{12})/2$ slow shear mode in In-Tl) . Landau and Lifshitz [1959] introduced the concepts on which this approach to phase transitions is based , and Cochran

[1960 and 1961] using these concepts realised that the soft mode instability could lead to transition . Reviews on the soft mode aspects of phase transitions may be found in publications by Fleury [1972a and b, 1973, and 1976] and Rehwald [1974] .

Previous studies investigating the possible mechanisms involved in the melting process have tried to link mode softening with the solid-liquid transition (Born [1939] , Herzfeld and Geoppert Mayer [1934]) but experimental work has generally failed to show the required vanishing shear mode elastic constant at the transition . More recent studies (e.g. Jackson and Leiberman [1974] have continued to develop Born's concept and have applied it , with some success , to alkali halides . There are now a large number of theories of melting based around a lattice instability model (eg. Slagle et al [1967], Tallon [1980], Ruffa [1982]), although no one has really succeeded in applying one single theory to a wide range of materials . Further discussion on instability-based melting theories may be found in section 1.1 .

5.4 PRESSURE DERIVATIVES OF ELASTIC CONSTANTS

The way in which acoustic modes behave under hydrostatic pressure is established by the pressure derivatives of the elastic constants . For indium the softest shear mode (k[101],e[Ø]) has a pressure derivative (table 1.1);

$$\delta C_s/\delta P = \delta(A - (A^2 - B + C^2\gamma^2/2)/\delta P$$

Previously (Flower et al [1984]) this pressure derivative had not been measured directly and so a room temperature value could only be obtained from calculations using other measured elastic constant pressure derivatives . The accumulation of errors from each individual reading (especially for that of $\delta C_{13}/\delta P$) lead to an uncertainty in the value of the pressure derivative which was actually larger than the value itself . The value so obtained was negative suggesting that the mode softened as pressure was applied, and leading to a large negative value of Grüneisen parameter for this mode .

The results presented here for the k[101],e[Ø] mode pressure derivative (Table 4.6 and Fig 4.26) represent direct measurements of the pressure derivative and so do not have excessively large errors associated with them (although the values for $\delta C_{13}/\delta P$ obtained from these results still have the same error limits) . The pressure derivative for the k[101],e[Ø] mode , measured directly ,

is positive right up through the temperature range and the results quite closely resemble those for the $\underline{k}[110],\underline{e}[1\bar{1}0]$ slow shear mode (Fig 4.25) .

The results shown in Fig 4.25 for the $\underline{k}[110],\underline{e}[1\bar{1}0]$ mode indicate a dramatic drop in the value of the mode pressure derivative just before the melting point . However , there is some doubt as to the validity of these results as they could not be repeated in any other runs , and readings against rising temperature did not agree with readings against falling temperature (although results for SOECs did show agreement , see comments in section 4.4) . This is the only evidence to suggest that any SOEC pressure derivatives or mode pressure derivatives might tend to zero (or go negative) near the melting point .

As long as all the mode pressure derivatives for a material are positive , application of pressure is stiffening the crystal structure , fixing it more firmly in its present state and tending to drive the material away from any transition . If a mode derivative is negative , application of pressure reduces the structure's ability to resist stress along the mode direction which tends to de-stabilize the structure and can drive the material towards a transition .

The results given in Figs 4.21-4.24 show that , for most of the modes measured , the mode pressure derivatives increase as the temperature is increased, and

that the responses generally become steeper as the melting point is approached . The values obtained for the pressure derivatives of the elastic constants have been used to obtain the temperature response for the pressure derivative of the adiabatic bulk modulus for indium . The response is presented in figure 5.1 and shows that from room temperature until about 100 deg.C the value of $\delta B/\delta P$ remains virtually constant. Above 100 deg.C , as the melting point is approached , the value of $\delta B/\delta P$ increases quite significantly . Such behaviour has previously been predicted for aluminium (Ho and Ruoff [1969]) .

FIG 5.1

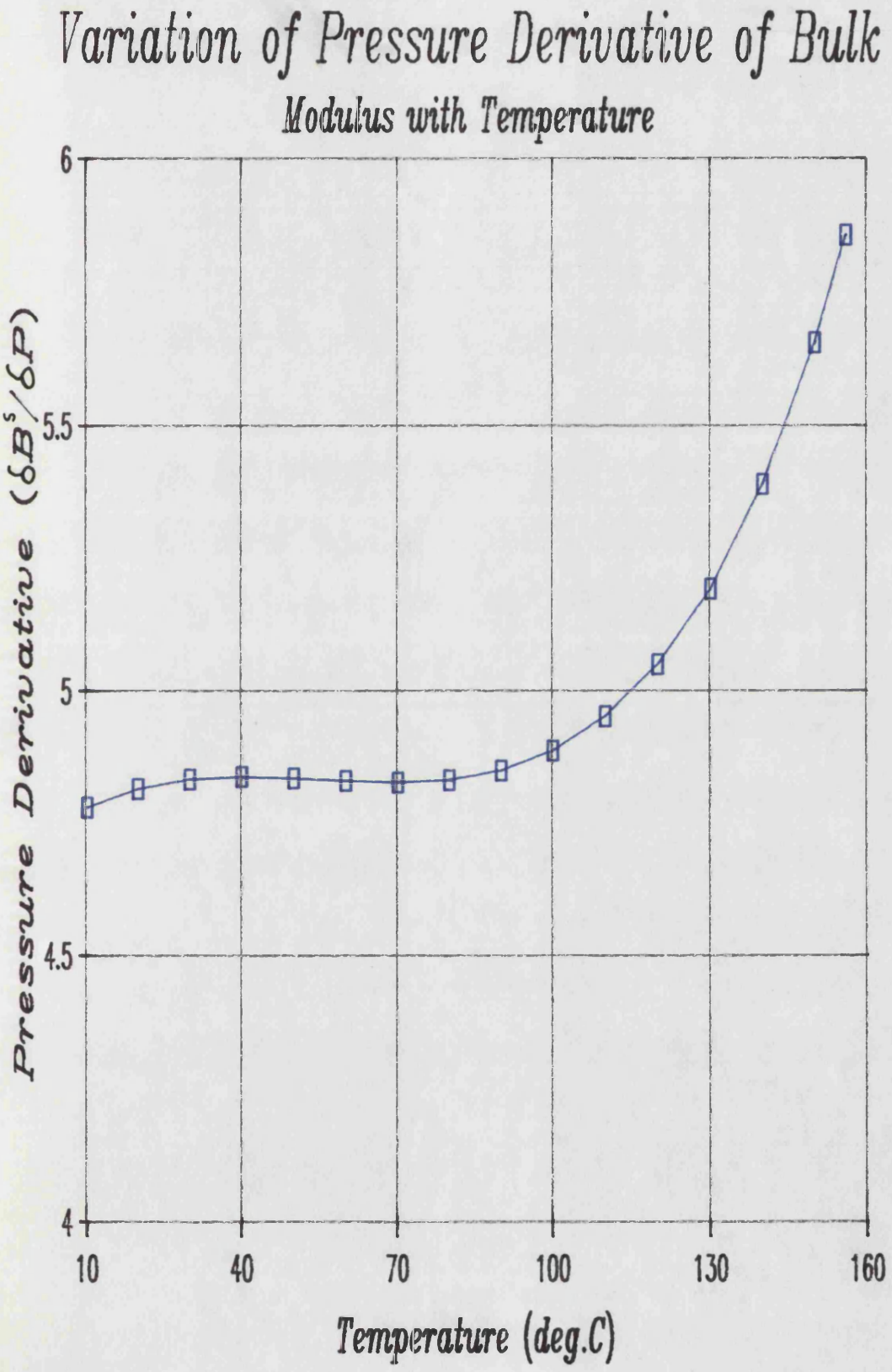
Variation of Pressure Derivative of Bulk
Modulus with Temperature
Pressure Derivative ($\delta B^S/\delta P$)
6
5.5
5
4.5
4
10
40
70
100
130
160
Temperature (deg.C)

5.5 GRÜNEISEN PARAMETERS

The Grüneisen parameters for a material characterise the anharmonicity of vibrational modes within the structure . In general all physical properties which depend upon the thermal motion of the atoms are much influenced by such anharmonicity , especially at high temperatures . Thermal expansion data is usually analysed and interpreted in terms of a thermal Grüneisen parameter γ^{th} which links the volume expansivity α with the compressibility χ and heat capacity C (see section 2.5)

$$\gamma^{th} = \alpha V / \chi^{T} C_{v} = \alpha V / \chi^{S} C_{p} \qquad (5.3)$$

Values of the thermal Grüneisen parameter γ^{th} have been given as 2.5 from room temperature down to temperatures of the order of $0.25\theta_D$ (where θ_D is the Debye temperature) by Madaiah and Graham [1964] , about 2.4 between 20 deg.K and 240 K by Munn [1969] and 2.419 at room temperature and pressure (Ramakrishnan et al [1978]) .

The thermal Grüneisen parameter is a weighted average of mode Grüneisen parameters (see section 2.5) . At high temperatures ($T >> \theta_D$) the heat capacity per mode becomes equal to Boltzman's constant k and phonons from every available state in the Brillouin zone should contribute equally to the thermal expansion and specific heat (and hence to γ^{th}) . At room temperature indium , with a θ_D

of 87 K , is close to the high temperature limit and so almost all available phonon states will be excited . Values for the mean acoustic mode Grüneisen parameter γ^{el} presented here have been obtained as an average over just the long wavelength phonon modes near the Brillouin zone centre . Hence any correlation between γ^{el} and γ^{th} will depend upon mode Grüneisen parameters from near the Brillouin zone centre having similar values to those further out in the zone .

The value of the mean acoustic Grüneisen parameter γ^{el} at room temperature was found to be about 3.2 . The fact that this is rather larger than the numbers given for the thermal Grüneisen parameter suggests that the average value of mode Grüneisen parameters from phonon modes further out in the Brillouin zone (shorter wavelength) will be rather smaller than this . The difference between results for γ^{el} and γ^{th} seems to be due mainly to contributions to γ^{el} from the slow shear vibrational modes (see fig. 4.32).

Early work during this study [Flower et al [1984]) seemed to find close agreement between thermal and mean gammas . This was due in part to the negative pressure derivative calculated for the $\underline{k}[101],\underline{e}[\emptyset]$ shear mode forcing some shear mode Grüneisen gammas to be negative , which tended to cancel with other shear mode gammas that were still positive . The negative value obtained was probably a result of accumulated errors in the calculation

of the pressure derivative (see section 5.4) . Direct measurement of the $\underline{k}[101],\underline{e}[\emptyset]$ mode pressure derivative has since found it to be positive and similar in value to the $\underline{k}[110],\underline{e}[1\bar{1}0]$ mode pressure derivative . This means that there are no modes with negative mode gammas and so the mean value for the long wavelength acoustic Grüneisen parameter is now found to be larger than before .

The data given by Kramer and NÖlting [1972] for the specific heat of indium (Fig 4.30) , combined with thermal expansion data (Graham et al [1955]) and compressibility data (from this work) , has allowed values of thermal Grüneisen parameter to be calculated over the temperature range studied here . Fig 4.33 shows the values obtained . The temperature response for this thermal gamma seems to be virtually linear with a room temperature value of about 2.6 (showing quite close agreement with previous data) climbing to about 3.0 near melting . The long wavelength mean acoustic mode Grüneisen parameter does not show particularly good agreement with this , its value at room temperature being about 3.2 , increasing to nearly 4.5 close to melting (fig 4.33). The temperature response for γ^{el} also shows an increasing slope (temperature derivative) as the temperature is increased , rather than the near linear response for γ^{th}. However , the fact that both responses show an increase in value with temperature indicates increasing vibrational anharmonicity as the melting point

is approached .

There are various views on what behaviour is expected of the Grüneisen parameters near the melting point . Feldman et al [1967] expected a rapidly decreasing γ^{th} for fcc argon , krypton , and xenon before the melting point was reached . Schouton and Swenson [1974] observed γ^{th} increasing for cubic potassium before melting (which they felt reflected the increased anharmonicity due to increasing numbers of defects) .

Some interesting work (in view of the results found here) was published by Hollenberg and Batterman [1974] , who found anomalously large temperature dependences of X-ray intensities reflected from isomorphous AuGa . They found that to fit the data a quasiharmonic treatment required a value for Grüneisen parameter that was considerably higher than the value obtained thermodynamically for thermal Grüneisen parameter . They went on to show that the discrepancy could be associated with the temperature dependence of the $(C_{11}-C_{12})/2$ shear modulus .

The results here (section 4.5) do show that it is mainly the values for the long wavelength shear mode Grüneisen parameters (in particular the $\underline{k}[110],\underline{e}[1\bar{1}0]$ and $\underline{k}[101],\underline{e}[\emptyset]$ modes) that force the mean value for zone centre modes above that for the thermal Grüneisen parameter . With the anharmonicity of long wavelength modes in indium seeming to rely quite heavily on the slow

shear mode contributions it is interesting to look more closely at the way in which these contributions vary with temperature . Figure 4.31 shows just the temperature responses for the three mode Grüneisen parameters in the [101] direction (the directionwith the highest value of shear mode Grüneisen parameter). The longitudinal mode and the fast shear mode (k[101],e[010]) show a fairly flat response with a slight rise as the melting point is approached . The results for the slow shear mode (k[101],e[Ø]) show a much steeper curve whose slope increases quite sharply towards the melting point . The steeper slope is due to the relatively much larger change in wave propagation velocity with temperature (when expressed as a fraction of the velocity itself) for this mode than for the others . Acoustic mode Grüneisen parameters can be represented as a fractional change in mode frequency ν_i divided by a fractional change in volume V (section 2.5);

$$\gamma_i = - d\ln\nu_i / d\ln V \qquad (5.4)$$

At any temperature the temperature derivative of the elastic wave propagation velocity , for any direction , divided by the velocity itself can be thought of as eqivalent to the fractional change in vibrational mode frequency .

The main conclusions to be drawn from this section are the following;

(i) Vibrational anharmonicity is seen to increase as the melting point is approached.

(ii) The mean acoustic mode Grüneisen parameter for long wavelength modes is seen to have a larger value than the thermal Grüneisen parameter (due mainly to shear mode contributions), showing that the average value for shorter wavelength modes further out in the Brillouin zone must be smaller than that at the zone centre.

5.6 MELTING CURVE FOR INDIUM

5.6.1 INTRODUCTION

The determination of melting curves is a central area of interest in high pressure research . The pressure dependence of melting temperature has been experimentally determined under static pressure for a great number of materials , including indium (Dudley and Hall [1959], Cannon [1974]) . However , at very high pressures (P < 10GPa) there is little experimental data , and melting temperatures often have to be calculated on the basis of various theoretical , or empirical , expressions . For instance Simon's formula (Simon and Glatzel [1929], Babb [1963]);

$$P_m / a = (T_m / T_{om})^c - 1 \qquad (5.5)$$

is often used to correlate the melting temperature , T_m, and the melting pressure , P_m , using two empirical constants , a and c which are taken to be related to internal pressure and interatomic forces respectively . T_{om} is the melting point at zero pressure . Although this equation has been quite successfully applied to a number of simple materials , it does not really provide a satisfactory basis for extrapolating melting data to very high pressures . The validity and deficiencies of Simon's

formula have been discussed by several workers (Babb [1963] , Kennedy [1956] and [1965]) .

Kraut and Kennedy [1966] put forward a new melting equation ;

$$T_m = T_{om} (1 + C \left| \Delta V/V_o \right|) \qquad (5.6)$$

when they found that by plotting melting temperature T_m at a given pressure against room temperature compression ($\Delta V/V_o$ obtained from compression data given by Bridgman [1949]) an approximate straight line was obtained . This equation was found to agree well with melting point and compression data for Li, Na, K, and Rb . Gilvarry [1966] used a reformulation of the classical Lindemann melting law (Lindemann [1910]);

$$T_{om} = Cm\Theta_D^2 v_m^2 \qquad (5.7)$$

(where Θ_D is the Debye temperature , m the molar weight, v_m the volume per atom at melting and C is a constant) to modify equation (5.6) and obtained the relation;

$$T_m = T_{om} (1 + 2(\gamma - 1/3) \left| \Delta V/V_o \right|) \qquad (5.8)$$

where γ is the Grüneisen coefficient . The same equation has also been put forward by Vaidya and Raja Gopal [1966] who were able to show that this linear relation between melting temperature and compression ratio agreed quite well with experimental results for several elements (including indium) for small compressions . However , as

with Simon's formula , equation (5.8) does not really provide a reliable basis for high pressure extrapolation . One reason for this could be that the Grüneisen coefficient is assumed to be a constant although in reality it is found to be both temperature dependent (Fig 4.33) and volume dependent . In addition Vaidya and Raja Gopal [1966] assume also that compression data measured at room temperature will be valid close to the melting point.

In this section equation (5.8) is tested using the high temperature data measured here for indium. The purpose is to see whether , by making due allowance for the effect of pressure on the Grüneisen parameter , the Givarry equation (5.8) may be shown to provide a good basis for high pressure calculations of the melting point of indium .

The values measured here for the temperature dependences of the bulk modulus of indium and the pressure derivative of the bulk modulus (section 4.3) are used with the Murnaghan equation of state to calculate compression as a function of pressure . The value used for the Grüneisen coefficient was that obtained here for the thermal Grüneisen parameter at high temperature (section 4.5) suitably corrected for pressure effects using an empirical relation given (for indium) by Ramakrishnan et al [1978].

5.6.2 COMPRESSION DATA

Knowledge of the compression ratio ($V(P)/V_0$) , where V(P) is the volume at pressure P , and V_0 the volume at atmospheric pressure , is useful in theoretical studies of physical properties of solids under pressure . One common procedure for calculating the compression of a material at high pressure is to extrapolate values from lower pressures using the Murnaghan [1944] equation of state (Anderson [1966]) . The central assumption of such a method is that values of isothermal and adiabatic bulk moduli vary linearly with pressure , ie;

$$\begin{aligned} B^T(P) &= -V(\partial P/\partial V) \\ &= B_0^T + P(\partial B^T/\partial P) \end{aligned} \qquad (5.9)$$

where B is the isothermal bulk modulus . By integrating equation (5.9) Murnaghan obtained the relation;

$$P = B_0^T / B_0'^T \{(V_0/V(P))^{B_0'^T} - 1\} \qquad (5.10)$$

where $B_0'^T$ is the pressure derivative of the isothermal bulk modulus at atmospheric pressure . This is the Murnaghan equation of state which may be expressed in the more easily used form;

$$\ln(V_0/V(P)) = (1/B_0'^T)\ln[B_0'^T (P/B_0^T) + 1] \qquad (5.11)$$

and which describes the compression of many solids well (Anderson [1966]).

Now ultrasonic measurements give adiabatic elastic moduli , so data must be transformed to isothermal values for use in equation 5.11 . The relationship between adiabatic and isothermal bulk moduli is given as (Anderson [1966]);

$$B_o^S = B_o^T (1 + \alpha\gamma^{th}T) \qquad (5.12)$$

where α is the thermal expansion coefficient and γ^{th} is the thermal Grüneisen parameter . By applying this equation to the measurements made here of the adiabatic bulk modulus of indium (fig. 4.19) , values for the isothermal bulk modulus between room temperature and 156 deg.C have been obtained . These results are presented in figure 5.2 where they are compared with the original adiabatic data .

The hydrostatic pressure derivative of the isothermal bulk modulus , $B_o'^T$, has been shown to be (Overton [1962] , Anderson [1966]);

$$B_o'^T = B_o'^S + T\alpha\gamma (B_o^T/B_o^S)[1 - (2/\alpha B_o^T)(\partial B_o^T/\partial T) - 2B_o'^S] + [T\alpha\gamma (B_o^T/B_o^S)]^2 (B_o'^S - 1 - (1/\alpha^2)(\partial\alpha/\partial T)_p] \qquad (5.13)$$

where $\partial B_o^T/\partial T$ can be obtained from;

$$(\partial B_o^T/\partial T) = (\partial B_o^S/\partial T)/(1 + T\alpha\gamma) - (B_o^S/T)(T\alpha\gamma/(1 + T\alpha\gamma)^2)[1 + (\partial\alpha/\partial T)/(\alpha/T)] \qquad (5.14)$$

These equations have been used , with data measured here for the adiabatic bulk modulus and its pressure derivative

FIG. 5.2

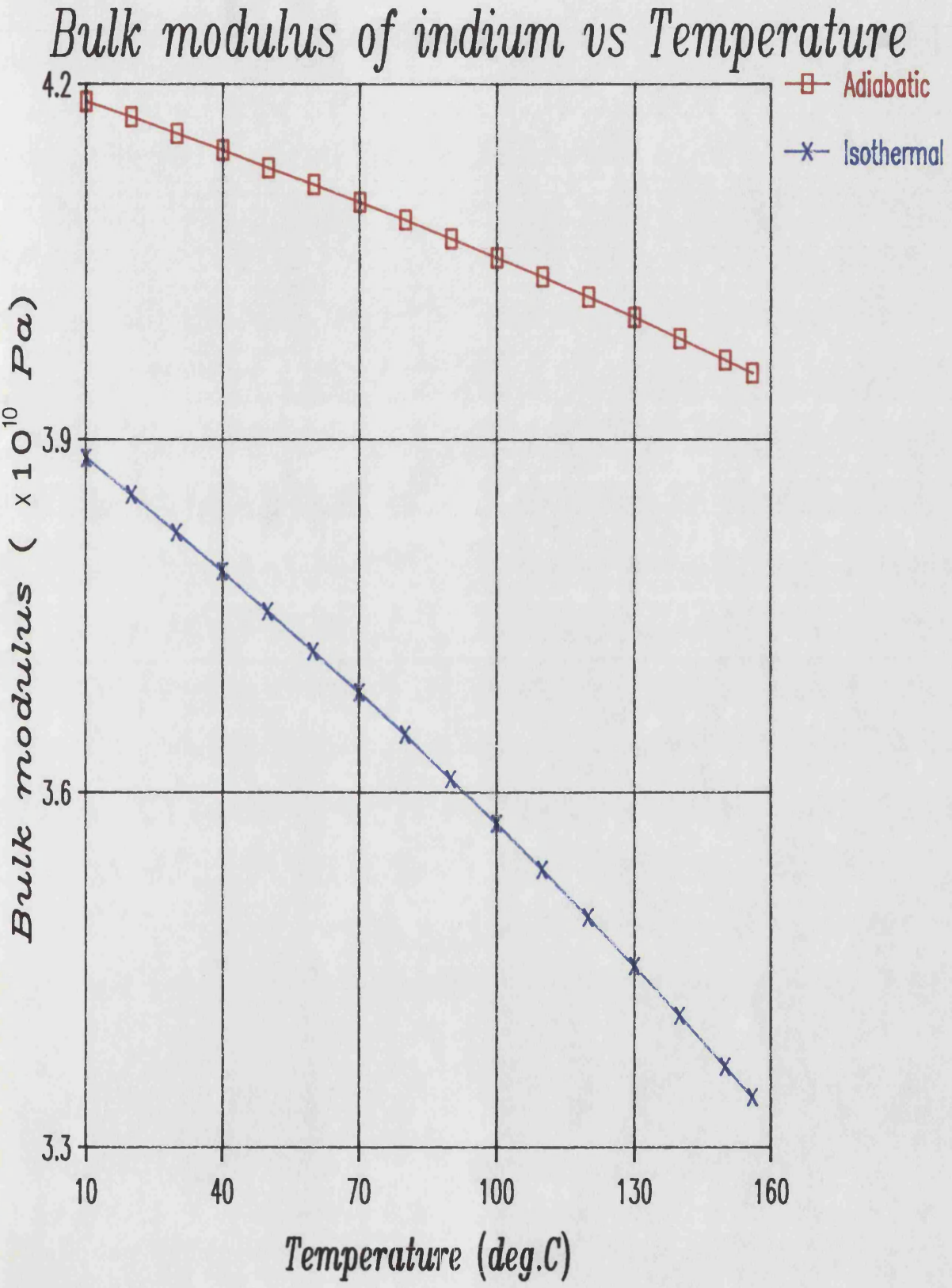
Bulk modulus of indium vs Temperature
Adiabatic
Isothermal
Bulk modulus (x 10^10 Pa)
4.2
3.9
3.6
3.3
10
40
70
100
130
160
Temperature (deg.C)

(sections 4.3 and 4.4) , to calculate the temperature dependences of $B_0'^T$ and $(\partial B_0^T/\partial T)$ (figures 5.3 and 5.4 respectively).

Compression data has been obtained for a range of pressures by substituting values for the isothermal bulk modulus , and its pressure derivative , into the equation of state (equation 5.11). The calculations have been done first using room temperature data and then with data from measurements taken close to the melting point . Previously (Vaidya and Raja Gopal [1966] , Romain et al [1979]) testing of the Gilvarry melting curve equation has relied on the assumption that compression data at room temperature is still valid at the melting point . The results presented here for the compression of indium at room temperature and 156 deg.C (fig 5.5) show that while this assumption is not unreasonable the two curves do start to diverge at higher pressures . Proper testing of the melting curve equation will obviously require data from as close to the melting point as possible .

The thermal Grüneisen parameter γ^{th} is usually taken as the Grüneisen coefficient in equation (5.8) . The value of γ^{th} near the melting point ($\gamma^{th}_{(156)}$ = 3.03) has been obtained by combining elastic moduli data , measured here , with high temperature values for thermal expansion (Graham et al [1955] and specific heat (Kramer and Nölting [1972])(see section 4.5). Before substitution into the melting curve equation this value was corrected for change

FIG. 5.3

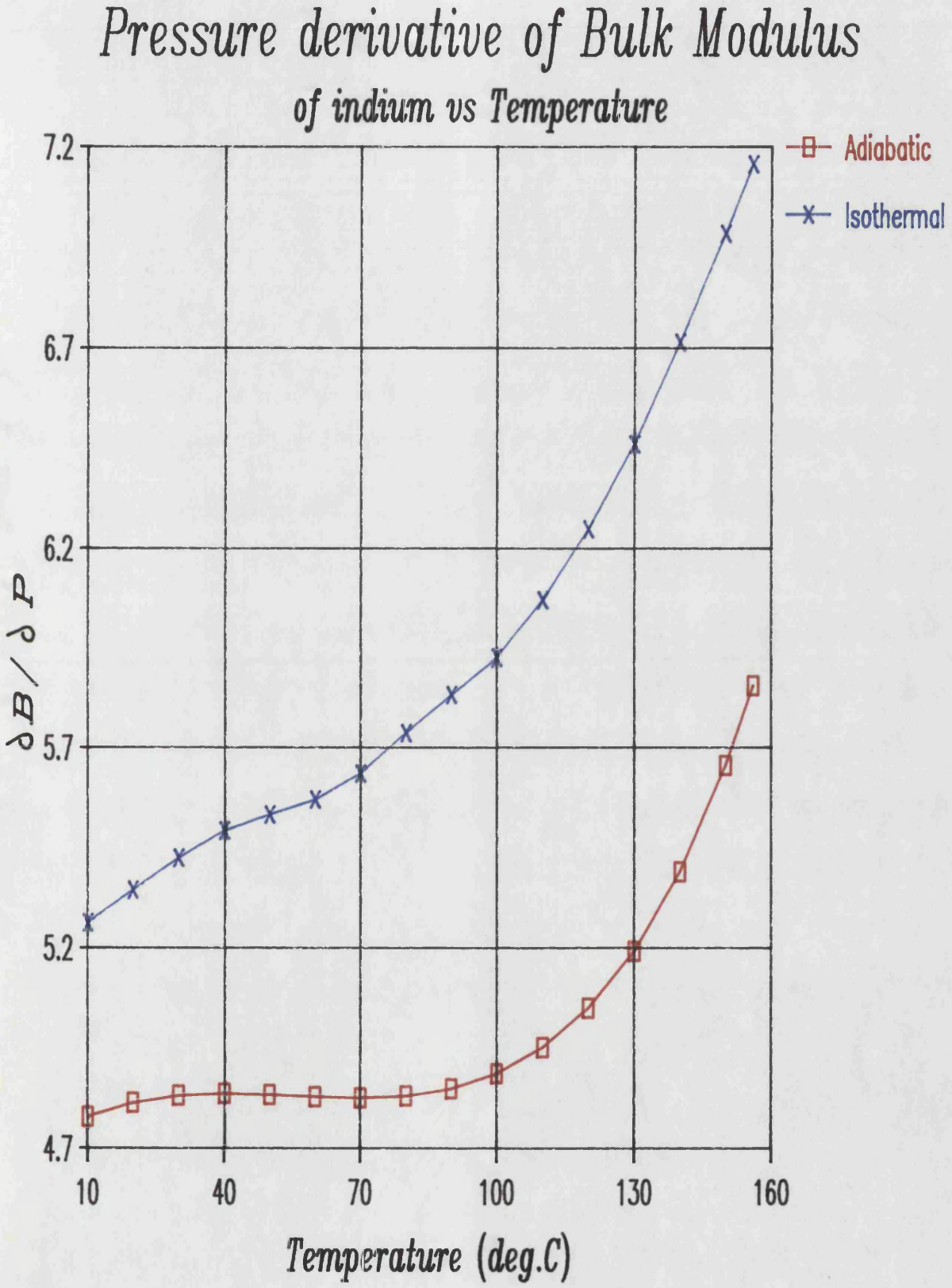
Pressure derivative of Bulk Modulus
of indium vs Temperature
Adiabatic
Isothermal
7.2
6.7
6.2
5.7
5.2
4.7
∂B/∂P
10
40
70
100
130
160
Temperature (deg.C)

FIG. 5.4

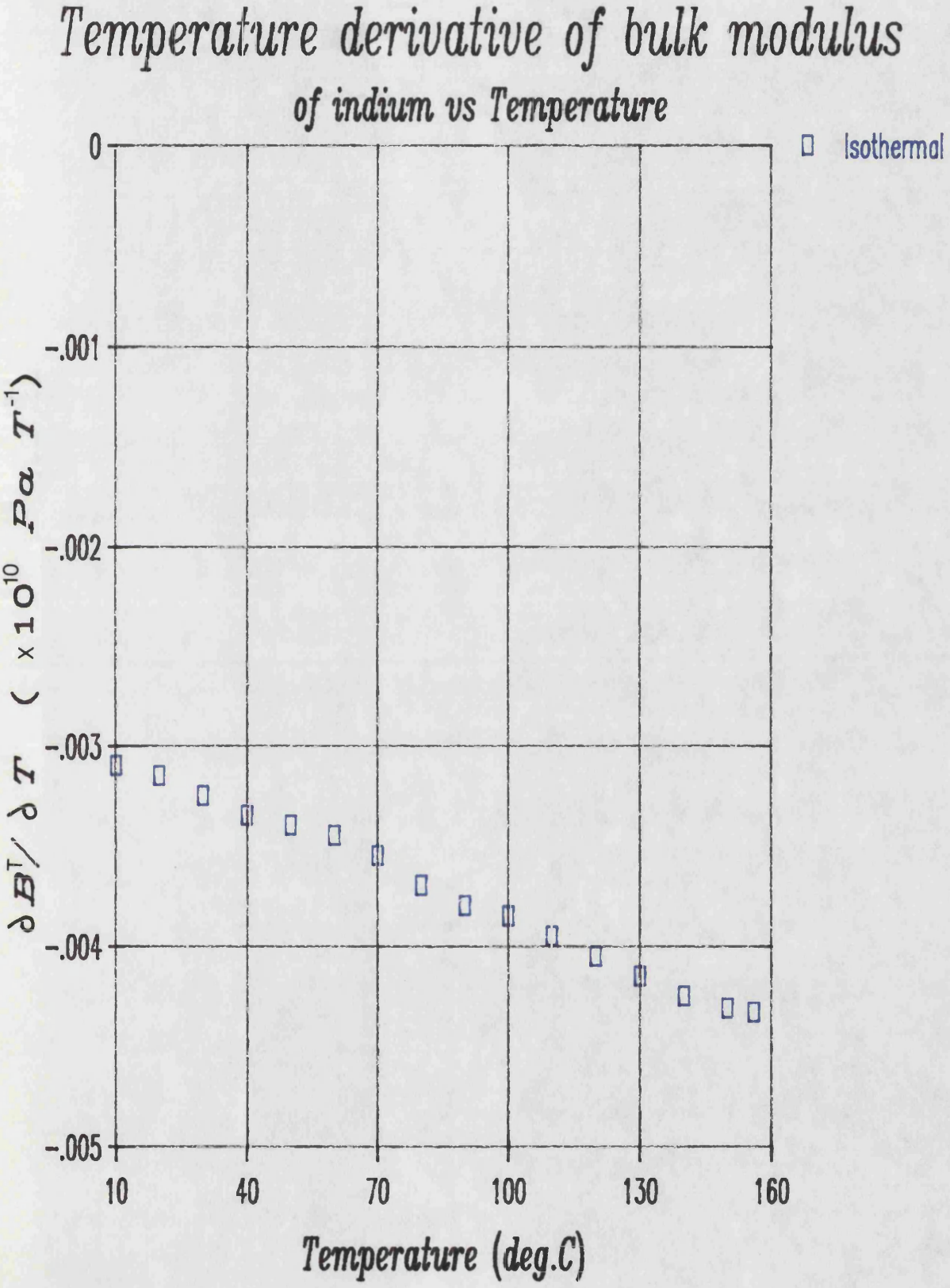
Temperature derivative of bulk modulus
of indium vs Temperature
Isothermal
0
-.001
-.002
-.003
-.004
-.005
10
40
70
100
130
160
∂B^T/∂T (×10^10 Pa T^-1)
Temperature (deg.C)

FIG. 5.5

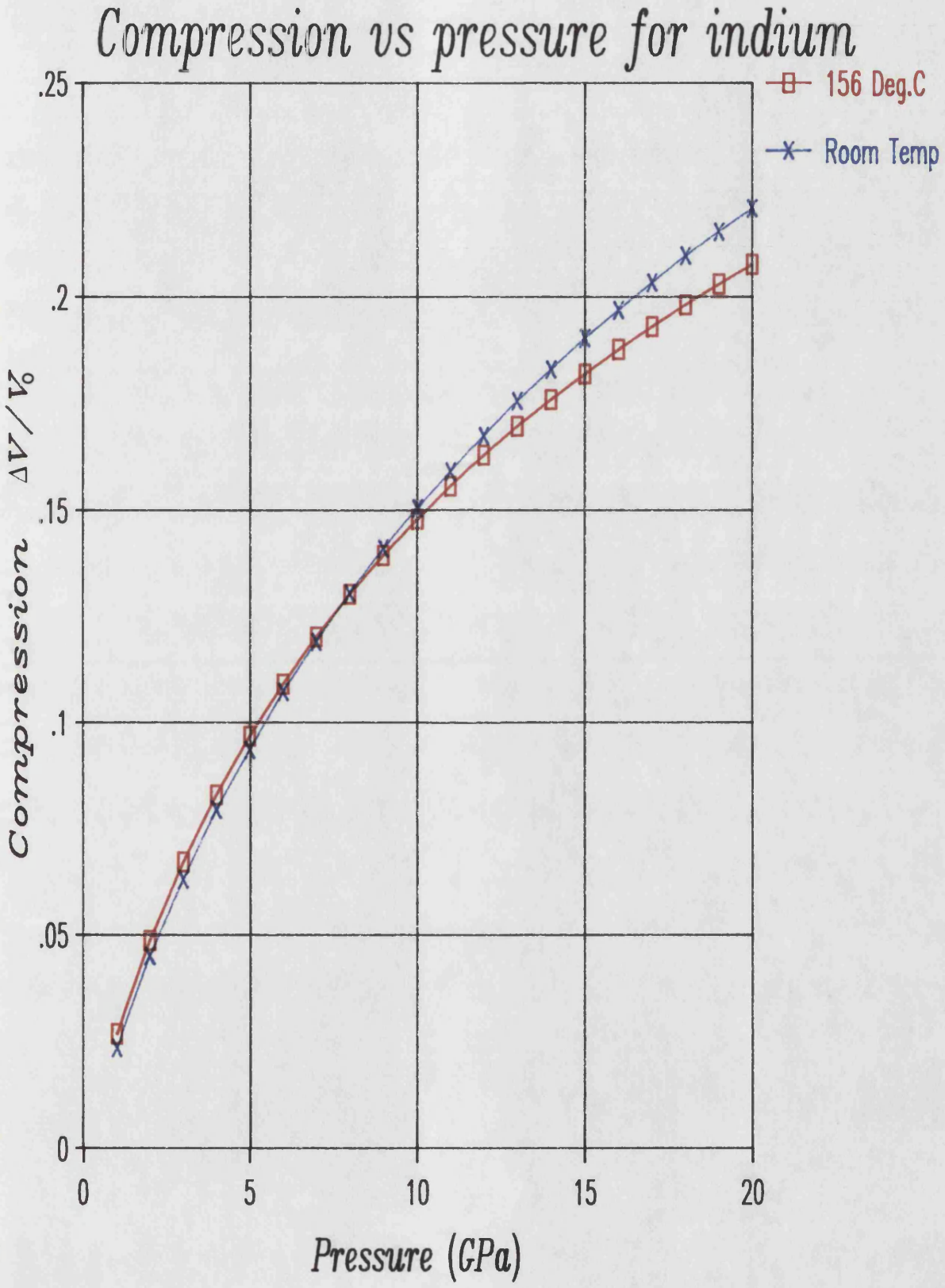
Compression vs pressure for indium
156 Deg.C
Room Temp
Compression ΔV/V₀
.25
.2
.15
.1
.05
0
0
5
10
15
20
Pressure (GPa)

in volume with pressure using the empirical relation (Ramakrishnan et al [1978]);

$$\gamma(P) = \gamma_0 (V(P)/V_0)^{1.8} \qquad (5.15)$$

The pressure dependence of the Grüneisen parameter calculated using equation 5.15 is shown in figure 5.6. It can be seen from these results that the pressure induced variation of the Grüneisen parameter cannot be assumed to be negliglble over the range studied .

5.6.3 MELTING CURVE

Substitution of high temperature compression and Grüneisen parameter data (obtained from this study) into the Gilvarry melting curve relation (equation 5.8) has allowed the pressure dependence of the melting point of indium to be calculated to high pressure (20 GPa) . The calculated results are presented in figure 5.7 where they are shown to be in very close agreement with experimental data for indium (Dudley and Hall [1960]). When the data is plotted out as melting temperature against compression (fig 5.8) it is also seen to be in very close agreement with the data given by Vaidya and Raja Gopal [1966]. Vaidya and Raja Gopal used room temperature compression data (Bridgeman [1949]) and Dudley and Hall's melting point data to try and show a linear relation between melting point and compression for a number of metals

FIG. 5.6

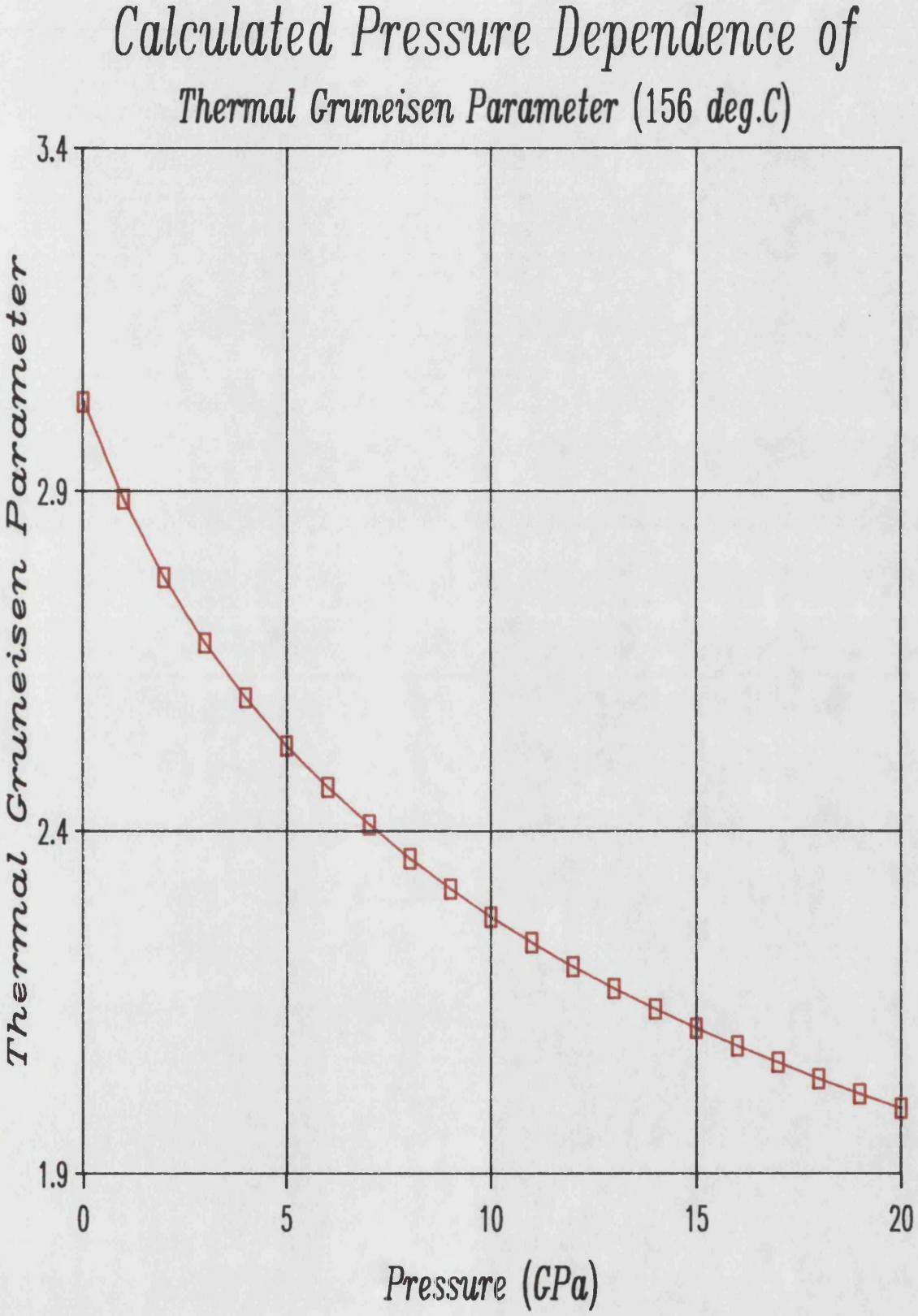
Calculated Pressure Dependence of
Thermal Gruneisen Parameter (156 deg.C)
Thermal Gruneisen Parameter
3.4
2.9
2.4
1.9
0
5
10
15
20
Pressure (GPa)

FIG. 5.7

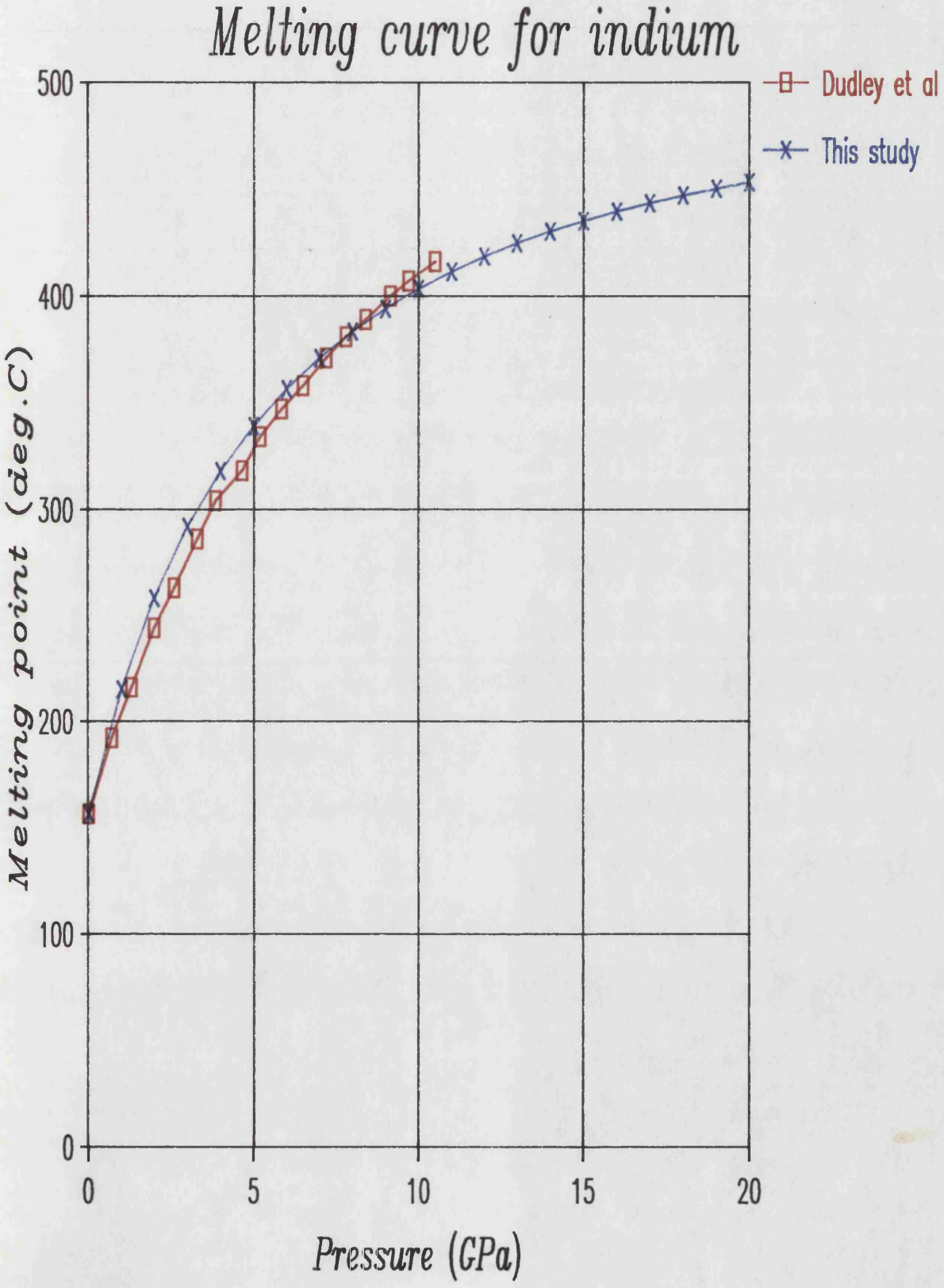
Melting curve for indium
Dudley et al
This study
Melting point (deg.C)
500
400
300
200
100
0
0
5
10
15
20
Pressure (GPa)

FIG. 5.8

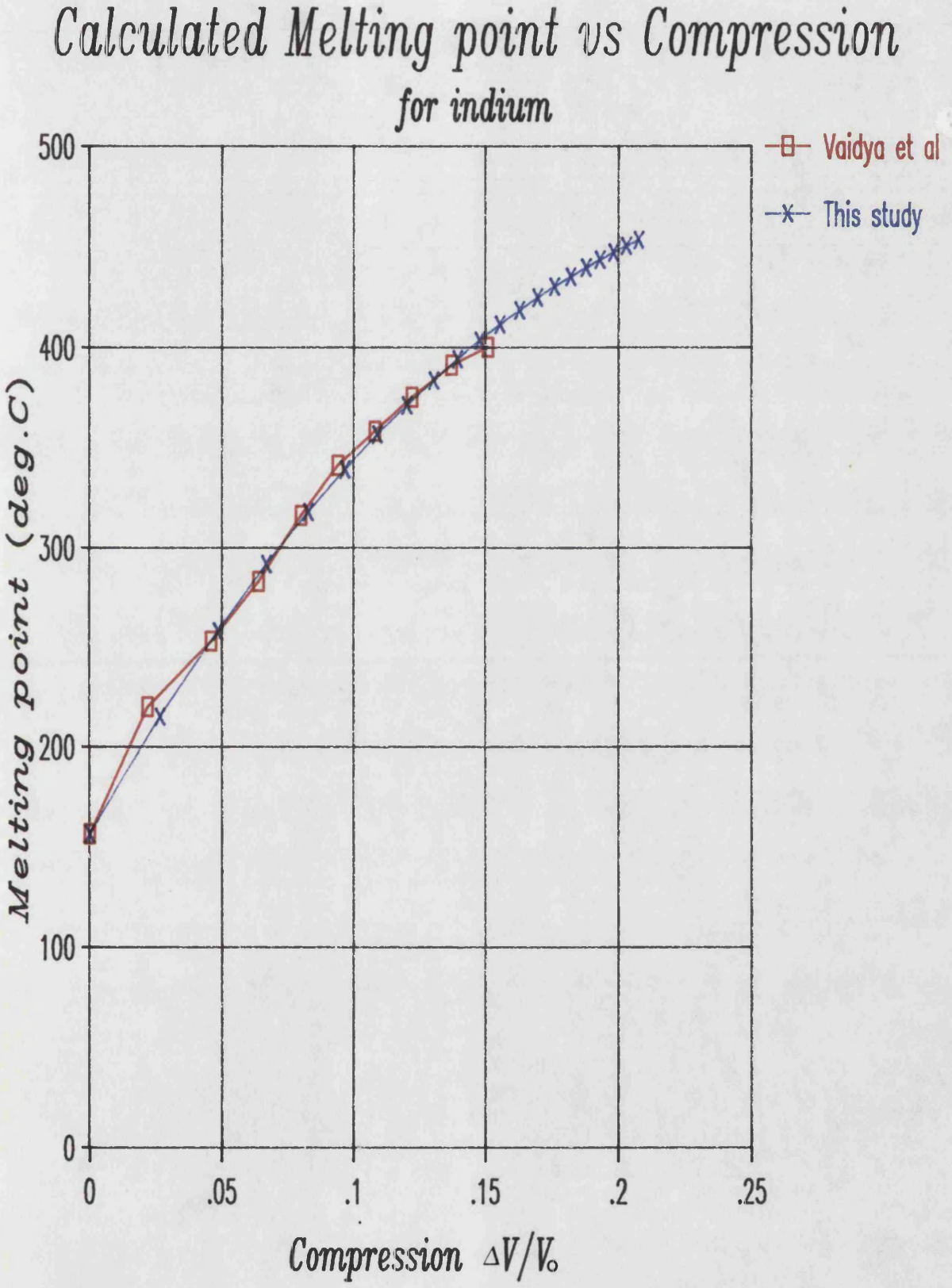
Calculated Melting point vs Compression
for indium
Vaidya et al
This study
Melting point (deg.C)
500
400
300
200
100
0
0
.05
.1
.15
.2
.25
Compression ΔV/V₀

including indium. They were looking for a linear relation because they assumed that the Grüneisen coefficient in equation 5.8 was invariant with pressure . They were able to show that the response was approximately linear for lower pressures (leading to a value of 2.61 for the Grüneisen coefficient), but the results clearly curve away at higher pressures .

For the results presented here the same equation that Vaidya and Raja Gopal were testing has actually been used to calculate the melting temperature as a function of pressure using data measured close to the melting point , and using a high temperature value of Grüneisen parameter corrected for for the effect of pressure . The close fit between the data from this study and the previous experimental results show that the melting curve equation (Gilvarry [1966], Vaidya and Raja Gopal [1966]) describes very well the pressure response of the melting temperature of indium up to the highest temperatures for which data is available .

6.0 CONCLUSIONS

Measurements of SOECs , hydrostatic pressure derivatives of SOECs , and Grüneisen parameters for single crystal indium have been made for temperatures between room temperature and close to the melting point (T_M =156.7 deg.C).

No mode elastic constants are seen to approach zero near the melting point , confirming previous results (Chung et al [1977]) and showing that , for indium at least , soft modes do not seem to play a central role in the melting process .

The temperature responses for the bulk modulus and volume compressibility show smooth curves right up to near the melting temperature , without the divergence predicted by Hertzfeld and Geoppert-Mayer [1934] .

Some pressure derivatives do show some change near melting . The pressure derivative of the adiabatic bulk modulus , in particular , shows a significant rise in value between about 100 deg.C and 156 deg.C .

The values for the mean acoustic mode Grüneisen parameter (averaged over long wavelength modes near the Brillouin centre) over the temperature range studied , are shown to be larger in value than the thermal Grüneisen parameter over the same range. As , even at room temperature , indium is near the high temperature limit ($T \gg \theta_D$; θ_D for indium = 87K) every mode in the Brillouin

zone should contribute equally to the specific heat (and so to the thermal Grüneisen parameter) . It may therefore be concluded that the mean of the shorter wavelength acoustic mode Grüneisen parameters (further out into the Brillouin zone) should be lower in value than the mean obtained for zone centre modes .

The use of high temperature elastic data, measured here, and the application of a pressure correction to the high temperature thermal Grüneisen parameter have provided a means of testing a melting curve equation based on the Lindemann melting law (Gilvarry [1966], Vaidya and Raja Gopal [1966]) . Previously (Vaidya and Raja Gopal [1966]) the equation has been tested with room temperature data and has only been shown to provide a good description of the pressure dependence of the melting temperature at relatively low pressures . The results presented here show that (after correcting the Grüneisen parameter for volume change due to application of pressure) the Gilvarry equation shows very close agreement with experimental data for indium up to the highest pressures so far measured .

APPENDIX A

Data Analysis Program

```
 10 MODE7
 20 REM PROGRAM TO CALCULATE PRESSURE
 30 REM DERIVATIVES OF SOEC'S OF INDIUM
 35 REM FROM ULTRASONIC DATA
 38 REM
 40 DIM T(100),G(100),I(100),L(100),V(100),P(100),D(100)
 50 CLS
 60 PRINT"D...LOAD DATA FROM DISC"
 70 PRINT:PRINT"K...LOAD DATA FROM KEYBOARD"
 80 O$=GET$
 90 IF O$="D"THEN GOTO 410
100 IF O$="K"THEN GOTO 120
110 GOTO 50
120 CLS
122 REM
124 REM INPUT DATA FROM KEYBOARD
126 REM
130 PRINT"INPUT PROPAGATION DIRECTION"
140 INPUT"L1,L2,L3 ";L1,L2,L3
150 PRINT:PRINT"SHEAR OR LONGITUDINAL (S/L)":O$=GET$
160 IF O$="S" GOTO 190
170 IF O$="L" GOTO 200
180 GOTO 150
190 S$="SHEAR":GOTO 210
200 S$="LONGITUDINAL"
210 PRINT:INPUT"ROOM TEMP. THICKNESS";L
220 IF L=0 GOTO 210
230 CLS
240 X=0
250 PRINT"INPUT DATA--TYPE IN '0' Deg.C TO STOP"
260 INPUT"TEMP (Deg.C)";T(X)
270 IF T(X)=0 GOTO 390
280 INPUT"GRADIENT (KHz/Kbar)";G(X)
290 INPUT"INTERCEPT (KHz)";I(X)
300 PRINT"CHANGE THICKNESS (Y/N)":Q$=GET$
310 IF Q$="Y" GOTO 340
320 IF Q$="N" GOTO 360
330 GOTO 300
340 PRINT:INPUT"NEW ROOM TEMP.THICKNESS";L(X)
350 L=L(X)
360 L(X)=L
370 X=X+1
380 PRINT:PRINT:GOTO 260
390 X=X-1
400 GOTO 600
405 REM
410 REM INPUT FROM DISC
415 REM
420 CLS:INPUT "FILENAME";I$
430 INPUT"DRIVE NUMBER";DN
440 IF DN=0 THEN *DRIVE0
450 IF DN=1 THEN *DRIVE1
460 IF DN=2 THEN *DRIVE2
470 IF DN=3 THEN *DRIVE3
480 IF DN>3 GOTO 430
490 K=OPENIN I$
500 INPUT£K,L1,L2,L3,O$
```

```
 510 X=0
 520 REPEAT
 530 INPUT£K,T(X),G(X),I(X),L(X)
 540 X=X+1
 550 UNTIL EOF£K
 552 CLOSE£K
 555 L=L(0)
 560 X=X-1
 570 IF O$="S" THEN S$="SHEAR"
 580 IF O$="L" THEN S$="LONGITUDINAL"
 590 REM
 600 REM DATA HANDLING
 605 REM
 610 CLS: PRINT"            CONTROL"
 620 PRINT:PRINT:PRINT"V...VIEW SECTION OF DATA"
 630 PRINT"      (D..delete data; C..change data)"
 640 PRINT:PRINT"A...APPEND DATA"
 650 PRINT:PRINT"P...PRINT OUT DATA"
 660 PRINT:PRINT"X...SAVE DATA TO DISC"
 665 PRINT:PRINT"D...CALC PRESS. DER'S"
 670 PRINT:PRINT"S...STOP PROGRAM"
 680 PRINT:PRINT:PRINT:PRINT:PRINT;L1;L2;L3;" ";S$;" MODE"
 690 U$=GET$
 700 IF U$="V" GOTO 760
 710 IF U$="P" GOTO 1250
 720 IF U$="A" GOTO 1350
 730 IF U$="X" GOTO 1370
 740 IF U$="S" GOTO 1520
 745 IF U$="D" GOTO 2010
 750 GOTO 610
 755 REM
 760 REM VIEW DATA
 765 REM
 770 Y=0
 780 CLS
 790 PRINT,L1;L2;L3;" ";S$;" MODE":PRINT
 800 PRINT"No. TEMP   GRADIENT INTERCEPT THICKNESS"
 810 FOR T=Y TO (Y+20)
 820 IF T>X GOTO 840
 830 PRINT;T;"   ";T(T)TAB(12);G(T)TAB(22);I(T)TAB(32);L(T)
 840 NEXT T
 850 PRINT:PRINT:PRINT"(V)-View data; (D)-Delete; (C)-Change"
 860 PRINT"ANY OTHER KEY RETURNS CONTROL"
 870 V$=GET$
 880 IF V$="V" GOTO 930
 890 IF V$="D" GOTO 970
 900 IF V$="C" GOTO 1080
 910 GOTO 610
 920 REM    . VIEW DATA
 930 INPUT"VIEW DATA FROM LINE No";Y
 940 IF Y>X GOTO 930
 950 GOTO 780
 960 REM      DELETE DATA
 970 CLS:INPUT"START OF DELETION";SD
 980 PRINT:INPUT"END OF DELETION";ED
 990 DD=ED-SD+1
1000 FOR M=SD TO (X-DD)
```

```
1010 T(M)=T(M+DD):G(M)=G(M+DD):I(M)=I(M+DD):L(M)=L(M+DD)
1020 NEXTM
1030 X=(X-DD)
1040 FOR M=(X+1) TO (X+DD)
1050 T(M)=0:G(M)=0:I(M)=0:L(M)=0
1060 NEXT M
1070 Y=SD:GOTO 780
1080 REM      CHANGE DATA
1090 PRINT:INPUT"LINE NUMBER TO BE CHANGED";NL
1100 PRINT:PRINT"ENTER DATA AS REQUESTED"
1110 PRINT"ENTER '0' TO LEAVE UNCHANGED"
1120 PRINT:INPUT"TEMPERATURE (Deg.C)";TT
1130 IF TT=0 GOTO 1150
1140 T(NL)=TT
1150 PRINT:INPUT"GRADIENT (KHz/Kbar)";GG
1160 IF GG=0 GOTO 1180
1170 G(NL)=GG
1180 PRINT:INPUT"INTERCEPT (KHz)";II
1190 IF II=0 GOTO 1210
1200 I(NL)=II
1210 PRINT:INPUT"ROOM TEMP THICKNESS (cm)";LL
1220 IF LL=0 GOTO 1240
1230 L(NL)=LL
1240 Y=NL:GOTO 780
1245 REM
1250 REM      PRINT OUT DATA
1255 REM
1260 CLS
1270 VDU2
1280 PRINT,L1;L2;L3;" ";S$;" MODE"
1290 PRINT:PRINT"No. TEMP   GRADIENT INTERCEPT THICKNESS"
1300 FOR M=0 TO X
1310 PRINT;M;"  ";T(M)TAB(12);G(M)TAB(22);I(M)TAB(32)L(M)
1320 NEXT M
1330 VDU3
1340 GOTO 610
1350 REM       APPEND DATA
1355 REM
1360 X=X+1:CLS:GOTO 250
1370 REM       SAVE DATA TO DISC
1375 REM
1380 CLS:INPUT"FILENAME";F$
1390 PRINT:INPUT"DRIVE No";DN
1400 IF DN=0 THEN *DRIVE0
1410 IF DN=1 THEN *DRIVE1
1420 IF DN=2 THEN *DRIVE2
1430 IF DN=3 THEN *DRIVE3
1440 IF DN>3 GOTO 1390
1450 I=OPENOUT F$
1460 PRINT£I,L1,L2,L3,0$
1470 FOR M=0TOX
1480 PRINT£I,T(M),G(M),I(M),L(M)
1490 NEXT M
1500 CLOSE£I
1510 GOTO 610
1520 REM STOP ROUTINE
1530 ENVELOPE 1,1,-26,-36,-45,255,255,255,127,0,0,-127,126,0
1540 SOUND 1,1,120,-1
```

```
1550 MODE 5
1560 FOR W=1 TO 1000
1570 A=RND(1028):B=RND(1280)
1580 DRAW B,A
1590 NEXT W
1600 STOP
1610 END
2000 REM
2005 REM TEMP & TRANSDUCER CORRECTIONS
2008 REM
2010 P=7290:CF=10
2020 C1=4.59:C2=4.4:C3=.660
2030 C4=1.23:C5=4.07:C6=4.06
2040 CLS
2310 INPUT"OUTPUT FILENAME";H$
2320 INPUT"DRIVE No";DN
2330 IF DN=0 THEN *DRIVE0
2340 IF DN=1 THEN *DRIVE1
2350 IF DN=2 THEN *DRIVE2
2360 IF DN=3 THEN *DRIVE3
2370 IF DN>3 GOTO 2320
2380 J=OPENOUT H$
2390 PRINT£J,L1,L2,L3,O$
2400 FOR M=0 TO X
2410 GOSUB 3200
2420REM TRANSDUCER CORRECTION
2430REM
2440IF O$="S" THEN GOTO 2460
2450IF O$="L" THEN Z=15.2:GOTO 2470
2460Z=10.3
2470FC=CF*1E6
2480LC=LL*1E-2:FA=I(M)*1E3
2490V=2*LC*FA:AI=D*V*1E-6
2500RF=(Z-AI)/(Z+AI):TC=(.1602*EXP(1.831*(RF+1)))/FC
2510IF RF>=-.6 AND RF<=.6 THEN GOTO 2530
2520PRINT"WARNING  REFLECTION COEFF. OUT OF RANGE"
2530VC=2*LC/((1/FA)-TC):ER=VC*100/V-100
2540FA=I(M)*1E3
2550 GOSUB 3330
2560PW=2*D*VC^2*G(M)/FA*1E-5
2570DC=PW+D*VC^2*(X-2*LCP)
2580PV=D*VC^2
2590CLS
2600 PRINT£J,T(M),I(M),G(M),D,LC,VC,PV,DC
2610 NEXT M
2620 CLOSE£J
2630 PRINT"PRINT OUT DATA Y/N"
2640 I$=GET$
2650 IF I$="Y" GOTO 2680
2660 IF I$="N" GOTO 3030
2670 GOTO 2640
2680 K=OPENIN H$
2690 INPUT£K,L1,L2,L3,O$
2700 VDU2
2710 PRINT;L1;L2;L3;" ";O$;" MODE":PRINT
2720 PRINT"       TEMP       FREQ      GRAD      DENS     PATH.L      VELC
  (PV^2)'"
2730 REPEAT
2740 INPUT£K,Z1,Z2,Z3,Z4,Z5,Z6,Z7,Z8
2750 @%=&0100050A
```

```
2760 PRINT Z1,Z2,Z3,Z4,Z5,Z6,Z7,Z8
2770 UNTIL EOF£K
2780 CLOSE£K
2790 VDU3
2800 GOTO 3030
2810REM PRINT OUT FILE FROM DISC
2820INPUT "FILENAME";H$
2830 INPUT"DRIVE No";DN
2840 IF DN=0 THEN *DRIVE0
2850 IF DN=1 THEN *DRIVE1
2860 IF DN=2 THEN *DRIVE2
2870 IF DN=3 THEN *DRIVE3
2880 IF DN>3 GOTO 2830
28900=OPENIN H$
2900 INPUT£0,L1,L2,L3,O$
2910VDU2
2920 PRINT;L1;L2;L3;" ";O$;" MODE":PRINT
2930PRINT"     TEMP      FREQ      GRAD       DENS    PATH.L      VELOC
  (PV^2)'"
2940REPEAT
2950INPUT£0,TEMP,F,G,D,LC,VC,PV,DC
2960@%=&0100050A
2970PRINT TEMP,F,G,D,LC,VC,PV,DC
2980UNTIL EOF£0
2990CLOSE£0
3000VDU3
3010CLS
3020 GOTO 3030
3030REM MENU
3040CLS
3050PRINT"CONTROL"
3060PRINT
3070PRINT"P---PRINT OUT STORED DATA"
3080PRINT
3090PRINT"D---CALCULATE PRESS.DER."
3100PRINT
3104 PRINT"G---PLOT GRAPHS"
3108 PRINT:PRINT"H---CHANGE INPUT DATA"
3110PRINT:PRINT"C---TO CHANGE PRESET DATA"
3120PRINT
3130 PRINT"S---STOP PROGRAM"
3140 F$=GET$
3150 IF F$="P" THEN GOTO 2810
3160 IF F$="D" THEN GOTO 2310
3170 IF F$="C" THEN GOTO 3470
3175 IF F$="G" THEN GOTO 4000
3177 IF F$="H" THEN GOTO 610
3180 IF F$="S" THEN GOTO 3720
3190 GOTO 3030
3195 REM
3200 REM CORRECTION FOR THERMAL EXP.
3205 REM
3210T=T(M)-20:K=T(M)+273
3220AL=4.5422*(1+2.59E-5*K+1.15E-10*K^3)
3230CL=4.9141*(1+2.59E-5*K-1.15E-10*K^3)
3240RTL=4.5422*(1+2.59E-5*293+1.15E-10*293^3)
3250RCL=4.9141*(1+2.59E-5*293-1.15E-10*293^3)
3260HT=(AL^2*L1+AL^2*L2+CL^2*L3)^.5
3270 RT=(RTL^2*(L1+L2)+RCL^2*L3)^.5
3280 COR=HT/RT
```

```
3290 LL=L(M)*COR
3295 REM
3300 REM DENSITY CORRECTION
3305 REM
3310 D=P/(1+7.77E-5*T+3.45E-10*K^2*T)
3320 RETURN
3325 REM
3330REM TEMP CORR FOR ELASTIC CONSTANTS
3335 REM
3340 R1=4.591E10-3.318E7*T(M)+17677*T(M)^2
3345 R2=4.442E10-2.744E7*T(M)-6630*T(M)^2
3350 R3=6.629E9-3.936E6*T(M)-7778*T(M)^2
3355 R4=1.241E10-1.893E7*T(M)-8473*T(M)^2
3360 R5=R1-2*(2.956E9-1.662E7*T(M)+22426*T(M)^2)
3362 A=R3+.5*(R1+R2)
3364 MC=2.358E9-1.228E7*T(M)+13761*T(M)^2
3366 R6=-C3+SQR((A-2*MC)^2-.25*((C1-C2)^2))
3370CC=(R2*(R1+R5)-2*R6^2)
3380S1=(.5*(R2/CC+1/(R1-R5)))
3382 REM CALCULATE COMPLIANCES
3384 REM
3390S2=(R1+R5)/CC
3400S3=1/R3:S4=1/R4
3410S5=0.5*(R2/CC-1/(R1-R5))
3420S6=-R6/CC
3430X=2*S1+S2+2*(S5+2*S6)
3440BM=1/X
3450LCP=(S1+S5+S6)-(S1+S5-S6-S2)*L3^2
3460 RETURN
3465 REM
3470 REM CHANGE PRESET DATA
3475 REM
3480 CLS
3490 PRINT"....ELASTIC CONSTANTS-"
3500 PRINT
3510 PRINT"1...C11=";C1;"E10    2...C33=";C2;"E10"
3520 PRINT
3530 PRINT"3...C44=";C3;"E10    4...C66=";C4;"E10"
3540 PRINT
3550 PRINT"5...C12=";C5;"E10    6...C13=";C6;"E10"
3560 PRINT:PRINT
3570 PRINT:PRINT:PRINT"7...ROOM TEMP DENSITY=";P;"Kg/M^3"
3580 PRINT:PRINT"8...CARRIER FREQUENCY=";CF;"MHz"
3590 PRINT:PRINT:PRINT"C...BACK TO CONTROL"
3600 PRINT:PRINT:PRINT"PRESS APPROPRIATE KEY"
3610M$=GET$
3620IF M$="1" THEN INPUT"C11*1E10=";C1
3630IF M$="2" THEN INPUT"C33*1E10=";C2
3640IF M$="3" THEN INPUT"C44*1E10=";C3
3650IF M$="4" THEN INPUT"C66*1E10=";C4
3660IF M$="5" THEN INPUT"C12*1E10=";C5
3670IF M$="6" THEN INPUT"C13*1E10=";C6
3680 IF M$="7"THEN INPUT"DENSITY(Kg/M^3)=";P
3690 IF M$="8" THEN INPUT"CARRIER FREQ(MHz)";CF
3700 IF M$="C" THEN GOTO 3040
3710 GOTO 3470
3720 P=0
3730 REPEAT
3740 PRINT"BYE NOW!";
3750 P=P+1
```

```
3760 UNTIL P=125
3770 STOP:END
4000 REM
4005 REM GRAPH PLOTTER
4010 REM
4020 MODE 4
4030 Z=0
4120Q=OPENIN H$
4130 INPUT£Q,L1,L2,L3,O$
4140 REPEAT
4150INPUT£Q,T(Z),F,G,D,LC,V(Z),P(Z),D(Z)
4160Z=Z+1
4170UNTIL EOF£Q
4180CLOSE£Q
4190 GOTO 4350
4200 CLS
4205 REM DRAW AXES
4210MOVE 200,150
4220DRAW 1200,150:DRAW 1200,950
4230DRAW 200,950:DRAW 200,150
4240 FOR N=0 TO 5
4250X=200+N*200
4260MOVE X,150:DRAW X,170
4270 MOVE X,950:DRAW X,930
4280 NEXT N
4290FOR N=0 TO 4
4300Y=150+N*200
4310MOVE 200,Y:DRAW 220,Y
4320MOVE 1200,Y:DRAW 1180,Y
4330NEXT N
4340 RETURN
4345 REM
4346 REM CALC. MAX AND MIN VALUES
4347 REM
4350 TMAX=T(0):VMAX=V(0):PMAX=P(0):DMAX=D(0)
4360  TMIN=T(0):VMIN=V(0):PMIN=P(0):DMIN=D(0)
4370 FOR M=1 TO Z-1
4380IFT(M)>TMAX THEN TMAX=T(M)
4390IFT(M)<TMIN THEN TMIN=T(M)
4400IFP(M)>PMAX THEN PMAX=P(M)
4410IFP(M)<PMIN THEN PMIN=P(M)
4420IFV(M)>VMAX THEN VMAX=V(M)
4430IFV(M)<VMIN THEN VMIN=V(M)
4440IFD(M)>DMAX THEN DMAX=D(M)
4450IFD(M)<DMIN THEN DMIN=D(M)
4460NEXT M
4470 XMIN=INT(TMIN/10)*10
4480 XMAX=(INT(TMAX/10)+1)*10
4490 XSTEP=(XMAX-XMIN)/5
4500 CLS
4510 PRINT"PRESS APPROPRIATE BUTTON"
4520 PRINT:PRINT:
4530 PRINT"V...Velocity vs temp.":PRINT
4540 PRINT"P...Elastic modulus vs temp.":PRINT
4550 PRINT"D...Pressure der. vs temp."
4560 PRINT:PRINT"E...View or edit data"
4570 PRINT:PRINT"C...RETURN TO CONTROL"
4572 PRINT:PRINT:PRINT"AFTER PLOTTING GRAPH PRESS 'D' FOR A"
4574 PRINT"SCREEN DUMP OF GRAPH (YOU NEED PROGRAM"
4576 PRINT"'PPLOT' ON YOUR DISC)"
```

```
4580 W$=GET$
4590 IF W$="V" GOTO 4650
4600 IF W$="P" GOTO 4690
4610 IF W$="D" GOTO 4730
4620 IF W$="E"THEN GOTO 5220
4630 IF W$="C" THEN MODE7:GOTO 3040
4640 GOTO 4500
4645 REM SCALE GRAPH
4650 YMAX=(INT(VMAX/10)+1)*10
4660 YMIN=(INT(VMIN/10))*10
4670 YSTEP=(YMAX-YMIN)/4
4680 GOTO 4770
4690YMAX=(INT(PMAX/1E9)+1)*1E9
4700YMIN=INT(PMIN/1E9)*1E9
4710 YSTEP=(YMAX-YMIN)/4
4720 GOTO 4770
4730YMAX=(INT(DMAX)+1)
4740YMIN=(INT(DMIN))
4750 YSTEP=(YMAX-YMIN)/4
4760 GOTO 4770
4770 GOSUB 4200
4780 Y=28
4790FOR L=0TO5
4800 X=36-L*6
4810 XX=XMAX-L*XSTEP
4820PRINT TAB(X,Y);XX
4830NEXT L
4840 X=0
4850 FOR L=0TO4
4860 Y=3+L*6
4870 YY=YMAX-L*YSTEP
4880 PRINT TAB(X,Y);YY
4890 NEXT L
4900 GX=1000/(XMAX-XMIN)
4910 GY=800/(YMAX-YMIN)
4920 IFW$="V" GOTO 4950
4930 IFW$="P" GOTO 5020
4940 IFW$="D" GOTO 5100
4950 C$="VELOCITY"
4960  FOR L=0 TO Z-1
4970 Y=(V(L)-YMIN)*GY+150
4980 X=(T(L)-XMIN)*GX+200
4990 PLOT 69,X,Y
5000NEXT L
5010 GOTO 5170
5020 @%=&01000509
5030 C$="MODE CONSTANT"
5040  FOR L=0 TO Z-1
5050 Y=(P(L)-YMIN)*GY+150
5060 X=(T(L)-XMIN)*GX+200
5070PLOT 69,X,Y
5080NEXT L
5090GOTO 5170
5100 C$="PRESS. DER."
5110  FOR L=0 TO Z-1
5120 Y=(D(L)-YMIN)*GY+150
5130 X=(T(L)-XMIN)*GX+200
5140 PLOT 69,X,Y
5150 NEXT L
5160 GOTO 5170
```

```
5170 PRINT TAB(1,30);"TEMP. vs ";C$;" FOR ";L1;L2;L3;" ";O$;" MODE":PF
,0)
5180 R$=GET$
5190 IF R$="D" THEN *PPLOT
5200 GOTO 4500
5210 GOTO 4500
5220 REM LIST DATA
5230 VDU 14
5240 CLS:PRINT"TEMP(Deg.C) VEL(m/sec) pV^2   PRES.DER"
5250 @%=&0100050A
5260 FOR L=0 TO Z-1
5270 PRINT;L;"  ";T(L),V(L),P(L),D(L)
5280 NEXT L
5290 IF GET$="" GOTO 5290
5300 VDU 15
5310 PRINT"CHANGE DATA (Y/N)"
5320 O$=GET$:IF O$="Y" GOTO 5380
5330 PRINT"DELETE DATA (Y/N)"
5340 O$=GET$:IF O$="Y" GOTO 5500
5350 PRINT"APPEND DATA (Y/N)"
5360 O$=GET$:IF O$="Y" GOTO 5600
5370 GOTO 4350
5380 INPUT "LINE NUMBER ";NL
5390 PRINT"INPUT NEW DATA. TYPE '0' TO"
5400 PRINT"LEAVE UNCHANGED"
5410 INPUT"TEMPERATURE (Deg.C) ";XD
5420 IF XD<>0 THEN T(NL)=XD
5430 INPUT"VELOCITY (m/sec)";XD
5440 IF XD<>0 THEN V(NL)=XD
5450 INPUT"ELASTIC CONSTANT";XD
5460 IF XD<>0 THEN P(NL)=XD
5470 INPUT"PRESSURE DER.";XD
5480 IF XD<>0 THEN D(NL)=XD
5490 GOTO 5220
5500 PRINT"LINE No. TO BE DELETED"
5510 INPUT"TYPE NEGATIVE No IF NO DELETION";NL
5520 IF NL<0 GOTO 5220
5530 IF NL>Z-1 GOTO 5220
5540 FOR L=NL TO Z-1
5550 T(L)=T(L+1):V(L)=V(L+1)
5560 P(L)=P(L+1):D(L)=D(L+1)
5570 NEXT L
5580 Z=Z-1
5590 GOTO 5220
5600 PRINT"DATA LINE ";Z
5610 PRINT:INPUT"TEMP (Deg.C)";T(Z)
5620 PRINT:INPUT"VELOCITY (m/sec)";V(Z)
5630 PRINT:INPUT"ELASTIC CONSTANT";P(Z)
5640 PRINT:INPUT"PRESSURE DERIV.";D(Z)
5650 Z=Z+1
5660 PRINT"AGAIN (Y/N)"
5670 O$=GET$:IF O$="Y" GOTO 5600
5680 GOTO 5220
```

APPENDIX B

Worked examples of conversion between adiabatic and isothermal pressure derivatives

APPENDIX B

This appendix contains worked examples illustrating a method for converting pressure derivatives of effective adiabatic elastic stiffnesses to the pressure derivatives of the isothermal stiffnesses (Thurston [1967]) . The method requires that data for the thermal expansion , the specific heat , and the temperature derivatives of the elastic constants , be available for the material under study .

The reason for including these calculations is to show that at high temperatures the difference between adiabatic and isothermal pressure derivatives is small compared with other experimental errors .

The calculations shown here are for single crystal indium at 157 deg.C . Elastic constant data and values for pressure derivatives have been obtained from the experimental results of the present work . Data on the thermal expansion coefficients of indium and their temperature derivatives was taken from previously published data (Graham et al [1955]) and the value for the specific heat at 157 deg.C was calculated from results obtained by Kramer and NÖlting [1972] .

STEP 1

Convert from temperature derivatives of effective elastic coefficients to temperature derivatives of

thermodynamic elastic coefficients .

When the pressure, P, = 0 we can assume that the material is undeformed and then thermodynamic elastic constants play the role of 'effective' coefficients when temperature changes are considered . Therefore the required values are simply the measured temperature derivatives . The values listed here were obtained by differentiation of the equations of best fit to measured elastic constant temperature responses :

Values for 157 (deg.C)

$\partial C_{11}^S/\partial T = -2.76 \times 10^7$ (Pa/deg.C)

$\partial C_{33}^S/\partial T = -2.95 \times 10^7$

$\partial C_{44}^S/\partial T = -6.38 \times 10^6$

$\partial C_{66}^S/\partial T = -2.16 \times 10^7$

$\partial C_{12}^S/\partial T = -8.44 \times 10^6$

$\partial C_{13}^S/\partial T = -1.26 \times 10^7$

STEP 2

Invert elastic stiffness tensor to obtain elastic compliance values .

The values found for the adiabatic elastic constants of indium at 156 deg.C were:

$C_{11}^S = 4.116 \times 10^{10}$ (Pa)

$C_{33}^S = 3.998 \times 10^{10}$

$C_{44}^S = 0.583 \times 10^{10}$

$C_{66}^S = 0.925 \times 10^{10}$

$$C^S_{12} = 3.935 \times 10^{10}$$
$$C^S_{13} = 3.901 \times 10^{10}$$

For the indium structure (fct) the inversion of the elastic constant matrix may be represented by the following equations (e.g. Nye [1972]):

$$S_{11} + S_{12} = C_{33}/X$$
$$S_{11} - S_{12} = 1/(C_{11} - C_{12})$$
$$S_{33} = (C_{11} + C_{12})/X$$
$$S_{44} = 1/C_{44}$$
$$S_{66} = 1/C_{66}$$
$$S_{13} = -C_{13}/X$$
$$\text{where } X = C_{33}(C_{11} + C_{12}) - 2C^2_{13}$$

The resulting compliance values (S_{ij}) are:

$$S^S_{11} = 3.95 \times 10^{-10} \quad (Pa^{-1})$$
$$S^S_{33} = 4.66 \times 10^{-10}$$
$$S^S_{44} = 1.72 \times 10^{-10}$$
$$S^S_{66} = 1.08 \times 10^{-10}$$
$$S^S_{12} = -1.64 \times 10^{-10}$$
$$S^S_{13} = -2.26 \times 10^{-10}$$

STEP 3

Use the equation:

$$S^T_{\lambda\mu} - S^S_{\lambda\mu} = T\alpha_\lambda\alpha_\mu/\rho C;$$

to find the isothermal compliance values . α_λ and α_μ are thermal expansion coefficients , ρ is the density and C is the heat capacity at constant thermodynamic

tensions (at zero tensions $C_i = C_\rho$) .

At 157 deg.C ,

$$\alpha_a = 8.97 \times 10^{-5} \qquad (K^{-1})$$

$$\alpha_b = -3.78 \times 10^{-5}$$

$$C_\rho = 260 \text{ J } K^{-1}kg^{-1}$$

Resulting values of isothermal compliances are:

$$S^T_{11} = 3.96 \times 10^{-10} \qquad (Pa^{-1})$$

$$S^T_{33} = 4.66 \times 10^{-10}$$

$$S^T_{44} = 1.71 \times 10^{-10}$$

$$S^T_{66} = 1.10 \times 10^{-10}$$

$$S^T_{12} = -1.64 \times 10^{-10}$$

$$S^T_{13} = -2.26 \times 10^{-10}$$

STEP 4

Invert isothermal compliance matrix to obtain values for the isothermal elastic constants .

Values obtained on inversion of compliance matrix are as follows:

$$C^T_{11} = 4.02 \times 10^{10} \qquad (Pa)$$

$$C^T_{33} = 3.92 \times 10^{10}$$

$$C^T_{44} = 0.58 \times 10^{10}$$

$$C^T_{66} = 0.91 \times 10^{10}$$

$$C^T_{12} = 3.71 \times 10^{10}$$

$$C^T_{13} = 3.82 \times 10^{10}$$

STEP 5

Convert from pressure derivatives of effective elastic constants, C'_{ij}, to pressure derivatives of thermodynamic

elastic coefficients, B_{ij}, (see section 2.5) .

C'_{11} = 6.55	B11 = 7.40
C'_{33} = 6.01	B33 = 8.30
C'_{44} = 1.26	B44 = 2.34
C'_{66} = 2.27	B66 = 3.24
C'_{12} = 5.68	B12 = 4.53
C'_{13} = 5.34	B13 = 4.88

STEP 6

Use the following equation to obtain pressure derivatives of isothermal elastic compliances:

$$\partial S^T_{\lambda\mu} / \partial P = -S^S_{\lambda\alpha} S^S_{\beta\mu} \partial C_{\alpha\beta} / \partial P + T/\rho C_p (\pi_\lambda S^S_{\mu\alpha} S^S_{\beta\lambda} \partial C^S_{\alpha\beta} / \partial T + \pi_\mu S^S_{\lambda\alpha} S^S_{\beta\mu} \partial C^S_{\alpha\beta} / \partial T) - 2T \pi_{ii} \pi_\lambda \pi_\mu / \rho^2 C_p^2 - (T^2 \pi_{ii} / \rho^2 C_p^2)(\pi_\lambda \partial \pi_\mu / \partial T + \pi_\mu \partial \pi_\lambda / \partial T) + (T^2 \pi_\lambda \pi_\mu / \rho^2 C_p^2)(2 \pi_{ii} \partial C_p / C_p \partial T - \partial \pi_{ii} / \partial T)$$

Once this has been done the final step is to convert pressure derivatives of isothermal compliances into pressure derivatives of isothermal stiffnesses . To obtain the relationship between the two quantities the stiffness-compliance relation for each coefficient must be differentiated with respect to pressure . For some coefficients this process is very complex and so only values for C_{44} and C_{66} are calculated here as the workings involved are relatively straightforward .

C_{44} Mode

$T = 430$ deg.K $\qquad \rho = 7150$ kg/m^3

$C_p = 260$ J K^{-1}kg^{-1} $\qquad \partial C_p/\partial T = 0.2807$ J K^{-2}kg^{-1}

$\pi_4 = 2.207 \times 10^{-5}$ K^{-1} $\qquad \partial \pi_4/\partial T = -8.22 \times 10^{-9}$ K^{-1}

For this mode the equation given above for $\partial S^T_{44}/\partial P$ deals only with C^S_{44} , $\partial C^S_{44}/\partial P$, $\partial C^S_{44}/\partial T$, and S_{44}. Substituting the appropriate values into the above equation gives the result:

$$\partial S^T_{44}/\partial P = -7.062 \times 10$$

Now $\qquad S_{44} = 1/C_{44}$

therefore $\qquad \partial S_{44}/\partial P = -(1/C^2_{44})\partial C_{44}/\partial P$

This leads to $\qquad \partial C^T_{44}/\partial P = 2.39$

which when compared with $\qquad \partial C^S_{44}/\partial P = 2.34$

shows a difference of less than 2% .

The equivalent calculations for the C_{66} mode gave a value for $\partial C^T_{66}/\partial P$ of 3.19 which again shows a difference of less than 2% from the adiabatic value .

REFERENCES

Anderson [1966], J. Phys. Chem. Sol., 27, 547

Arenberg D.L. [1950], J. Appl. Phys., 21, 941

Babb S.E. [1963], Rev. Mod. Phys., 35, 400

Barsch G.R. and Shull H.E. [1971], Phys. Stat. Sol., (b) 43, 637

Betteridge W. [1938], Proc. Phys. Soc., 50, 519

Born M. [1939], J. Chem. Phys., 7, 591

Boyer L.L. [1979], Phys. Rev. Lett., 42, 584

Boyer L.L. [1985], Phase Transitions, Vol. 5, 1-48

Bradley C.C. [1969], High pressure methods in solid state research, Butterworth, London

Brassington M.P. [1982], PhD thesis, University of Bath

Brassington M.P. and Saunders G.A. [1983], Proc. R. Soc. Lond., A387, 289

Bridgman P.W. [1911], Proc. Amer. Acad. Arts. Sci., 47, 321

Bridgman P.W. [1949], Proc. Amer. Acad. Arts. Sci., 77, 187

Brillouin L. [1938], Phys. Rev., 54, 916

Brugger K. [1964], Phys. Rev., 133, A1611

Brugger K. [1965], Phys. Rev. 137, A1826

Brugger K. [1965], J. Appl. Phys., 36, 759

Brugger K. and Fritz T.C. [1967], Phys. Rev., 157, 524

Cannon J.F. [1974], J. Phys. Chem., 3, 781

Chi-Yuen Wang [1967], Rev. Sci. Instrum., 38, 24

Choquard P.F. [1967], "The Anharmonic Crystal", W.A. Benjamin Inc., New York

Chung D.Y., Gunton D.J. and Saunders G.A. [1976], Phys. Rev., B13, 3239

Cochran W. [1960] Adv. Phys. 9, 387

Cochran W. [1961] Adv. Phys. 10, 401

Coterill R.M.J. [1980], J. Cryst. Growth, 48, 582

Coterill R.M.J., and Madsen J.U. [1982], Nature, 299, 188

Dieulesaint E. and Royer D. [1980], Elastic waves in solids, Wiley, Chichester

Dudley J.D. and Hall H.T., [1960], Phys. Rev., 118, 1211

Enck F.D., [1960], Phys. Rev. 119, 1873

Feldman C., Feldman J.L., Horton G.K. and Klein M.L. [1967], Proc. Phys. Soc., 90, 1182

Fleury P.A., [1972a], J. Acoust. Soc. Am. 49, 1041

Fleury P.A., [1972b], Comments Solid State Phys. 4, 149, 167

Fleury P.A., [1973], "Phase transitions", ed. L.E. Cross, Pergamon Press, New York

Fleury P.A., [1976], "Annual review of Materials Science", ed. R.A. Huggins, Annual Reviews Inc., Palo Alto (Calif.)

Flower S.C., Saunders G.A. and Yogurtcu Y.K. [1985], J. Phys. Chem. Solids, 46, 97

Gilvarry J.J. [1966]. Phys. Rev. Lett., 16, 1089

Graham J., Moore A. and Raynor G.V. [1955], J. Inst. Metals, 84, 87

Grose R., Krause P., Meissner M. and Tausend A. [1978], J. Phys., C11, 45

Grüneisen E. [1908], Ann. Phys., 25, 825

Grüneisen E. [1962], "Handbuchder Physik", 10, 2, Springer-Verlag, Berlin

Guinea F., Rose J.H., Smith J.R. and Ferrante J. [1984], Appl. Phys. Lett. 44, 53

Gunton D.J. [1973], PhD thesis, University of Bath

Gunton D.J. and Saunders G.A. [1973], Solid state commun., 12, 569

Gunton D.J. and Saunders G.A. [1974], Solid state commun., 14, 865

Hailing Tu. [1983], PhD thesis, University of Bath

Hailing Tu., Saunders G.A., Lampson W.A., and Fegelson R.F. [1982], J. Phys. C: Solid state Phys. 15, 1399

Herzfeld K.F. and Goeppert-Mayer [1934], Phys. Rev., 46, 995

Hollenberg W.C. and Batterman B.W. [1974], Phys. Rev., B10, 2148

Hunter L. and Siegel [1942], Phys. Rev., 61, 84

Ida Y. [1969], Phys. Rev. 61, 84

Ida Y. [1970], Phys. Rev., B1, 2488

Jackson I.N.S. and Leiberman R.C. [1974], J. Phys. Chem. Solids 35, 1115

Kane G. [1939], J. Chem. Phys., 7, 603

Kennedy G.C. [1956], Phys. Rev., 102, 325

Kennedy G.C. [1965], J. Geophys. Res., 70, 1979

Kharoo H.L., Gupta O.P. and Hemkar M.P. [1978], J. Phys. Chem. Solids, 39, 45

Kittinger E. [1977], Ultrasonics (GB), 15, 30

Kramer W. and Nölting J. [1972], Acta Metall., 20, 1353

Kraut E.A. and Kennedy G.C. [1966], Phys. Rev. Lett., 16, 608

Landau L.D. and Lifshitz E.M. [1959],"Statistical Physics" Pergamon Press, London

Liakos J.K. and Saunders G.A. [1982], Phil. Mag., 46, 217

Lindemann F. [1910], Phys. Z., 11, 609

Madaiah N. and Graham G.M. [1964], Can. J. Phys., 42, 221

Madhava M.R. [1977], PhD thesis, University of Bath

Madhava M.R. and Saunders G.A. [1977], Phil. Mag., 36, 777

Mason W.P. and McSkimin H.J., [1947], J. Acoust. Soc. Am., 19, 464

McSkimin H.J. and Andreatch P. [1966], J. Acoust. Soc. Am. 41, 1052

Moleko L.K. and Glyde H.R. [1983], Phys. Rev., B27, 6019

Munn R.W., Adv. Phys., 18, 515

Murnaghan F.D. [1944], Proc. Nat. Acad. Sci. (USA), 30, 244

Nardi V. and Persus J.K. [1967], Phys. Rev., 160, 259

Newman R.M. [1980], Phys. Lett., 77A, 55

Nye J.F. [1957], 'Physical properties of crystals and their representation by tensors and matrices', O.U.P.

Nye J.F. [1960], 'Physical properties of crystals', Clarendon Press, Oxford.

Overton W.C. [1962], J. Chem. Phys., 37, 116

Pace N.G. and Saunders G.A. [1972], Proc. Roy. Soc. A 326, 521

Papadakis E.P. [1967], J. Acoust. Soc. Am., 42, 1045

Pershin V.K. and Pershin Vl.K. [1982], Theor. and Math. Phys., 52, 821

Pfann W.G. [1958], "Zone Melting", Wiley, New York

Plakida N.M. and Siklos T. [1978], Acta. Phys. Acad. Sci. Hung., 45, 37

Pollard H.F. [1977], 'Sound waves in solids', Pion, London

Ramakrishnan J., Boehler R., Higgins G. and Kennedy G.C. [1978], J. Geophys. Res. (USA), 83, 3535

Rewald W. [1973], Adv. Phys., 22, 721

Romain J.R., Migault A. and Jaquesson J. [1979], J. Phys. Chem. Sol., 41, 323

Ruffa A.R. [1981], Phys. Rev., B24, 6915

Ruffa A.R. [1982], Phys. Rev., B25, 5895

Schouten D.R. and Swensen C.A. [1974], Phys.Rev., B10, 2175

Seung-Am Cho [1982], J. Phys. F, 12, 1069

Shapiro J.N. [1970], Phys. Rev., B1, 3982

Simon F.E. and Glatzel G. [1929], Z. anorg. n. allgem. Chem., 178, 309

Slagle O.D. and McKinstry H.A. [1967], J. Appl. Phys., 38, 437

Stroud D. and Ashcroft N.W. [1972], Phys. Rev., B5, 371

Swensen C.A. [1955], Phys. Rev., 100, 1607

Tallon J.L. [1980], Phys. Lett. 76A, 139

Tallon J.L. [1980], Phys. Lett., 76A, 139

Tallon J.L. [1982], Nature, 299, 188

Tallon J.L. and Robinson W.H. [1982], Phys. Lett., 87A, 365

Tallon J.L., Robinson W.H. and Smedley S.I. [1977], Nature, 266, 337

Thurston R.N. [1965], Proc. IEEE 53, 1320

Thurston R.N. and Brugger K. [1964], Phys. Rev., 133, A1604

Thurston R.N., McSkimin H.J. and Andreatch P. [1966], J. Appl. Phys., 37, 267

Truell R., Elbaum C. and Chick B.B. [1959], Ultrasonic methods in solid state physics, Acad. Press, New York

Ubbelohde A.R. [1978], "The molten state of matter", John Wiley & Sons, New York

Vaidya S.N. [1984], Phys. Stat. Sol. (a) 86, 565

Vaidya S.N. [1985], Phys. Stat. Sol. (a) 87,181

Vaidya S.N. and Raja Gopal E.S. [1966], Phys. Rev. Lett., 17, 635

Vaygham R.W. and Drickamer H.G. [1965], J. Phys. Chem. Solids, 26, 1549

Vereshchagin L.F., Kabalkina S.S. and Troitskaya Z.V. [1964], Sov. Phys.- J.E.T.P., 20, 267

Vladimirov V.I. [1969], Sov. Phys.- solid state, 10, 2077

Vold C.L., Glicksman M.E., Kammer E.W., and Cardinal L.C., [1977], J. Phys. Chem. Solids, 38, 157

Winder D.R. and Smith C.S. [1958], J. Phys. Chem. Solids, 4, 128

Zhdanov G.S. [1981], Sov. Phys. Crystallogr., 26, 740

Zubov V.I. [1978], Phys. Status Solidi B, 88, 43

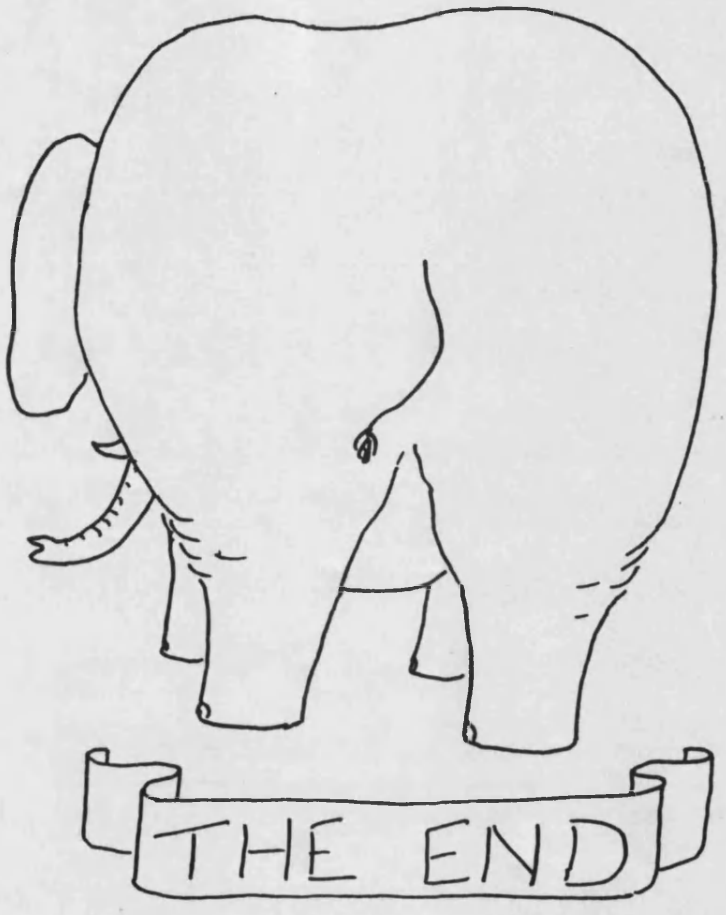
THE END